Post-Synthesis Modifications on Zeolites for Improved Accessibility and Catalytic Performance

Post-synthese modificaties van zeolieten voor
verbeterde toegankelijkheid en katalytische activiteit

(met een samenvatting in het Nederlands)

Proefschrift

ter verkrijging van de graad van doctor aan de Universiteit Utrecht op gezag van de rector magnificus, prof. dr. G.J. van der Zwaan, ingevolge het besluit van het college voor promoties in het openbaar te verdedigen op dinsdag 19 april 2011 des middags te 2.30 uur

door

Adrianus Nicolaas Cornelis van Laak

geboren op 15 januari 1980, te Vught

Promotor: Prof. dr. ir. K. P. de Jong

Co-promotor: Dr. P. E. de Jongh

The research described in this thesis was financially supported by ACTS-ASPECT.

Voor jou Marleen

ISBN: 978-90-393-5541-1

Printed by GVO drukkers & vormgevers B.V. | Ponsen & Looien

Contents

1

General Introduction

1.1 Zeolites and Catalyis

History

In 1756 the first zeolite (stilbite) was discovered by Axel Fredrik Crønsted [1] who observed that by heating the stone-like material, large amounts of steam were formed. By translating these two characteristics into classic Greek the term zeolite was introduced, where ζέω (zeo) means to boil and λίθος (lithos) means stone. In the next century more natural occurring zeolites were discovered including faujasite (1842) and mordenite (1864) [2]. Nowadays the Structure Commission of the International Zeolite Association (IZA) has accepted 194 different framework structures [3, 4].

Structure

Zeolites are crystalline solids with a structure that comprises a three dimensional and regular framework formed by SiO_4 and AlO_4^- or other TO_4 tetrahedra, in which the oxygen atoms are shared between two neighboring tetrahedra [5] (Fig. 1). With these tetrahedra a limited number of secondary building units (SBU) can be build, from which the different unique zeolite unit cells can be constructed. Depending on the linking of the SBU, different pore sizes can be obtained that are classified according to the number of tetrahedra involved. Most common are small- medium- and large pore zeolites that have channels with 8, 10 or 12 membered rings (MR). These channels are considered micropores and have diameters ranging from 3 to 8 Å. Multiple pores with different sizes can be present in a zeolite, and depending on whether they are interlinked or not, the resulting zeolites have a 1-, 2- or 3- dimensional channel system. Micropores can host several species, such as water, small organic molecules and charge compensation cations. Charge compensating cations are necessary to compensate for the negative charge when trivalent aluminum is inserted into the framework. This is often a sodium cation (Na^+), as it offers excellent stabilization of the framework during synthesis and is easily ion-exchanged for other cations. Upon ion exchange with NH_4^+ followed by a subsequent calcination a proton (H^+) cation can be obtained, that has strong acidic properties. The combination of the proton and the presence of the micropore network makes it possible to differentiate on molecule size (molecular sieving), while the acid sites catalyze reactions [6] inside the micropores.

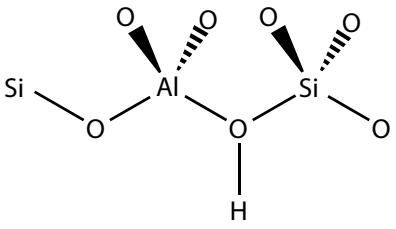

Fig. 1. Simplified zeolite structure and Bröndsted acid site.

The combination of these two features in one solid material has made zeolites into a very effective class of shape selective acid catalysts with many applications for the chemical industry. The downside of the shape selectivity is that molecules in micropores (< 2 nm) have a strong interaction with the pore wall, which leads to diffusivities that are orders of magnitude lower than in macropores (> 50 nm) or in mesopores (2-50 nm), which may result in mass transfer limitations (Fig. 2) [7]. To overcome the slow diffusion zeolites with channels larger than 12-MR have been synthesized such as VPI-5 [8] (18 MR, 12.7 Å, aluminum phosphate) , cloverite [9] (20 MR, 13.2 Å, gallium phosphate), and ITQ-15 [10] (interconnection 14 and 12 MR, 9.6 Å, germanium silicate).

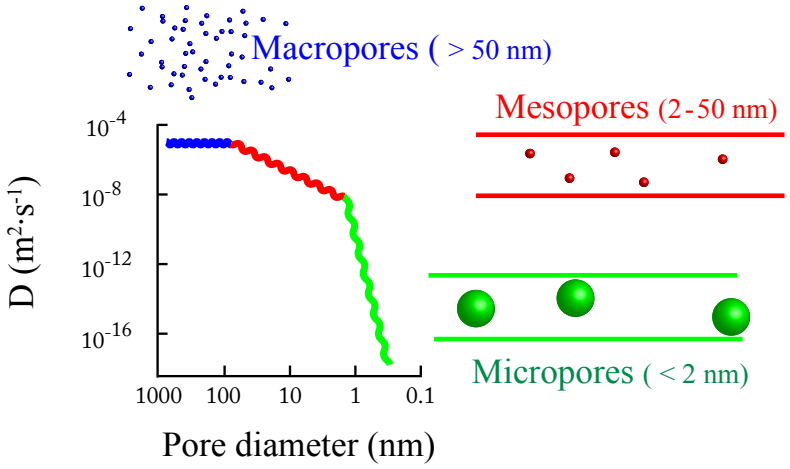

Fig. 2. Different diffusion regimes in macro-, meso- and micropores.

Applications

Despite the large variety of zeolites only a few are used in large scale industrial processes. One of the first applications was made by Mobil Oil that used a modified faujasite (FAU) for the catalytic cracking of gas oil [11]. The catalyst was over 100 times more active with 20 percent higher gasoline yields than the amorphous silica-alumina catalysts that were used before. Until this day zeolite Y is the most abundantly used zeolite in industry for processes such fluid catalytic cracking (FCC), alkylation and hydrocracking. Other important zeolites are; ZSM-5 (MFI), that is used for several reactions including FCC [12], methanol to olefins [13] and ethylbenzene production [14]; mordenite (MOR) [15] for C_5-C_6 n-alkane isomerization and the alkylation of aromatics for which zeolite

Beta and MCM-22 are used as well[14]; ferrierite (FER) for dewaxing [16]. Zeolites that are used in this research are zeolite Beta, ZSM-5 and ZSM-12 (Fig. 3). The focus however, will be on mordenite (Fig. 4).

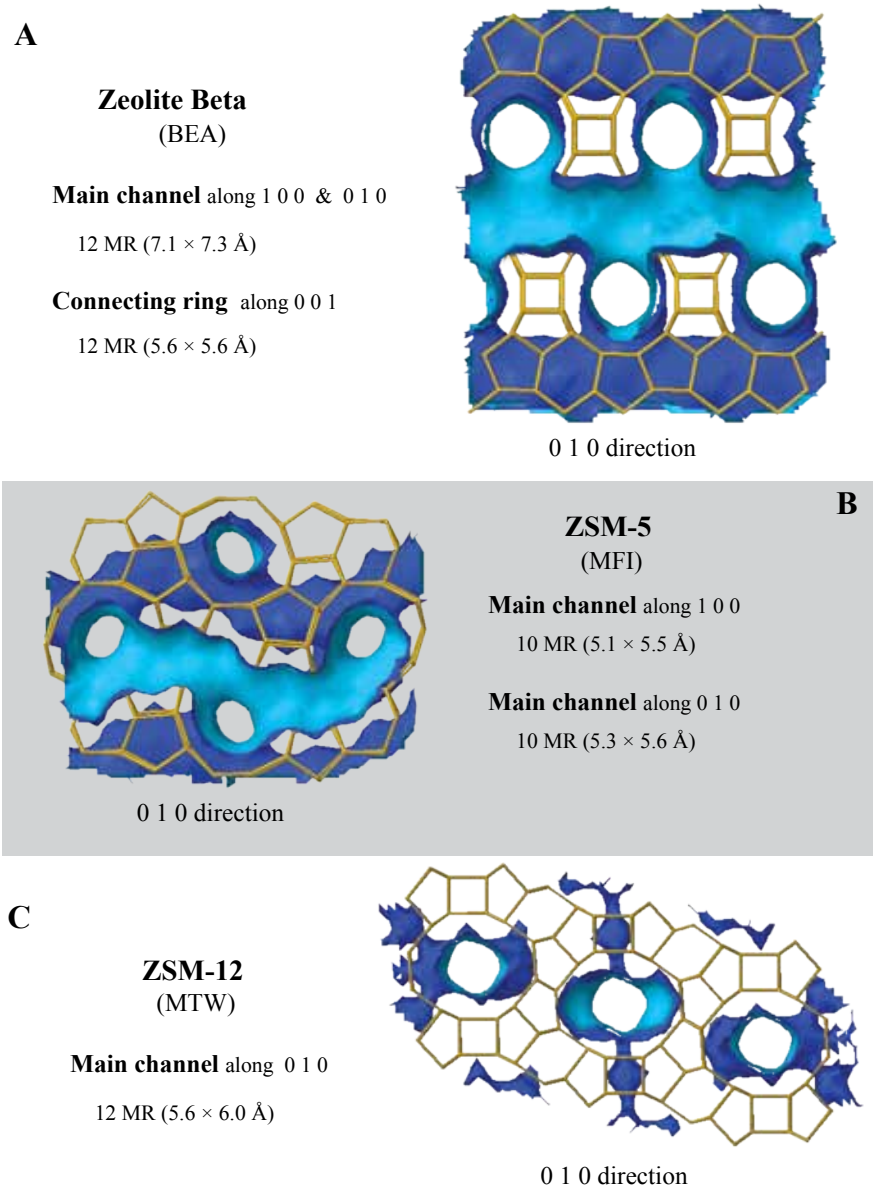

Fig. 3. Framework structures of the three zeolites, with a combined wireframe (yellow) and channel surface (blue) view: Beta (A), ZSM-5 (B) and ZSM-12 (C) [4].

1.2 Mordenite

Structure

Mordenite (ideal composition: $Na_8Al_8Si_{40}O_{96}{\cdot}nH_2O$) is a large-pore zeolite with a 12-MR channel (6.7 × 7.0 Å) that runs parallel to the c-axis (0 0 1). A second 8-MR channel runs along the direction of the b-axis (3.4 × 4.8 Å), this channel connects only to one 12-MR channel and is therefore often referred to as a sidepocket as is depicted in Figure 4 [17]. Since the side pockets do not inter-connect the 12 MR channels, mordenite is considered a one-dimensional zeolite. The channel-system of mordenite is best seen along the a-axis (1 0 0) in Figure 4B.

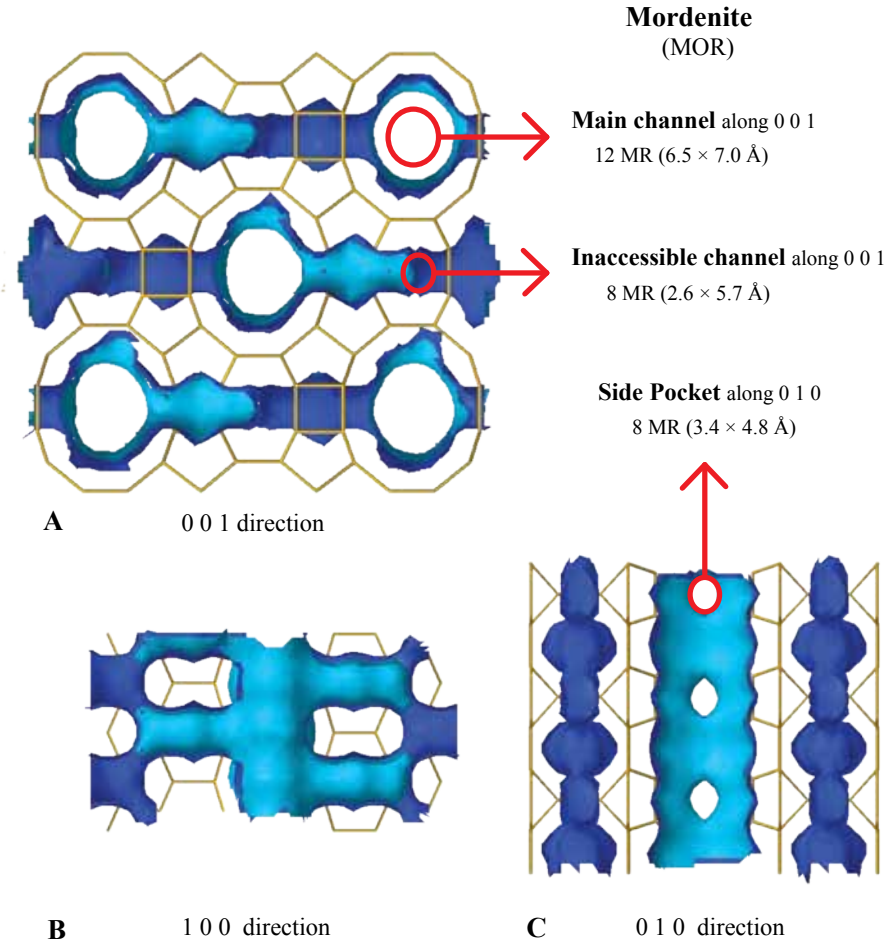

Fig. 4. Framework structure of mordenite along 3 axes with a combined wireframe (yellow) and channel surface (blue) view [4].

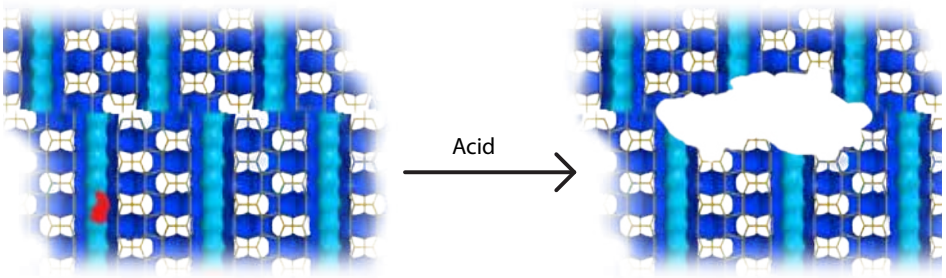

Fig. 5. The presence of stacking faults in mordenite and the removal of extraframework species and mesopore formation upon acid treatment.

Synthesis

Mordenite was one the earliest zeolites that was produced synthetically, and is important because of its high (hydro) thermal stability and for its high acid strength. It was observed that some mordenite samples were accessible for reactants while others were inaccessible. This difference in accessibility has been described frequently in literature as small- and large-port mordenite and has been the topic of a long discussion [18]. Because of the 1-dimensional channel system the micropores of mordenite are easily blocked by extra framework material. It has been described that by ion exchange or acid treatment [19] pore blockades can be removed (Fig. 5), thereby converting an inaccessible mordenite into an accessible mordenite [18]. Rudolf et al. [20] showed that stacking faults of half a unit cell can occur within mordenite crystallites, which could also be the cause of inaccessible mordenite. These boundaries are suggested to be weak points within the framework and upon acid treatment mesopores are formed, thereby increasing the accessibility of the micropores (Fig. 5). The number of stacking faults and pore blockades scales with the size (length) of the mordenite crystal. Small crystallites are, therefore, highly desirable. For several zeolites such as zeolite Beta and ZSM-5 routes to nano crystallites have been found [21]. For mordenite no route to nano crystallites has been found so far, although it is claimed by Chung et al. [22] based on the thickness (64 nm) of the crystallites. Mordenite however, has a tendency to form needle-like structures with the 12 MR channels directed along the length [23] of the crystallite, which was in this case well above 200 nm. The mordenite samples which are used in this thesis are fully accessible and are commercially available. The crystallites are on average between 100 and 200 nm in size and have formed agglomerates of 0.5-2 μm.

1.3 Post synthesis treatments and mesoporosity.

Acid treatment (dealumination, acid leaching)

Post synthesis treatment with steam and acid results in the removal of aluminum from the framework and is therefore often referred to as dealumination. Steaming is generally performed at high temperatures, typically above 723 K, in which aluminum is extracted from the framework and deposited on the external surface (A_{ext}) of the zeolite. In order to remove these extra framework species an additional acid treatment is necessary [24]. The combined steam and acid treatment, or acid treatment only, leads to an increased performance of the catalyst for several reasons: Decreasing the aluminum content leads to isolation of the remaining aluminum atoms, thereby increasing the acid site strength, which is maximum for Si/Al ratio (at/at) ~10 and higher. 2) A lower amount of aluminum in the framework results in improved (hydro) thermal stability. 3) Mesopores are created, thereby improving the accessibility of the crystallite [25]. Removal of aluminum also leads to a decrease in the total number of active sites. Consequently, the activity as a function of the silicon to aluminum ratio is going through a maximum [26].

Janssen et al. [27] showed by using electron tomography that two different mesopores can be distinguished upon combined steam and acid treatment of zeolite Y, i.e. mesopores that are connected to the external surface and mesopores within the crystallites, so-called cavities. The mesopores connected to the external surface are decreasing the intracrystalline diffusion path length (= half the length of the crystallite), by splitting the micropore channels into shorter segments. The transport of reactants and products to and from the newly created micropore entrances will proceed via the mesopore. A cavity is much less effective, as the molecules have to re-enter a micropore in order to leave the crystallite. The intracrystalline diffusion path length is therefore only decreased by the radius of the mesopore. In Figure 6 the effects of the two types of mesopores are illustrated for a 1 dimensional zeolite such as mordenite. Decreasing the diffusion path length is essential for increasing the activity of mordenite for diffusion limited processes like in the liquid-phase production of cumene [14]. For the isomerization of the n-hexane molecule, which can more easily migrate in the micropores, diffusion limitations become less severe. In a non mesoporous mordenite large parts of a one dimensional zeolite can be deactivated by a small number of blockades. In figure 6A a mordenite crystallite is depicted which is partly deactivated by plugs shown in red. These plugs result in blocking of ~60% of the micropores channels and thus reducing 60 % of the active sites. In figure 6B mesopores are present and only a small fraction (~15%) of the micropore channels is inaccessible for reactants.

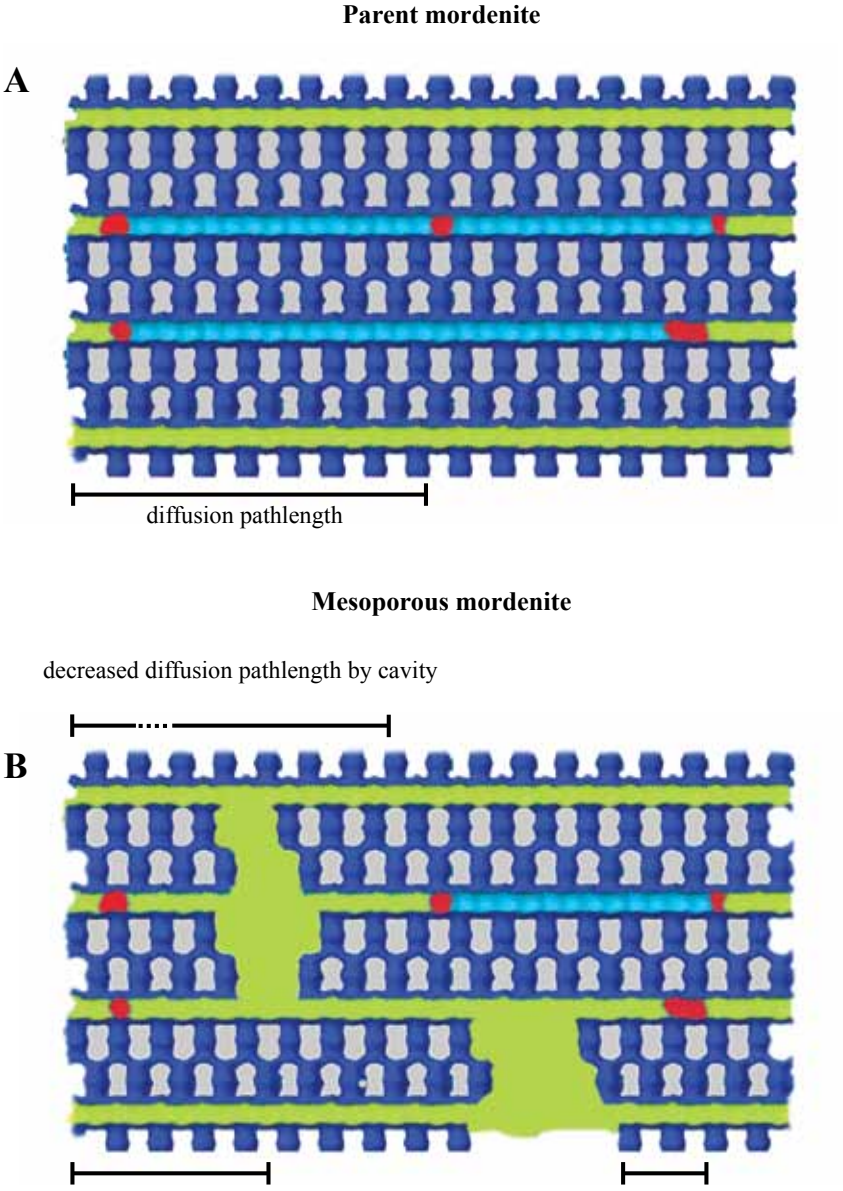

Fig. 6. Deactivation of parent mordenite by coke formation (red) resulting in the loss of 60 % of the micropores and thus acid sites (A) and decreased deactivation and diffusion path length by the presence of mesopores [4] (B).

Dealumination of mordenite

Dealumination of mordenite has been studied extensively and it is generally known to enhance the isomerization activity of n-hexane on Pt/mordenite, which is industrially applied by Shell in the HYSOMER process. A second example of an industrial application for mordenite is the Dow-Kellogg process for cumene production [28]. This process was partially commercialized in 1992 as an add-on trans-alkylation (diisopropylbenzene and benzene to form cumene) process. Most interesting about the unique performance and stability of this catalyst was that for the trans-alylation an undistilled heavies stream was used, which was possible because of its deep level of dealumination and mesoporosity [29, 30]. The dealumination and mesoporosity was obtained by subjecting the mordenite to treatment with nitric acid (3-6 M) followed by calcination at approximately 973 K. This procedure was repeated several times resulting in deeply dealuminated mordenite with Si/Al ratios as high as 315 at/at. Mesoporosity was presumably formed at the boundaries of stacking faults present inside the 0.5 to 2 μm crystallites (Fig. 5). This treatment resulted in an external surface area of ~100 $m^2 \cdot g^{-1}$ and a maximum mesopore volume of 0.11 $cm^3 \cdot g^{-1}$. The reported mesopore volume however, was defined between 1 and 100 nm instead of 2 to 50 nm. Several other dealumination studies are reported [22, 31-41], in which the maximum external surface areas are close to the values reported for the catalysts in the Dow Kellogg process. In some publications it was reported that a large amount of small (3-4 nm) mesopores were created [22, 34] upon acid treatment. However, on close inspection, this can be ascribed to misinterpretation of the nitrogen physisorption results, i.e. if the BJH pore size distribution is obtained from the desorption branch, a spike is observed at ~4 nm due the cavitation effect, that indicates that cavities are present with a neck smaller than ~4 nm and a radius larger than ~4 nm [42].

Alkaline treatment (desilication, base leaching)

Desilication is a post synthesis treatment in which primarily silicon is removed from the framework. In the late nineteen sixties and seventies several patents [43-47] were filed that described enhanced catalytic activity upon treatment with caustic solutions, primarily NaOH solutions. A revival of desilication as an effective post-synthesis treatment was initiated by Ogura et al. [48, 49] in 2000/2001. In his papers it was shown that treating a ZSM-5 crystal (~5 μm, Si/Al 20 (at/at)) in 0.05/0.1 M NaOH leads to an increase in mesoporosity, resulting in enhanced catalytic activity for cumene cracking. The desilication process for ZSM-5 was further improved by Groen et al. [50-52], who showed that the success of this procedure is closely related to the Si/Al ratio of the parent

material. An optimal mesoporosity was obtained for Si/Al ratios between 25 and 50 at/at [50], at lower values the aluminum is acting as a shield for desilication, thereby limiting mesopore formation, while at higher values complete dissolution occurs. In the past 10 years [53] it has been shown that desilication can be an effective post-synthesis treatment for other zeolites than ZSM-5, including zeolite beta (BEA) [54], ZSM-12 (MTW) [55], ferrierite (FER) [56], ITQ-4 (IFR) [57] and mordenite (MOR) [58-61].

Desilication of mordenite

Desilication or alkaline treatment on mordenite is described in 2 patents [43, 44] and 4 publication [58]. The patents assigned to Young (Mobil) disclose that caustic treatment preferably between 1 and 10 M NaOH at moderate temperatures (302-352 K) resulted in three-fold enhanced hydrocracking activity. In the publication by Groen et al. [58] (2007) as synthesized mordenite with a Si/Al ratio of 27 at/at was contacted with alkaline solution 0.2 M NaOH for 30 minutes at 338 K. This resulted in an increase of the external surface area from 5 to 115 $m^2 \cdot g^{-1}$ and enhanced catalytic performance for the production of ethylbenzene. Bokhoven et al. [59] (2009) showed that as synthesized mordenite with Si/Al ratio 13 at/at was not receptive towards alkaline treatment in 0.2 M NaOH solution at 338 K. By pre-treating the mordenite crystals in 3M HNO_3, thereby boosting the Si/Al ratio to 25, followed by alkaline treatment in 0.2 M NaOH a mesoporous mordenite was obtained (A_{ext} 174 $m^2 \cdot g^{-1}$, V_{micro} 0.15 $cm^3 \cdot g^{-1}$). Tsai et al. [60] (2009) showed that alkaline treatment of mordenite (Si/Al ratio of 6.8) in 0.1 M NaOH for 30 min at 333 K did not result in an increased external surface area although mesopores were formed. The alkaline treatment did result in improved catalytic activity and stability. Paixão et al. [61] (2010) showed that alkaline treatment can be used on aluminum rich mordenite (Si/Al ratio 10), thereby creating mesopores and increasing the external surface area of the mordenite to 133 $m^2 \cdot g^{-1}$, without changing the acidity of the zeolite.

1.4 Scope and outline of the thesis

The main goal of the work described in this thesis is to obtain (meso-) porous zeolites by alkaline treatment for improved catalytic performance, with a focus on mordenite and cumene synthesis. Most zeolite samples used in this thesis are commercially available or can be synthesized with the recipe provided. The zeolite samples consist of small

crystallites in the range between 20 and 200 nm that have agglomerated into larger particles of ~0.5 to 2.0 μm.

In chapter 2 aluminum rich zeolites with Si/Al ratio between 5 and 10 are treated in 1 M NaOH at 343 K. At these conditions both silicon and aluminum are extracted from the mordenite, resulting in the formation of inter- and intra-crystalline mesopores. It is shown that the compensating cation, besides the Si/Al ratio, is an important factor for mesoporosity development. Catalytic tests for the production of cumene show enhanced activity for alkaline treated mordenite with similar selectivity.

Acid and alkaline treatments as well as combinations thereof are discussed in chapter 3. It is shown that the combination of acid and alkaline treatment results in porous mordenite. Electron tomography reveals that mostly intra-crystalline mesopores are formed that are in contact with the external surface. Catalytic tests for the production of cumene shows that the activities of these porous mordenites are close to the activity of a commercial catalyst based on zeolite Beta, with reduced selectivity towards the formation of undesirable n-propylbenzene.

In chapter 4 alkaline treatment on various template containing zeolites (mordenite, ZSM-5, ZSM-12 and zeolite Beta) is studied. Treatment in 1 M NaOH at 343 K resulted in purely intercrystalline mesopores and increased external surface areas, independent of the Si/Al ratio. The added porosity was obtained without changing the Brønsted acid sites because of the protection of the template molecules. This enables us to decouple acidity and accessibility of zeolites.

Chapter 5 presents the key findings and concluding remarks

References

1. Cronstedt, A.F.; *Akad. Handl. Stockholm*, **1756** 120
2. How, H.; *J. Chem. Soc.*, **1964** 100
3. Bearlocher, C.; McCusker, L.B.; Olsen, D.H.; *Atlas of zeolite framework types*. 6th ed, (Bearlocher, C.; McCusker, L.B.; Olsen, D.H., Eds). Amsterdam. Elsevier. **2007**
4. http://www.iza-structure.org
5. Van Bekkum, H.; Flanigen, E.M.; Jacobs, P.A.; *Introduction to zeolite sciences and practice*. Elsevier. **1991**
6. Weisz, P.B.; Frilette, V.J.; Maatman, R.W.; Mower, E.B.; *J. Catal.*, **1962** 307
7. Ruthven, D.M.; Post, M.F.M.; *Diffusion in zeolite molecular sieves*, in *Introduction to zeolite science and practice* (van Bekkum, H.; Flanigen, E.M.; Jacobs, P.A.; Jansen, J.C., Eds), Elsevier: Amsterdam. **2001** 525-577.
8. Davis, M.E.; Saldarriaga, C.; Montes, C.; Garces, J.; Crowdert, C.; *Nature*, **1988** 698-699
9. Estermann, M.; McCusker, L.B.; Baerlocher, C.; Merrouche, A.; Kessler, H.; *Nature*,

1991 (352) 320-323
10. Corma, A.; Díaz-Cabaña, M.J.; Martínez-Triguero, J.; Nicolopoulus, S.; Boulahya, K.; *Chem. Commun.*, **2004** 1356 - 1357
11. Plank, C.J.; Rosinski, E.J.; Hawthorne, W.P.; *Ind. Eng. Chem. Prod. Res. Dev.*, **1964** 165-169
12. Degnan, T.F.; Chitnis, G.K.; Schipper, P.H.; *Microporous Mesoporous Mater.*, **2000** (35-36) 245-252
13. Stöcker, M.; *Microporous Mesoporous Mater.*, **1999** (29) 3-48
14. Perego, C.; Ingallina, P.; *Catal Today*, **2002** (73) 3-22
15. Tanabe, K.; Hölderich, W.F.; *Appl. Catal., A* **1999** (181) 399-434
16. Cook, B.R.; Johnson, J.W.; G. Cao, G.; McEvoy, R.A., **2000**
17. Meyer, W.M.; *Z. Kristallogr.*, **1961** (115) 439-450
18. Raatz, F.; Marcilly, C.; Freund, E.; *Zeolites*, **1985** (5) 329-333
19. van Donk, S.; Broersma, A.; Gijzeman, O.L.J.; Van Bokhoven, J.A.; Bitter, J.H.; de Jong, K.P.; *J. Catal.*, **2001** (204) 272-280
20. Rudolf, P.R.; Garces, J.M.; *Zeolites*, **1994** (14) 137-146
21. Tosheva, L.; Valtchev, V.P.; *Chem. Mater.* , **2005** (17) 2494-2513
22. Chung, K.-H.; *Microporous Mesoporous Mater.*, **2008** (111) 544-550
23. van Donk, S.; Bitter, J.H.; Verberckmoes, A.; Versluijs-Helder, M.; Broersma, A.; de Jong, K.P.; *Angew. Chem. Int. Ed.* , **2005** (44) 1360-1363
24. Janssen, A.H.; Koster, A.J.; de Jong, K.P.; *Angew. Chem. Int. Ed.*, **2001** (40) 1102-1104
25. van Donk, S.; Janssen, A.H.; Bitter, J.H.; de Jong, K.P.; *Catal. Rev. Sci. Eng.* , **2003** (45) 297 - 319
26. Corma, A.; *Chem. Rev.* , **1997** (97) 2373-2420
27. Janssen, A.H.; Koster, A.J.; de Jong, K.P.; *J. Phys. Chem. B*, **2002** (106) 11905-11909
28. Lee, G.S.J.; Garces, J.M.; Meima, G.R.; Van Der Aalst, M.J.M., The Dow Chemical Company,US Patent 5 198 595, **1993**
29. Olken, M.M.; Garces, J.M. *Proceedings of the 9th International Zeolite Conference*. 1992. Montreal: Butterworth-Heinemann.559-566
30. Garcés, J.M.; Olken, M.M.; Lee, G.J.; Meima, G.R.; Jacobs, P.A.; Martens, J.A.; *Top. Catal.*, **2009** (52) 1175-1181
31. Viswanadham, N.; Kumar, M.; *Microporous Mesoporous Mater.*, **2006** (92) 31-37
32. Debras, G.; Gourgue, A.; B.Nagy, J.; Clippeleir, G.D.; *Zeolites*, **1986** (6) 241-248
33. Lee, G.S.; Maj, J.J.; Rocke, S.C.; Garcés, J.M.; *Catal. Lett.* , **1989** (2) 243-247
34. Fernandes, L.D.; Bartl, P.E.; Monteiro, J.F.; da Silva, J.G.; de Menezes, S.C.; Cardoso, M.J.B.; *Zeolites*, **1994** (14) 533-540
35. Hong, Y.; Fripiat, J.J.; *Microporous Mater.*, **1995** (4) 323-334
36. Maache, M.; Janin, A.; Lavalley, J.C.; Benazzi, E.; *Zeolites*, **1995** (15) 507-516
37. O'Donovan, A.W.; O'Connor, C.T.; Koch, K.R.; *Microporous Mater.*, **1995** (5) 185-202
38. Dutartre, R.; de Menorval, L.C.; Di Renzo, F.; McQueen, D.; Fajula, F.; Schulz, P.; *Microporous Mater.*, **1996** (6) 311-320
39. Moreno, S.; Poncelet, G.; *Microporous Mater.*, **1997** (12) 197-222
40. Giudici, R.; Kouwenhoven, H.W.; Prins, R.; *Appl. Catal., A*, **2000** (203) 101-110
41. Boveri, M.; Marquez-Alvarez, C.; Laborde, M.A.; Sastre, E.; *Catal. Today*, **2006** (114) 217-225
42. Zhang, L.; van Laak, A.N.C.; de Jongh, P.E.; de Jong, K.P.; *Zeolites and Catalysis: Synthesis, Reactions and Applications*, (Cejka, J.; Corma, A.; Zones, S., Eds). Weinheim. Wiley-VHC. **2010** 237-282
43. Young, D.A., Union Oil. Co.,US Patent 3 326 797, **1967**

44. Young, D.A., Union Oil. Co.,US Patent 3 374 182, **1968**
45. Rosback, D.H.; Neuzil, R.W., UOP Inc.,US Patent 4 048 111, **1977**
46. Rein, A.J.; Saperstein, D.D.; Pines, S.H., Merck & Co.,US Patent 4 134 965, **1979**
47. Kokotailo, G.T.; Rohrman, A.C., Mobil Oil Corp.,US Patent 4 703 025, **1987**
48. Ogura, M.; Shinomiya, S.; Tateno, J.; Nara, Y.; Kikuchi, E.; Matsukata, M.; *Chem. Lett.* , **2000** (29) 882
49. Ogura, M.; Shinomiya, S.; Tateno, J.; Nara, Y.; Nomura, M.; Kikuchi, E.; Matsukata, M.; *Appl. Catal., A*, **2001** (219) 33-43
50. Groen, J.C.; Jansen, J.C.; Moulijn, J.A.; Perez-Ramirez, J.; *J. Phys. Chem. B*, **2004** (108) 13062-13065
51. Groen, J.C.; Peffer, L.A.A.; Moulijn, J.A.; Pérez-Ramírez, J.; *Colloids Surf., A,* **2004** (241) 53-58
52. Groen, J.C.; Peffer, L.A.A.; Moulijn, J.A.; Pérez-Ramírez, J.; *Microporous Mesoporous Mater.*, **2004** (69) 29-34
53. Perez-Ramirez, J.; Christensen, C.H.; Egeblad, K.; Christensen, C.H.; Groen, J.C.; *Chem. Soc. Rev.*, **2008** (37) 2530-2542
54. Groen, J.C.; Abelló, S.; Villaescusa, L.A.; Pérez-Ramírez, J.; *Microporous Mesoporous Mater.*, **2008** (114) 93-102
55. Wei, X.; Smirniotis, P.G.; *Microporous Mesoporous Mater.* , **2006** (97) 97-106
56. Bonilla, A.; Baudouin, D.; Pérez-Ramírez, J.; *J. Catal*, **2009** (265) 170-180
57. Verboekend, D.; Villaescusa, L.A.; Thomas, K.; Stan, I.; Pérez-Ramírez, J.; *Catal Today*, **2010** (152) 11-16
58. Groen, J.C.; Sano, T.; Moulijn, J.A.; Pérez-Ramírez, J.; *J. Catal.*, **2007** (251) 21-27
59. Li, X.; Prins, R.; van Bokhoven, J.A.; *J. Catal.*, **2009** (262) 257-265
60. Tsai, S.T.; Chen, C.H.; Tsai, T.C.; *Green Chem.*, **2009** (11) 1349-1356
61. Paixao, V.; Carvalho, A.P.; Rocha, J.; Fernandes, A.; Martins, A.; *Microporous Mesoporous Mater.*, **2010** (131) 350-357

2

Alkaline Treatment on Commercially Available Aluminum Rich Mordenite

Abstract

Several commercially available samples consisting of agglomerated small mordenite crystallites with low Si/Al ratios (5.7-10 at/at) have been treated in aqueous NaOH solution. It was found that the porosity can be enhanced when the sodium hydroxide solution is sufficiently concentrated. Treatment in 1 M NaOH for 15 minutes resulted in inter-crystalline porosity and the mesopore volume was increased from 0.01 to 0.21 $cm^3 \cdot g^{-1}$ together with an increased external surface area from 36 to 85 $m^2 \cdot g^{-1}$. The micropore volume and crystallinity were preserved after the treatment. Both H-MOR and Na-MOR mordenite agglomerates have been successfully treated: the Na-MOR requires a longer contact time to obtain similar porosity. By carefully choosing the alkaline concentration and contact time, intra-crystalline mesoporosity can be obtained for mordenite with Si/Al ratios as low as 10. Catalytic tests with proton mordenite showed that alkaline treatment leads to more than one order of magnitude of activity gain in the liquid-phase alkylation of benzene with propene to form cumene, while selectivity is preserved. These results demonstrate that alkaline treatment also on high-aluminum content mordenites is an effective tool to enhance accessibility and thereby its catalytic performance.

1 Introduction

Zeolites are microporous crystalline materials that present an important class of catalysts because of their specific properties such as high Brønsted acidity, thermal stability, facile regeneration and shape selectivity [1]. There are over 191 different types of zeolite framework structures [2], but only a limited number is used in industrial applications. Mordenite, with an ideal composition of $Na_8Al_8Si_{40}O_{96}{\cdot}nH_2O$, is one of the industrially important zeolites and has been used for hydroisomerization, alkylation and dewaxing processes [3-5]. The micropore system of mordenite consists of two pore channels: an elliptical 12 membered ring (MR) channel (6.7 Å × 7.0 Å) which runs parallel to the c-axis, and an 8 MR side pocket (3.4 Å × 4.8 Å) [6] that runs in the b-axis direction. Mordenite is considered a one-dimensional zeolite due to inaccessibility of the 8 MR side pocket for all but the smallest molecules [7].

The shape selectivity is a result of the micropores that are of similar size as the reacting molecules and the intended products. As the catalytic sites are located within these micropores, the formation of high molecular weight side products is suppressed resulting in high selectivity. The drawback of this size similarity is slow intra-crystalline diffusion, due to strong interaction of the molecules with the micropore walls [8]. A second disadvantage of the micropore structure, especially with one-dimensional zeolites such as mordenite, is that they are prone to pore blocking [9]. A reduction of the diffusion path length, however, may alleviate these problems and increase the activity and stability. A first approach is the reduction of the crystal size by altering the synthesis routes [10, 11]. This has been proven successful over the years for numerous zeolites. Mordenite is challenging in this respect because the range of synthesis conditions are very narrow. Industrial zeolite producers such as Zeolyst and Tosoh have been able to synthesize small crystallites ~100 nm but those are most often agglomerated into larger particles of 1-5 μm.

A second approach to decrease the diffusion path length is by introducing mesoporosity [12, 13]. This can be realized during synthesis or by using post-synthesis treatments such as steaming and acid leaching [7, 14-19]. For the last two methods the introduction of mesoporosity is closely linked with the Si/Al ratio of the zeolite. As a high silicon to aluminum ratio often also has a positive effect on the catalytic performance of zeolites these methods have been thoroughly investigated in the past decades. One of the industrial applications of acid treatment was described by Dow [20, 21]. They reported that by deep dealumination they obtained mordenite that provided shape selective, active

and stable catalysis of the trans-alkylation of mononuclear aromatics. This was the first zeolite to be commercialized in a cumene synthesis process, as an add-on trans-alkylation process.

Another post-synthesis treatment to introduce mesopores involves alkaline solutions and was studied in the late 1960s and 1970s [22-26] and has recently seen a revival. This method is referred to as desilication, base leaching or alkaline treatment [27-31]. In a typical experiment the zeolite is treated with a low concentration of NaOH in water at 333 to 353 K for a short time. During contact with the solution, silicon is extracted from the framework resulting in mesoporous zeolites. Results have been published for various zeolites such as MFI [29, 31, 32], BEA [33] and MOR [22, 23, 34, 35]. There are however some general requirements reported for successful alkaline treatment. Firstly, the zeolite must have preferably a Si/Al ratio (at/at) between 25 and 50 [36]. At lower values there is a limited effect of alkaline treatment due to the relatively high aluminum content, while at higher values the structural integrity of the zeolite crystal is lost. Secondly for mordenite only large zeolite crystals, in the micrometers range, have been successfully treated using this method. Groen et al. [34] reported the generation of intra-crystalline mesoporosity for mordenite crystals of 4 and 12 μm in diameter having Si/Al ratios of 20 and 30, respectively. A commercially available mordenite, Zeolyst CBV 20A, was found to be hardly susceptible for desilication. Van Bokhoven and co-workers [35] reported no mesoporosity for a 13 μm crystal with Si/Al ratio of 15 at/at upon desilication. Mesoporosity was obtained after boosting the Si/Al ratio of the parent mordenite with acid to 25 at/at .

In this study we use commercially available mordenites, which most often have low Si/Al ratios and consist of small crystallites that are assembled in agglomerates. The effect of alkaline treatment to improve the porosity of these systems and their catalytic properties for the production of cumene from propene and benzene will be discussed.

2 Experimental

2.1 Sample preparation

Three samples of mordenite were supplied by BP Amoco, BASF and Zeolyst named LZM-5, BASF and CBV 21A with Si/Al ratios of 5.7, 8.5 and 10, respectively. LZM-5 and BASF mordenite were provided in sodium form, Zeolyst CBV 21A was provided in ammonia form.

As received LZM-5 mordenite, referred to as Na-MOR-parent, was ion-exchanged under stirring in an aqueous 1 M ammonium nitrate solution at 353 K for 24 hours, followed by filtering and washing. Per gram of mordenite 12 ml of ammonia nitrate solution was used [7]. This procedure was repeated twice to ensure complete removal of sodium ions. The sample was then converted from the ammonia form to the proton form by calcination at 723 K for 3 hours at a heating rate of 1 $K \cdot min^{-1}$; the obtained sample will be referred to as H-MOR-parent.

Two gram of H-MOR-parent was stirred in pre-heated 100 ml sodium hydroxide solution (0.2, 0.5 or 1.0 M) at 343 K for 15 or 30 minutes. The solid sample was subsequently filtered and washed with demineralised water until the pH of the filtrate was neutral. After drying at 333 K the resulting solid was named H-MOR-at-[NaOH]-time. One sample, H-MOR-at-1.0-15, was re-ion-exchanged/calcined into the H-MOR as described above and will be referred to as H-MOR-at. Na-MOR-parent was likewise treated with NaOH solutions and referred to as Na-MOR-at-[NaOH]-time. The following sample code H-MOR-at-1.0-15 than translates into: alkaline treatment on the parent H-MOR for 15 minutes in 1 M NaOH that has sodium as a compensating cation.

As received BASF and Zeolyst CBV 21A mordenite were referred to as BASF-parent and CBV 21A-parent. After alkaline treatment of the parent an identical naming scheme was used as described above.

2.2 Structural characterization

Powder X-ray diffraction (XRD) patterns were obtained using a Bruker-Axs D8 series 2 with a $Co_{\alpha 1,2}$ source (λ = 0.179 nm). The porosity of the samples was studied using N_2-physisorption isotherms, which were recorded with a Micromeritics Tristar 3000 at 77 K. Prior to the physisorption measurements, the mordenite samples were dried overnight at 573 K in flowing nitrogen. The t-plot method [37] was applied to obtain the micro pore volume and external surface area. Pore size distributions were obtained from the adsorption branch using the BJH-method [38]. The mesopore volume was calculated by integrating these plots from 2 to 50 nm. Ammonia temperature programmed desorption (TPD) was performed with a Micromeritics Autochem II. About ~130 mg of sample was dried at 573 K with a heating ramp of 5 $K \cdot s^{-1}$ and kept there for 30 minutes after which the sample was cooled down to 473 K. After saturating the sample with ammonia a 30 minutes dwell time was applied to obtain a stabile baseline. Subsequently the temperature was increased to 923K with a heating rate of 10 $K \cdot s^{-1}$ and was kept there for 30 minutes. Morphology and crystal sizes were determined with a Tecnai FEI XL 30SFEG

Scanning Electron Microscope (SEM) at 15 kV and with a Tecnai 20 Transmission Electron Microscope operated at 200 kV. Electron tomography (ET) grids, to which 10 nm gold fiducial markers were added to aid alignment on a polymer coated copper grid. Mordenite samples were suspended in ethanol and dispersed for 30 minutes in an ultrasonic bath and deposited on the TEM grids using a thin film. ET was performed in bright field TEM by acquiring tilt angles from -67º to +67º. Reconstruction of the tomogram was performed in IMOD [39].

^{27}Al MAS NMR experiments were performed at room temperature on a 500 MHz Varian Inova Spectrometer using a 4 mm probe. In the experiments, a single pulse of 1 μs, a relaxation delay of 2 s, and a spinning rate of ca. 13 kHz were used. The ^{27}Al chemical shift was referenced to 1M $Al(NO_3)_3$ in H_2O.

2.3 Adsorption and catalytic measurements

Cumene uptake was measured with a tapered element oscillating microbalance (TEOM) (Rupprecht & Pataschnick TEOM 1500 PMA). Prior to the measurements the catalyst was pelletized at a pressure of 1 ton/cm^2 for 25 seconds and subsequent crushed and sieved, resulting in particles between 150 and 425 μm. Approximately 50 mg of catalyst powder was then transferred into a 100 ml sample container of the TEOM and held in place between two layers of quartz wool. The sample was dried for 4 hours at 623 K in nitrogen flow (grade 5.0). Cumene (Acros 99.9% pure) uptake was measured with using nitrogen as a carrier gas at a total pressure of 1.3 bar at 623 K. Liquid cumene was injected into the system using an ISCO 260D syringe pump with 3 ml min^{-1} and was evaporated in flowing nitrogen resulting in a cumene partial pressure of 9 mbar. For a detailed description of the TEOM we refer to Chen et al [40] and Zhu et al. [41].

The catalytic tests were carried out in a stirred autoclave at 400 rpm. Benzene and propylene were tapped from industrial streams (99% plus) supplied by Dow Terneuzen, The Netherlands. For the alkylation approximately 1 g of catalyst powder (sieve fraction 425-800 μm) and 270 g of benzene were loaded into a nitrogen purged 1 l autoclave. After raising the temperature to 423 K approximately 38 g of propylene was fed to the reactor resulting in a benzene to propylene molar ratio ~4. The reactor was then pressurized to ~40 bar by feeding nitrogen. During reaction samples were withdrawn from the reactor and analyzed by GC. Similar experiments have been described by Bellussi et al [42].

3 Results and discussion

Figure 1 presents SEM images of LZM-5, BASF and Zeolyst CBV 21A mordenite samples. All three samples consist of sub-micron sized crystals that have agglomerated into larger particles. LZM-5 mordenite was chosen as a model system to study mesopore development upon alkaline treatment because of its overall uniform morphology. LZM-5 consists of coffin-shaped crystallites with typical dimensions of ~100 nm × 40 nm and a Si/Al atomic ratio of 5.7. These crystallites are mostly organized in a parallel fashion into particles of about 0.5-2 μm.

3.1 H-MOR-parent (LZM-5)

The H-MOR-parent sample was treated in 0.2 M sodium hydroxide for 30 minutes, similar to what is described in earlier studies for introducing mesopores in large mordenite crystals [34]. This treatment did not result in significant changes in the porosity of the mordenite most likely due to the Si/Al ratio which is well below the Si/Al ratio of 25-50 that is reported to be necessary to introduce mesoporosity [36, 43]. Increasing the sodium hydroxide solution to 0.5 M resulted in a slight increase in mesoporosity as illustrated with N_2-physisorption (Fig. 2). Surprisingly, a NaOH concentration of 1.0 M brought about a sharp increase in adsorption at high relative pressures, indicating the formation of large mesopores and small macropores (Figure 3). Simultaneously, a substantial part of micropore volume was lost, indicating that the applied conditions resulted in the degradation of the framework. However, when the experiment in 1 M NaOH was repeated with a contact time of only 15 minutes (to obtain the H-MOR-at-1.0-15 sample), a similar increase in mesoporosity was observed, while the micropore volume was preserved (Fig. 3). Table 1 summarizes the N_2-physisorption results for the different samples. In general the external surface area and total pore-volume both increase with increasing alkaline concentration and contact times, with the exception of the H-MOR-at-1.0-30 sample. In picture 3B the pore size distribution is shown for the H-MOR-at-1.0-15

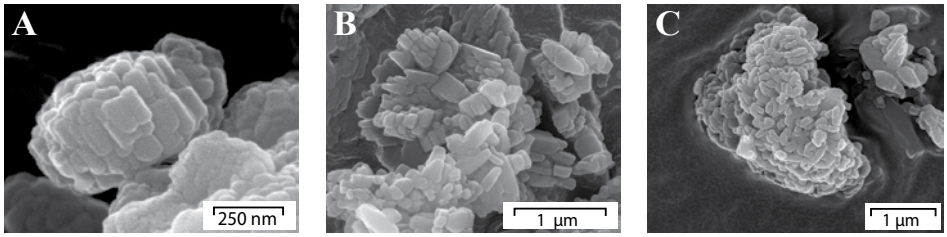

Fig. 1. SEM image of (A)LZM-5, (B) BASF and (C) Zeolyst CBV 21A.

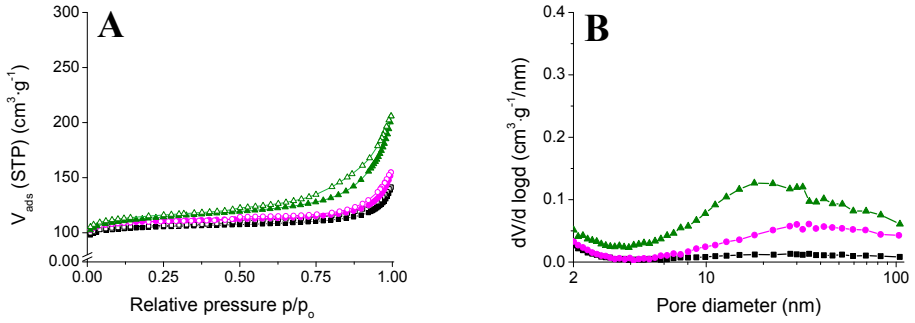

Fig. 2. (A) N_2 adsorption (solid symbols) and desorption (open symbols) isotherm; and (B) BJH pore- size distribution: (■) H-MOR-parent, (●) H-MOR-at-0.2-30 and (▲) H-MOR-at-0.5-30.

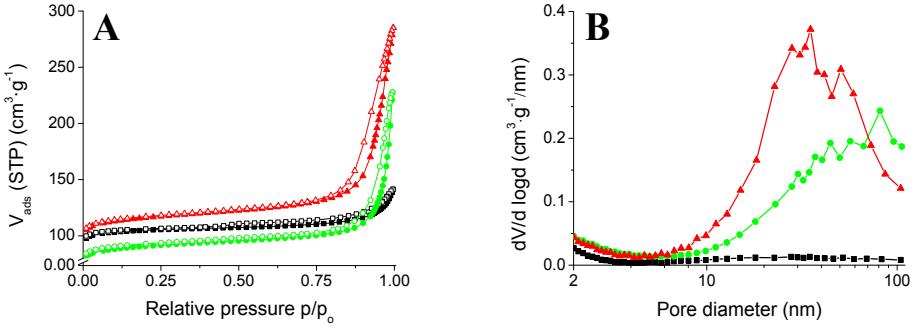

Fig. 3. (A) N_2 adsorption (solid symbols) and desorption (open symbols) isotherm; and (B) BJH poresize distribution: (■) H-MOR-parent, (●) H-MOR-at-1.0-30 and (▲) H-MOR-at-1.0-15.

Table 1. Textural properties of parent and alkaline treated LZM-5 H-mordenite.

Sample	V_{micro} [a] ($cm^3 \times g^{-1}$)	A_{ext} [a] ($m^2 \times g^{-1}$)	V_{meso} [b] ($cm^3 \times g^{-1}$)	V_{total} [c] ($cm^3 \times g^{-1}$)	Si/Al [d] (at/at)	Cumene uptake (wt.%)
Na-MOR-Parent	0.15	35	0.02	0.21	5.5	
H-MOR-Parent	0.17	36	0.01	0.20	5.5	4.1
H-MOR-at-0.2-30	0.15	35	0.04	0.24	-	
H-MOR-at-0.5-30	0.15	55	0.11	0.30	-	
H-MOR-at-1.0-30	0.12	54	0.09	0.35	-	
H-MOR-at-1.0-15	0.15	67	0.16	0.44	5.0	
filtrate					*6.1*	
H-MOR-at	0.17	85	0.21	0.53	5.0	3.6

[a] t-plot method
[b] BJH-method (adsorption branch)
[c] @ $p/p_o = 0.995$
[d] ICP-AES

sample and an average pore size of 35 nm was observed. These pores are too large to be intra-crystalline mesopores, as the crystallites have a dimension of 40nm × 100 nm. The resulting mesopores are therefore most probably inter-crystalline. Si/Al ratios were determined for the H-MOR-at-1.0-15 and showed a decrease from 5.7 to 5.0 at/at. This suggests that upon alkaline treatment predominantly silicon was dissolved. The Si/Al ratio in the filtrate after alkaline solution was 6.1, showing that during this treatment both silicon and aluminum are being dissolved and in rather large amounts. For this particular sample the dry weights before and after the alkaline experiment was determined, which indicated that 35-40 % of the mordenite was dissolved. Similar experiments were performed by Cundy et al. [44, 45], who showed that large 1 μm sized ZSM-5 crystals can also be subjected to controllable dissolution.

The H-MOR-at-1.0-15 sample was chosen for further studies. It was exchanged with ammonium nitrate to remove sodium ions followed by calcination to obtain the proton form that is referred to as H-MOR-at. When H-MOR-parent and H-MOR-at are compared we observed that the micropore volume as determined with N_2 is similar for both samples. The uptake of benzene however, is ~15% lower for the H-MOR-at indicating that as a result of alkaline treatment some micropores have become partially blocked. This could be due to the precipitation of amorphous species during alkaline treatment or due to the formation of extra framework aluminum upon calcination. From ^{27}Al MAS NMR (Fig. 9) we did not observe a significant change in framework to extra-framework aluminum species upon calcination, which indicates that the former reason is most likely the cause of the partial blockade. Figure 4 depicts the XRD patterns of both samples, showing that there is no significant change in crystallinity after alkaline treatment. If the crystallinity is calculated according to O' Donovan et al. [46] the crystallinity is 100 and 102 % for H-MOR-parent and H-MOR-at respectively. Ammonia TPD (Fig. 4A)

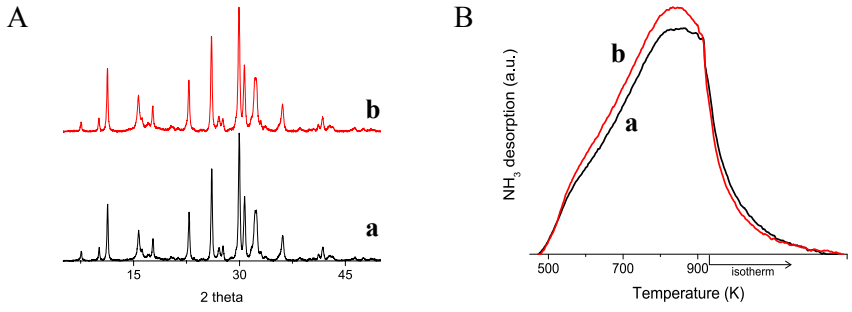

Fig. 4. (A) XRD patterns and (B) NH_3-TPD curves of LZM-5 mordnite: H-MOR-parent (a) and H-MOR-at (b).

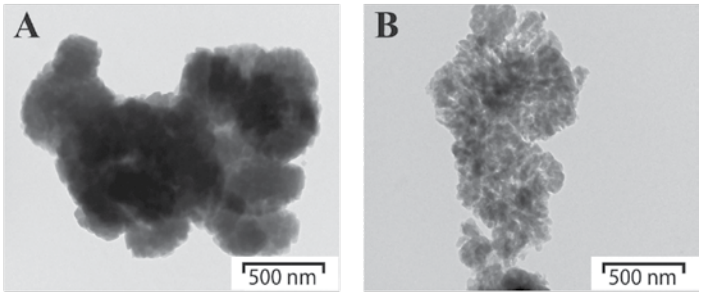

Fig. 5. TEM images of LZM-5 mordenite: (A) H-MOR-parent and (B) H-MOR-at.

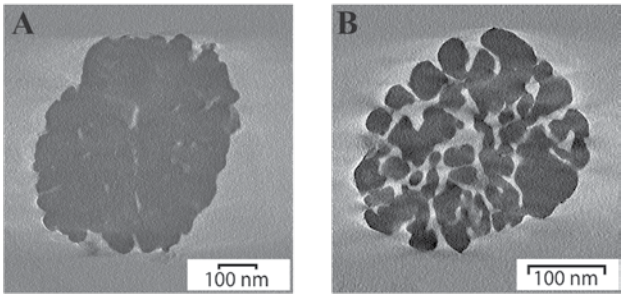

Fig. 6. Reconstructed thin slices obtained from electron tomography of LZM-5 mordenite (A) H-MOR-parent and (B) H-MOR-at.

measurements show that H-MOR-parent and H-MOR-at have a similar desorption curve, indication that the alkaline treatment did not affect acidity. The H-MOR-at has only slightly more (~8%) acid sites when compared to H-MOR-parent, which is close in agreement with the decrease in Si/Al ratio as determined with ICP (15%). Figure 5 shows TEM images of the H-MOR-parent sample and the H-MOR-at sample. After alkaline treatment the density of the agglomerates has decreased significantly and individual crystallites can be observed throughout the whole sample, while the parent sample is much more compact. To study the changes in porosity in more detail we applied electron tomography. Figures 6A and 6B are thin slices obtained from the center of the reconstructed tomograms. For the H-MOR-parent this illustrates the tight packing of crystallites, leading to dense particles. Between the crystallites small cavities are visible that are most probably inkbottle type mesopores originating from imperfect stacking. However, for the treated sample a very open structure is observed. An average mesopore size of about 30 nm is observed from tomography, thereby supporting the results obtained with N_2 physisorption.

3.2 Na-MOR-parent (LZM-5)

Direct alkaline treatment on the Na-MOR-parent would be very attractive, because in this case the additional exchange and calcination to obtain H-MOR could be avoided. Identical conditions were applied on the Na-MOR-parent as on the H-MOR-parent, i.e., 1 M NaOH solution. However, less mesoporosity was introduced than for the H-MOR-parent. A series of measurements was performed to investigate the mesoporosity development in time (Table 2). After 15 minutes of alkaline treatment the mesopores are still very small and with SEM (Fig. 7A) a similar morphology is observed, although it appears that the crystallites have become more round compared to the parent (Fig. 1A). After 45 minutes of treatment the small mesopores have expanded into large mesopores and small macropore that result in open particles that are close to falling apart

Table 2. Textural properties of parent and alkaline treated LZM-5 Na-mordenite.

Sample	V_{micro} [a] ($cm^3 \times g^{-1}$)	A_{ext} [a] ($m^2 \times g^{-1}$)	V_{meso} [b] ($cm^3 \times g^{-1}$)	V_{total} [c] ($cm^3 \times g^{-1}$)	Si/Al [d] (at/at)	Na/Al [d] (at/at)
Na-MOR-Parent	0.15	35	0.03	0.18	5.5	0.96
Na-MOR-at-1.0-5	0.15	45	0.08	0.26		
Na-MOR-at-1.0-10	0.15	48	0.08	0.28		
Na-MOR-at -1.0-15	0.16	52	0.11	0.27	5.3	0.90
Na-MOR-at -1.0-23	0.15	65	0.14	0.37		
Na-MOR-at -1.0-30	0.15	79	0.17	0.49	5.3	0.88
Na-MOR-at -1.0-45	0.15	82	0.18	0.50		
Na-MOR-at -1.0-60	0.13	101	0.13	0.53		
Na-MOR-at -1.0-90	0.14	84	0.12	0.66		
Na-MOR-at -1.0-120	0.13	99	0.14	0.53	4.9	0.66

[a] t-plot method
[b] BJH-method (adsorption branch)
[c] @ $p/p_o = 0.995$
[d] ICP-AES

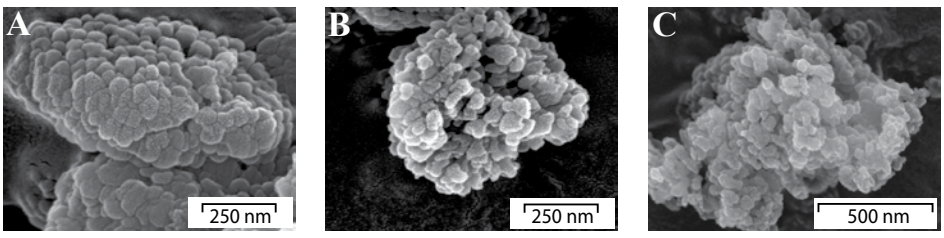

Fig. 7. SEM images of LZM-5 mordenite: (A) Na-MOR-at-1.0-15; (B) Na-MOR-at-1.0-45 and (C) Na-MOR-at-1.0-120.

(Fig. 7B). After 120 minutes of treatments the particles are no longer observed (Fig. 7C), and a uniform structure with large macropores is observed.

We observed a slight decrease in Si/Al ratios upon alkaline treatment (Table 2, right column), and after 120 minutes the Si/Al ratio was lower than 5, suggesting the presence of extra-framework aluminum. Simultaneously we observe a decrease in Na/Al ratio that is combined with a decreasing micropore volume. This leads to the conclusion that some extra-framework aluminum has exchanged with sodium or is being deposited on the outer surface. Both might lead to blocking of the micropores.

From the N_2-physisorption data we can conclude that Na-MOR-at-1.0-30 is very similar to the H-MOR-at-1.0-15 (Fig. 8A) in terms of porosity. Hence sodium mordenite can be used as a starting material for alkaline treatment, but requires a longer treatment time due to higher stability. An additional advantage is that longer treatment times provide more control, which might be necessary for large scale treatment. A possible explanation for the higher stability of sodium mordenite towards alkaline treatment can be the result of its larger cations, effectively shielding the framework of the mordenite from the alkaline treatment. A second possibility is that although the bulk Si/Al ratios are similar some extra-framework aluminum was formed in H-MOR upon calcination [47, 48] leading to structural defects and thus higher susceptibility towards alkaline treatment. In Figure 8B, ^{27}Al MAS NMR is shown for the Na-MOR-Parent. Only one peak is visible at 54 ppm chemical shift, which represents tetrahedrally coordinated aluminum [49], and can be ascribed to framework aluminum. In the H-MOR-Parent (Fig. 8B, b) three types of Al coordinations were observed; tetrahedrally (peak at 54 ppm) coordinated aluminum (Al^{IV}), octahedrally (peak at -1 ppm) coordinated aluminum (Al^{VI}) and a shoulder at 41 ppm which is suggested to represent penta-coordinated aluminum [50]

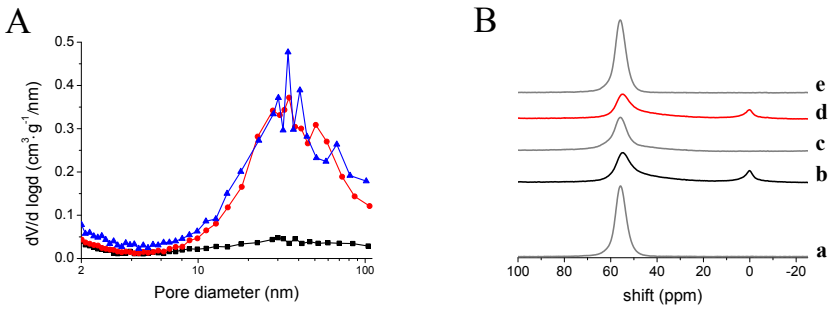

Fig. 8. (A) BJH pore size distribution derived from adsorption branch of LZM-5 mordenite: (■) Na-MOR-parent; (●) H-MOR-at-1.0-15 and (▲) Na-MOR-at-1.0-30 and (B) ^{27}Al MAS NMR spectra of LZM-5 samples: (a) Na-MOR-parent; (b) H-MOR-parent; (c) H-MOR-at-1.0-15, (d) H-MOR-at and (e) Na-MOR-at-1.0-15.

(Al^{V}). The Al^{VI} is probably extra-framework, which could explain a higher susceptibility towards alkaline treatment. After alkaline treatment (Fig. 8B, c) Al^{VI} is no longer observed and the intensity of the shoulder at 41 ppm is greatly diminished. The absence of Al^{VI} suggests that the extra-framework aluminum species are dissolved or re-inserted into the lattice [51, 52]. After ion exchange and consecutive calcination Al^{VI} is present (Fig. 8B, d) in similar Al^{IV}/Al^{VI} ratio as for H-MOR-Parent. No changes in the aluminum coordination were observed with ^{27}Al MAS NMR upon direct alkaline treatment on Na-MOR-Parent (Fig. 8B, e).

3.3 BASF and Zeolyst CBV 21A mordenites

The acquired insight for alkaline treatment on Na LZM-5 (Si/Al ratio 5.5 at/at) was applied to two other commercial mordenite samples from BASF (Si/Al ratio 7.5 at/at) and Zeolyst (Si/Al ratio 10 at/at). BASF-parent mordenite (sodium form) was treated similar as the parent sodium LZM-5 sample, although the contact time was slightly shorter (15 minutes), in view of the higher Si/Al ratio of the BASF mordenite. This resulted in an increased external surface area from 36 to 80 $m^2 \cdot g^{-1}$, enhanced porosity and the preservation of the micropore volume (Table 3), similar to what was observed for the LZM-5 mordenite. The pore size distribution (Fig. 9) after alkaline treatment shows that a large variety of pores are present, both smaller and larger compared the LZM-5 mordenite. This is most likely a direct influence of the morphology of the material which, compared to the LZM-5 sample, is more diverse in terms of particle and crystallite size. For the NH_4-Zeolyst CBV 21A material an even shorter contact time of 10 minutes was applied, because the starting Si/Al ratio of 10 is considerable higher than for LZM-5 mordenite, resulting in a faster desilication process. Upon alkaline treatment

Table 3. Textural properties of BASF (Na-MOR) and Zeolyst CBV 21A (NH_4-MOR).

Sample	V_{micro} [a] ($cm^3 \times g^{-1}$)	A_{ext} [a] ($m^2 \times g^{-1}$)	V_{meso} [b] ($cm^3 \times g^{-1}$)	V_{total} [c] ($cm^3 \times g^{-1}$)	Si/Al [d] (at/at)
BASF-parent	0.17	36	0.03	0.26	8.5
BASF-at-1.0-15	0.17	80	0.09	0.36	-
CBV-21A-parent	0.17	45	0.04	0.25	10
CBV-21A-at-1.0-10	0.17	88	0.03	0.37	-
CBV-21A-at-0.5-20	0.16	106	0.10	0.36	-

[a] t-plot method
[b] BJH-method (adsorption branch)
[c] @ $p/p_o = 0.995$
[d] ICP-AES

we observed an increase in external surface area (45-88 $m^2 g^{-1}$), while the micropore volume was preserved. Additionally an average pore size of 100 nm was observed, thus resulting in a low mesopore volume (Table 3). From these results it can be concluded that at these conditions fast dissolution of the sample occurs. To slow down this process a 20 minutes experiment with 0.5 M NaOH was performed. This resulted in an external surface area of 106 $m^2 \cdot g^{-1}$ and a mesopore volume of 0.10 $cm^3 \cdot g^{-1}$ (Table 3). When these

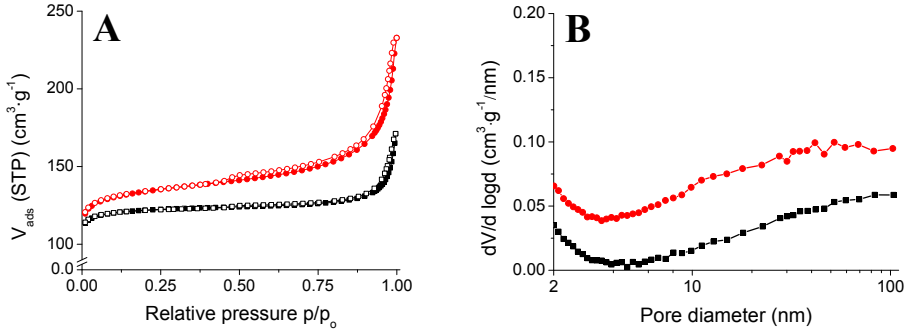

Fig. 9. (A) N_2 adsorption (open symbols) and desorption (solid symbols) isotherm of BASF mordenite; and (B) BJH pore size distribution): (■) BASF and (●)BASF-at-1.0-15.

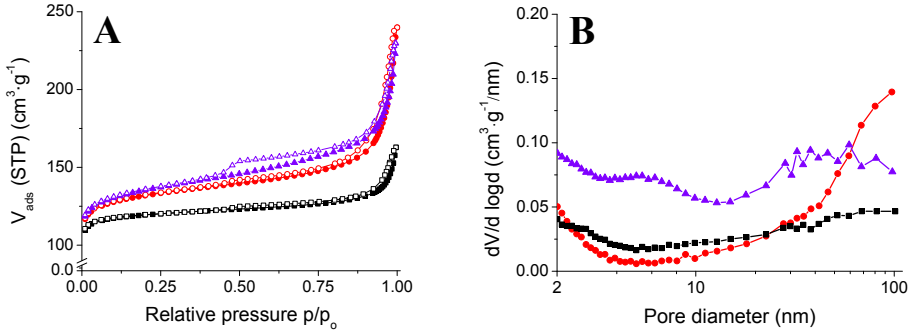

Fig. 10. (A) N_2 adsorption (open symbols) and desorption (solid symbols) isotherm of Zeolyst CBV 21A mordenite; and (B) BJH pore size distribution): (■) CBV-21A; (●) CBV 21A-at-1.0-10 and (▲) CBV 21A-at-0.5-15.

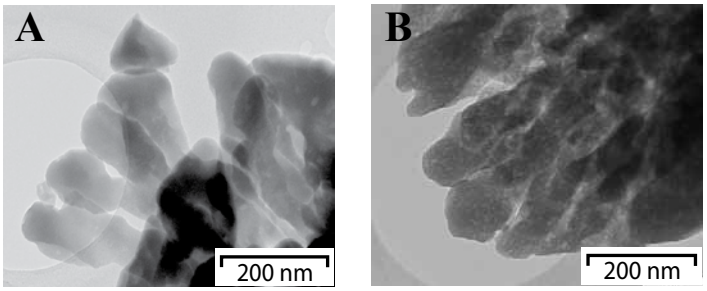

Fig. 11. TEM images of (A) Zeolyst CBV 21A and (B) Zeolyst CBV 21A-at-0.5-20.

conditions are applied not only large mesopores and small macropores are present but also a considerable amount of mesopores in the 3-8 nm range (Fig. 10). TEM images of CBV 21A-parent and of CBV-21A-at-0.5-20 (Fig. 11) show that small intra-crystalline mesopores are formed upon alkaline treatment. Groen et al. [34] reported that the Zeolyst 20A sample with similar Si/Al ratio was not reactive towards 0.2M NaOH for 30 min. We can conclude that the porosity of the 21A mordenite can be improved using a 0.5M NaOH for 20 minutes, which results in intra- and intercrystalline mesoporosity.

3.4 Liquid phase Benzene alkylation with propylene

The alkylation of benzene with propylene to form cumene was chosen as a model reaction to evaluate the effect of the introduced mesoporosity in LZM-5 on the activity and selectivity. At the start of the reaction an excess of benzene was used (benzene to propylene molar ratio ~4), and ~1g of catalyst (H-MOR-parent or H-MOR-at) was added. As can be seen in Figure 12 and Table 4 alkaline treatment results in improved catalytic activity, as measured by the initial rate constant, of more than an order of magnitude. After 4 hours of reaction 60 percent of the propene has reacted with the alkaline treated sample, while only 10 % of propene has reacted using the parent mordenite as catalyst. After 4 hours the selectivity towards cumene is slightly higher than for the parent mordenite. However, if we assume that di-substituted benzenes can also be transformed back into cumene via a trans-alkylation reaction the selectivity of both samples effectively was about 99 %.

The comparable selectivity gives an indication that no strong Lewis acid sites have formed on the surface as a result of alkaline treatment [53], otherwise it is expected that propene oligomerization would have taken place. It is unlikely that the increase in activity is related to an increase in acid site density, as based on the increase in Si/

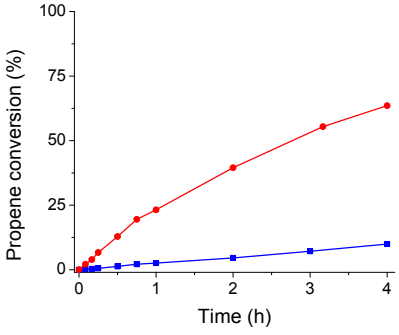

Fig. 12. Benzene alkylation with propylene on LZM-5 mordenite: (■) H-MOR-parent and (●) H-MOR-at.

Table 4 . Benzene alkylation with propene; parent and alkaline treated LZM-5 mordenite.

	H-MOR-parent	H-MOR-at
Activity		
Initial rate ($mol \cdot g^{-1} \cdot s^{-1}$)	2.9 E-5	5.5 E-4
Initial rate (normalized)	1	19
Propene selectivity [a] (mol %)		
cumene	82.6	85.7
di-isopropylbenzene	16.1	13.3

[a] after 4h of reaction

Al ratio only a slight increase in acid site density would be expected, as was confirmed by ammonia TPD (Fig. 4B). Furthermore, also for the heavily dealuminated mordenite reported previously by Dow [21, 54] an increase in activity was observed, showing that the acid site density or strength is not the limiting factor in this process. Rather the observed increase in activity can be ascribed to a decrease in average diffusion distances, and related to two parameters that were changed as result of alkaline treatment. First, inter-crystalline mesopores were generated to increase the accessibility of the mordenite agglomerates, thereby preventing possible mass transfer limitations between the particles. Secondly, the mordenite crystallites were slightly decreased in size resulting in a shorter intra-particle diffusion path length.

Conclusion

Commercially available, aluminum rich mordenites comprised of small (100-200 nm) agglomerated crystallites, were subjected to alkaline treatment. Alkaline treatment in a NaOH solution of 1 M for 15 minutes at 343 K on proton mordenite resulted in the formation of inter-crystalline porosity, while the microporosity as well as the crystallinity were preserved. It was also possible to apply alkaline treatment directly on the sodium parent mordenite. However, with an identical alkaline treatment, the treatment time had to be prolonged by a factor 2 to obtain similar porosity as compared to the proton mordenite. Using sodium mordenite has the advantage that the whole process involves less steps and as the reaction is slower it is more easily controlled, especially relevant for scale-up. Different commercial samples of mordenite have been successfully treated, although slightly different conditions had to be applied as a result of slight differences in

Si/Al ratios and morphology of the parent mordenite. With careful adjustments of time and alkaline concentration, it was possible to obtain both inter- and intra-crystalline porosity for mordenite samples with Si/Al ratio as low as 10. Upon alkaline treatment of mordenite with a Si/Al ratio of 5.7 an increase in catalytic activity by more than one order of magnitude was observed without losing selectivity. Hence alkaline treatment of aluminum rich mordenite is an effective post-synthesis treatment to enhance porosity and thereby catalytic activity.

Acknowledgements

We would like to thank Dr. J.T. Miller (BP Amoco, USA), Dr. K.R. Bayense (BASF, Utrecht, The Netherlands) and Dr. F. Winter (Shell, Amsterdam, The Netherlands) for supplying mordenite samples, Dr M.J. Janssen (ExxonMobil, Belgium) for ^{27}Al MAS NMR measurements, M.S.U. Samson, Dr. M.J. van der Aalst, and Dr. G. Meima (Dow Terneuzen, The Netherlands) for catalytic tests and ACTS-ASPECT for financial support.

References

1. Van Bekkum, H.; Flanigen, E.M.; Jacobs, P.A.; *Introduction to zeolite sciences and practice*. Elsevier. **1991**
2. Bearlocher, C.; McCusker, L.B.; Olsen, D.H.; *Atlas of zeolite framework types*. Elsevier, 6th edition. **2007**
3. Meima, G.R.; *cattech*, **1998** (June 1998) 5-12
4. van Donk, S.; Bitter, J.H.; de Jong, K.P.; *Appl. Catal., A* **2001** (212) 97-116
5. Guisnet, M.; Fouche, V.; Belloum, M.; Bournonville, J.P.; Travers, C.; *Appl. Catal.*, **1991** (71) 283-293
6. Meyer, W.M.; *Z. Kristallogr.*, **1961** (115) 439-450
7. Tromp, M.; van Bokhoven, J.A.; Garriga Oostenbrink, M.T.; Bitter, J.H.; de Jong, K.P.; Koningsberger, D.C.; *J. Catal.*, **2000** (190) 209-214
8. Ruthven, D.M.; Post, M.F.M.; *Diffusion in zeolite molecular sieves*, in *Introduction to zeolite science and practice* (van Bekkum, H.; Flanigen, E.M.; Jacobs, P.A.; Jansen, J.C., Eds), Elsevier: Amsterdam. **2001** 525-577.
9. van Donk, S.; Bitter, J.H.; Verberckmoes, A.; Versluijs-Helder, M.; Broersma, A.; de Jong, K.P.; *Angew. Chem. Int. Ed.*, **2005** (44) 1360-1363
10. Schmidt, I.; Madsen, C.; Jacobsen, C.J.H.; *Inorg. Chem.*, **2000** (39) 2279-2283
11. Tosheva, L.; Valtchev, V.P.; *Chem. Mater.*, **2005** (17) 2494-2513
12. van Donk, S.; Broersma, A.; Gijzeman, O.L.J.; Van Bokhoven, J.A.; Bitter, J.H.; de Jong, K.P.; *J. Catal.*, **2001** (204) 272-280
13. van Donk, S.; Janssen, A.H.; Bitter, J.H.; de Jong, K.P.; *Catal. Rev. Sci. Eng.*, **2003** (45) 297 - 319

14. Giudici, R.; Kouwenhoven, H.W.; Prins, R.; *Appl. Catal., A*, **2000** (203) 101-110
15. Boveri, M.; Marquez-Alvarez, C.; Laborde, M.A.; Sastre, E.; *Catal. Today*, **2006** (114) 217-225
16. Fernandes, L.D.; Bartl, P.E.; Monteiro, J.F.; da Silva, J.G.; de Menezes, S.C.; Cardoso, M.J.B.; *Zeolites*, **1994** (14) 533-540
17. Janssen, A.H.; Koster, A.J.; de Jong, K.P.; *J. Phys. Chem. B*, **2002** (106) 11905-11909
18. Janssen, A.H.; Koster, A.J.; de Jong, K.P.; *Angew. Chem. Int. Ed.*, **2001** (40) 1102-1104
19. Koster, A.J.; Ziese, U.; Verkleij, A.J.; Janssen, A.H.; de Jong, K.P.; *J. Phys. Chem. B*, **2000** (104) 9368-9370
20. Lee, G.S.J.; Garces, J.M.; Meima, G.R.; Van Der Aalst, M.J.M., The Dow Chemical Company, **1993**
21. Garcés, J.M.; Olken, M.M.; Lee, G.J.; Meima, G.R.; Jacobs, P.A.; Martens, J.A.; *Top. Catal.*, **2009** (52) 1175-1181
22. Young, D.A., Union Oil. Co.,US Patent 3 326 797, **1967**
23. Young, D.A., Union Oil. Co.,US Patent 3 374 182, **1968**
24. Rosback, D.H.; Neuzil, R.W., UOP Inc.,US Patent 4 048 111, **1977**
25. Rein, A.J.; Saperstein, D.D.; Pines, S.H., Merck & Co.,US Patent 4 134 965, **1979**
26. Kokotailo, G.T.; Rohrman, A.C., Mobil Oil Corp.,US Patent 4 703 025, **1987**
27. Le Van Mao, R.; Le, S.T.; Ohayon, D.; Caillibot, F.; Gelebart, L.; Denes, G.; *Zeolites*, **1997** (19) 270-278
28. Ogura, M.; Shinomiya, S.; Tateno, J.; Nara, Y.; Kikuchi, E.; Matsukata, M.; *Chem. Lett.*, **2000** (29) 882
29. Ogura, M.; Shinomiya, S.; Tateno, J.; Nara, Y.; Nomura, M.; Kikuchi, E.; Matsukata, M.; *Appl. Catal., A*, **2001** (219) 33-43
30. Groen, J.C.; Peffer, L.A.A.; Moulijn, J.A.; Pérez-Ramírez, J.; *Microporous Mesoporous Mater.*, **2004** (69) 29-34
31. Groen, J.C.; Peffer, L.A.A.; Moulijn, J.A.; Pérez-Ramírez, J.; *Colloids Surf., A* **2004** (241) 53-58
32. Groen, J.C.; Moulijn, J.A.; Pérez-Ramírez, J.; *Microporous Mesoporous Mater.*, **2005** (87) 153-161
33. Groen, J.C.; Abelló, S.; Villaescusa, L.A.; Pérez-Ramírez, J.; *Microporous Mesoporous Mater.*, **2008** (114) 93-102
34. Groen, J.C.; Sano, T.; Moulijn, J.A.; Pérez-Ramírez, J.; *J. Catal.*, **2007** (251) 21-27
35. Li, X.; Prins, R.; van Bokhoven, J.A.; *J. Catal.*, **2009** (262) 257-265
36. Groen, J.C.; Jansen, J.C.; Moulijn, J.A.; Pérez-Ramirez, J.; *J. Phys. Chem. B*, **2004** (108) 13062-13065
37. Lippens, B.C.; de Boer, J.H.; *J. Catal.*, **1965** (4) 319-323
38. Barrett, E.P.; Joyner, L.G.; Halenda, P.P.; *J. Am. Chem. Soc.* , **1951** (73) 373-380
39. Kremer, J.R.; Mastronarde, D.N.; McIntosh, J.R.; *J. Struct. Biol*, **1996** (116) 71-76
40. Chen, D.; Rebo, H.P.; Moljord, K.; Holmen, A.; *Chem. Eng. Sci.* , **1996** (51) 2687-2692
41. Zhu, W., Van de Graaf, J. M., Van den Broeke, L. J. P., Kapteijn, F.; Moulijn, J. A.; *Ind. Eng. Chem. Res.*, **1998** (37) 1934-1942
42. Bellussi, G.; Pazzuconi, G.; Perego, C.; Girotti, G.; Terzoni, G.; *J. Catal.*, **1995** (157) 227-234
43. Groen, J.C.; Peffer, L.A.A.; Moulijn, J.A.; Pérez-Ramírez, J.; *Chem. Eur. J.*, **2005** (11) 4983-4994
44. Cundy, C.S.; Henty, M.S.; Plaisted, R.J.; *Zeolites*, **1995** (15) 342-352

45. Meza, L.I.; Anderson, M.W.; Agger, J.R.; Cundy, C.S.; Ruren Xu,; *Stud. Surf. Sci. Catal.* 170, Elsevier. **2007** 177-184.
46. O'Donovan, A.W.; O'Connor, C.T.; Koch, K.R.; *Microporous Mater.* , **1995** (5) 185-202
47. Katada, N.; Takeguchi, T.; Suzuki, T.; Fukushima, T.; Inagaki, K.; Tokunaga, S.; Shimada, H.; Sato, K.; Oumi, Y.; Sano, T.; *Appl. Catal., A*, **2005** (283) 63-74
48. Katada, N.; Takeguchi, T.; Suzuki, T.; Fukushima, T.; Inagaki, K.; Tokunaga, S.; Shimada, H.; Sato, K.; Oumi, Y.; Sano, T.; *Appl. Catal., A*, **2005** (283) 75-84
49. Engelhardt, G.; Michel, D.; *Wiley, New York*, **1987**
50. Sanz, J.; Fornés, V.; Corma, A.; *J. Chem. Soc., Faraday Trans. 1 F*, **1988** (84) 3113-3119
51. Bourgeat-Lami, E.; Massiani, P.; Di Renzo, F.; Espiau, P.; Fajula, F.; Des Courières, T.; *Appl. Catal.*, **1991** (72) 139-152
52. Omegna, A.; van Bokhoven, J.A.; Prins, R.; *J. Phys. Chem. B*, **2003** (107) 8854-8860
53. Holm, M.S.; Svelle, S.; Joensen, F.; Beato, P.; Christensen, C.H.; Bordiga, S.; Bjørgen, M.; *Appl. Catal., A*, **2009** (356) 23-30
54. Olken, M.M.; Garces, J.M. *Proceedings of the 9th International Zeolite Conference*. 1992. Montreal: Butterworth-Heinemann.559-566

3

Mesoporous Mordenites Obtained by Sequential Acid and Alkaline Treatments - Catalysts for Cumene Production with Enhanced Accessibility

Abstract

Two commercially available mordenites, obtained from Zeolyst (Si/Al = 10 at/at) and BASF (Si/Al = 8 at/at), were subjected to post synthesis treatments. The impact of acid treatment, alkaline treatment (desilication), and a combination of both on porosity, crystallinity and catalysis were studied in detail. It was found that sequential acid and alkaline treatments were most effective to obtain mesoporous mordenite with external surface areas up to 250 $m^2 \cdot g^{-1}$. Electron tomography was used to visualize the mesoporosity of a series of sequential acid and alkaline treated mordenite samples. Mesopore formation started close to the external surface area and progressed towards the center of the crystallites for higher porosities. Liquid-phase alkylation of benzene with propylene to cumene was chosen to study the catalytic performance of the enhanced accessibility of various mordenite samples. The activity of the most porous mordenite was found to be close to that of a commercial zeolite Beta, while selectivity towards the undesired n-propylbenzene was found to be significantly lower for mordenite (~70 ppm) than for zeolite Beta (~175 ppm). These catalytic data indicate that the acid plus alkaline treated mordenite could be a viable catalyst in the cumene process.

1 Introduction

Alkylation of benzene with propene to form isopropylbenzene (cumene) is an important industrial process with an annual production of 8 million tonnes [1]. Cumene is primarily used as feedstock for the co-production of phenol and acetone. Until the mid-nineties cumene was produced with solid phosphoric acid (SPA) or $AlCl_3$ as catalysts. Because of superior selectivities and environmental benefits the first cumene plants based on zeolite catalysts started to operate in 1996 [2] . Due to the size of the cumene molecule, 12-ring zeolites were found to be the most promising, including ultrastable Y (USY/FAU), mordenite (MOR), zeolite Beta (BEA), MCM-22 (MWW) and ZSM-12 (MTW) [1], although the 10-ring zeolite ZSM-5 was found to be promising as well [3]. Because of slow diffusion in the micropores [4] it was found that zeolites with a small diffusion path length such as MCM-22 and zeolite Beta were most active. In the MCM-22 process (Mobil-Raytheon) alkylation is believed to take place in cups located on the outer surface of the crystallites [5] thereby avoiding diffusion limitations. The high activity of zeolite Beta (UOP, Q-Max^{tm} process) is the result of nano-crystallites [6] and an efficient 3-dimensional micropore system that consist of 2 interconnecting 12-ring channels [7]. Typical byproducts in the cumene synthesis [8] are diisopropylbenzene (DIPB), triisopropylbenzene (TIPB), propene oligomers and *n*-propylbenzene (NPB). DIPB is converted into cumene in a subsequent trans-alkylation step, whereas TIPB and oligomers are considered waste. NPB formation [9, 10] has to be prevented because in the downstream phenol production propionaldehyde is formed, an acetone contaminant. In 1996 the specification for NPB was 300 ppm [2], the Q-Max^{tm} process claims to operate at lower than 250 ppm [11] (alkylation + transalkylation). It was found that of the zeolites mentioned above, mordenite had the lowest production of *n*-propylbenzene [12, 13] and from this perspective mordenite could be a very attractive catalyst.

The micropore system of mordenite consists of two pore types: 12-ring channels in the c-axis direction (6.7 × 7.0 Å) and 8-ring channels along the direction of the b-axis (3.4 × 4.8 Å) that are inaccessible above C_3-molecules [14]. Since the 8-ring channels do not inter-connect the 12-ring channels, mordenite is considered a one-dimensional zeolite. So far there is no synthesis route for nano-crystalline mordenite available although thin needles (60 nm width) can be produced [15, 16]. Commercially available mordenite crystallites have typical dimensions between 100 and 200 nm and typically form larger particles. Post synthesis treatments with steam and acid have been described in detail in literature. The mesoporosity after these treatment was reported as limited [17-22]. DOW

reported that by cyclic dealumination a highly active pseudo 3 dimensional mesoporous mordenite (3DDM) was obtained that was commercially applied as an add-on trans-alkylation catalyst in the cumene production [23-25]. In a study by Van Donk et al. the formation of mesopores upon acid treatment were visualized with electron tomography [26, 27].

Alkaline treatment or desilication [28-31] with NaOH can be a very effective post synthesis treatment to improve the porosity of zeolites. During contact with the alkaline solution, silicon is extracted from the framework resulting in mesoporous zeolites. Successful alkaline treatment depends on the silicon to aluminum ratio of the zeolite. If the Si/Al ratio is too low no mesopores are formed, and when it is too high complete dissolution occurs. The optimal Si/Al ratio for alkaline treatment was found to be between 25 and 50 at/at [30]. It was shown that direct alkaline treatment on as-synthesized mordenite crystals in this optimal range indeed resulted in the formation of mesopores [32]. Van Bokhoven et al. [33] showed that acid treatment can be used to boost the Si/Al ratio of mordenite into this optimal range, leading to mesopore formation upon successive alkaline treatment. The crystallites used in both studies however, are up to two orders of magnitude larger than those prevailing in commercially available mordenite samples. It was shown by Van Laak et al. [34] that alkaline treatment on commercially available mordenite with Si/Al ratios as low as 10 at/at can result in the formation of intra-crystalline mesopores.

In this chapter we discuss the effects of sequential acid and alkaline treatments on the structural and catalytic properties of mordenite. Initial results were acquired on a readily available commercial mordenite obtained from Zeolyst International (CBV 21A). The sequential treatments resulted in the formation of mesoporous mordenite, although the Zeolyst mordenite was found to have a limited thermal stability. Hence, the procedure as described is also applied to a more stable second zeolite sample obtained from BASF. A comprehensive study was made on post-synthesis treatments on the BASF mordenite porosity including imaging by electron tomography. Although we realize that the changes in porosity can affect the acidity of the mordenite to some extent, we have not extensively studied the latter parameter. The catalytic properties of the treated BASF mordenite samples were tested for the liquid-phase production of cumene and are compared to an industrial catalyst based on zeolite Beta.

2 Experimental

2.1 Sample preparation

Mordenite samples were provided by Zeolyst International (CBV 21A) and BASF (formerly Engelhard). Zeolyst CBV 21A was delivered in NH_4 form with a Si/Al ratio of 10 at/at, BASF mordenite in sodium form with Si/Al ratio of 8 at/at. Two zeolite Beta samples were supplied by Zeolyst International. The first sample, CP814N CY (Si/Al ratio at/at 9), was an extrudate (20 wt.% SiO_2) in proton form. The second sample, CP814E (Si/Al ratio of 12.5) was supplied in NH_4 form.

As received Zeolyst mordenite, referred to as NH_4-Zeolyst-*parent* was converted from the ammonia form to the proton form by calcination at 773 K for three hours using a heating rate of 1 $K \cdot min^{-1}$; the obtained sample will be referred to as H-Zeolyst-*parent*. As received BASF mordenite, referred to as Na-BASF-*parent*, was ion-exchanged three times under stirring in an aqueous 1 M NH_4NO_3 (p.a. Acros) solution at 353 K for 24 hours, followed by filtering and washing. Per gram of mordenite 12 ml of ammonia nitrate solution was used. The ion-exchanged NH_4-BASF-*parent* was calcined as described above: the obtained sample will be referred to as H-BASF-*parent*. Acid treatment was performed by adding ten grams of H-Mordenite-*parent* in 100 ml 3 M nitric acid (65 % p.a. Acros) solution at reflux conditions for 1 h, while stirring. This was followed by filtering and washing with hot demineralized water until the pH is the filtrate was ~4. The obtained mordenite is called H-Mordenite-*acid*, subsequent calcination as described above resulted in H-Mordenite-*acid-c*.

Alkaline treatment on Zeolyst samples was performed by adding 0.7 g mordenite in 40 ml pre-heated alkaline solution (0.05 to 1M NaOH) (p.a. Merck) or 1 M NH_4OH (p.a. Acros) at 343 K, while stirring. This was followed by centrifugation (Eppendorf centrifuge 5804, 5000 rpm) and decantation of the liquid followed by re-suspension with hot demineralized water. This procedure was repeated until the pH was ~7. Conversion to proton form was performed as described above. BASF samples were treated similarly; the centrifugation step was carried out at 18.000 rpm using a SS34 rotor of a Sorvall *RC5*$^+$ ultracentrifuge for 1 minute. Conversion to proton form was performed as described above with 1 M NH_4NO_3, followed by calcination at 723 K. Alkaline treated samples are indicated with –*at* added to the name. One combined acid and alkaline treated sample was subsequently treated in 0.1 M HNO_3 solution at 323 K for 15 minutes. The flow diagram for the separate synthesis steps including sample designations for the as received mordenite parent to the sequential acid/alkaline/acid treated mordenite is represented in Scheme 1.

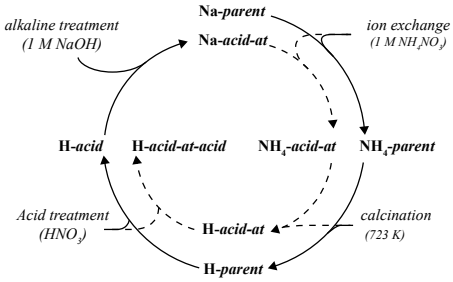

Scheme 1. Flow diagram of sequential acid, alkaline and acide treatment synthesis steps

2.2 Structural characterization

Powder X-ray diffraction (XRD) patterns were obtained using a Bruker-Axs D8 series 2 with a $Co_{1,2}$ source (λ = 0.179 nm). *In situ* XRD during calcination was performed in 20 % O_2 in N_2 (heating with 1 K·min^{-1} to 393 K for 3 h followed by heating with 1 K min^{-1} to 773 K for 3 h). Crystallinity was determined according to O'Donovan et al [20] by the summed up intensities of the (330), (150), (202), (350) and (511) reflections. The parent mordenite was assigned a crystallinity of 100 %

The porosity of the samples was studied using N_2 physisorption isotherms, which were recorded using a Micromeritics Tristar 3000 at 77 K. Prior to the physisorption measurements, the mordenite samples were dried overnight at 573 K in flowing nitrogen. The t-plot method was applied to obtain the micropore volume and external surface area. Pore size distributions were obtained from the adsorption branch using the BJH-method. The mesopore volume was calculated by integrating these plots from 2 to 50 nm. Pore size distributions are plotted from 2-100 nm. Although pore sizes >50 nm obtained with the BJH method are less reliable they are still indicative of the volume of small macropores in the sample.

Morphology and crystal sizes were determined with a Tecnai FEI XL 30SFEG Scanning Electron Microscope (SEM) at 15 kV and with a Tecnai 20 Transmission Electron Microscope operated at 200 kV. Samples for electron tomography (ET) were prepared in two steps. First, colloidal gold particles of 10 nm in size were deposited from suspension on a carbon support film on a standard Cu parallel-bar TEM grid, followed by drying in air. The carbon support film consisted of a <20 nm thick Quantifoil R2/1 carbon film with a ~ 3nm thin continuous carbon layer on top (Quantifoil Microtools GmbH, Jena, Germany). Second, a few drops of a dilute suspension of mordenite crystals in ethanol were applied to the grid, again followed by drying in air. Tilt series data were collected on a Tecnai 20 transmission electron microscope, which was equipped with a LaB6 electron

gun (200 keV) and a TWIN objective lens. Tilt-series were recorded in bright-field TEM mode on a 2k × 2k CCD camera (TVIPS GmbH, Gauting, Germany) over an angular range of -75° to +75° at 1° or 2° increments. The nominal defocus was set to -600 nm (14.5 k×) and -500 nm (19 k×). Alignment of the datasets (using the 10 nm colloidal gold particles as fiducial markers) and reconstruction (by weighted backprojection) was performed in IMOD [35]. Prior to reconstruction, the aligned tilt-series was binned by a factor of 2 resulting in a final pixel size of 1.1 nm (14.5 k×) or 0.82 nm (19 k×).
Analysis of the pore network was carried out by manual segmentation in Amira (Visage Imaging, Inc.) and automated segmentation in Matlab (The Mathworks) using in part functions of the TOM toolbox [36] and the Delft image processing library (www.diplib.org). Segmentation in Matlab proceeded via: 1) median filtering of the reconstruction; 2) thresholding using the isodata algorithm [37]; 3) binary erosion; 4) selection of the largest connected object; 5) binary dilation; and 6) binary closing. Following this automated segmentation procedure pores of at least 4 pixel in diameter, e.g. ~ 2.5 nm at a magnification of 19 k×, could be detected. The results of the reconstruction, manual and automated segmentation were visualized by numerical cross-sections using Amira, Matlab or IMOD.
^{27}Al MAS NMR experiments were carried out with a Bruker Avance 700 NMR spectrometer using a 2.5-mm double-resonance probe-head. The resonance frequency for ^{27}Al was 182.4 MHz, and the pulse length was 6 μs. All the spectra were obtained at a spinning speed of 15 kHz, and scans were added with a recycle delay of 1 s. The ^{27}Al chemical shifts were referenced to $(NH_4)Al(SO_4)_2 \cdot 12H_2O$.
Ammonia temperature programmed desorption (TPD) was performed with a Micromeritics Autochem II. About ~150 mg of sample was dried at 573 K. After saturating the sample at 473 K with ammonia a 30 minutes dwell time was applied. Subsequently TPD was measured while the temperature was increased to 923K with a heating rate of 10 $K \cdot min^{-1}$ and kept constant for 30 minutes.

2.3 Catalytic measurements

Catalytic tests were carried out in an autoclave stirred at 400 RPM. Benzene and propylene were tapped from industrial streams (99% plus) supplied by Dow Terneuzen, The Netherlands. For the alkylation approximately 0.75 g of catalyst powder (sieve fraction 425-800 μm) and 270 g of benzene were loaded into a nitrogen purged 1 l autoclave. After raising the temperature to 423 K approximately 38 g of propylene was fed to the reactor resulting in a benzene to propylene molar ratio ~4. The reactor was then

pressurized to ~40 bars by feeding nitrogen. During reaction samples were withdrawn from the reactor and analyzed by GC. A similar catalytic setup was used by Bellussi et al [38]

3 Results and discussion

In Figure 1 SEM images are shown of mordenite samples from Zeolyst and BASF as well as zeolite Beta (Zeolyst CP 814E). Both mordenite samples contain small crystallites of 100-200 nm that have agglomerated into larger particles. The BASF mordenite contains also larger crystallites up to 500 nm in length. The Zeolyst material was chosen as the starting material for post-synthesis treatments because of its more homogenous morphology compared to the BASF mordenite. Zeolite Beta consists of nano-crystallites with sizes between 15 and 20 nm, that are clustered into agglomerates of about 60-100 nm, which then form larger particles up to several μm.

3.1 Mordenite: Zeolyst

3.1.1 Acid treatment

NH_4-Zeolyst-*parent* was calcined to obtain H-Zeolyst-*parent* that was subsequently acid treated in 3 M HNO_3 for 1 h, thereby increasing the Si/Al ratio from 10 to 30 at/at (H-Zeolyst-*acid)*. With nitrogen physisorption it was determined that the porosity did not change significantly upon acid treatment (Table 1). The crystallinity was preserved even though about three quarters of the total aluminum content of the parent mordenite was removed. This illustrates the validity of acid treatment as a tool to modify the Si/Al ratio of mordenite. However, after subsequent calcination at 773 K the crystallinity decreased to ~50% when compared to the H-Zeolyst-*acid* sample. Despite the decrease in crystallinity after calcination no significant change on the porosity of mordenite was observed. Apparently small changes in the framework are made during calcination that

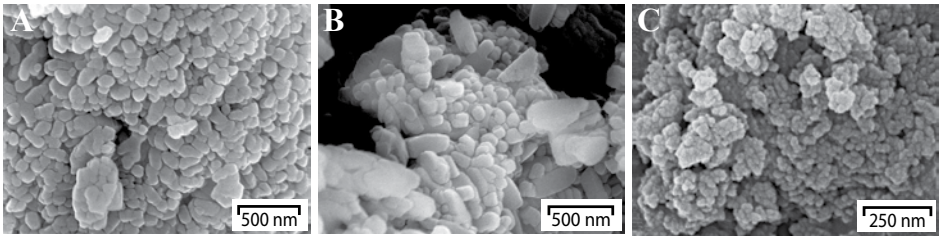

Fig. 1. SEM image (A) NH4-Zeolyst-parent (mordenite), (B) Na-BASF-parent (Mordenite) and (C) NH4-Zeolyst CP 814E (zeolite beta).

are affecting the crystallinity of the mordenite, without altering the microporosity. *In-situ* XRD measurements were performed to study at which temperatures the decrease in crystallinity occurs. Calcination of the as received NH_4-Zeolyst-*parent* (Fig. 2A) resulted in a small decrease in crystallinity that started around 623 K and ended when 773 K was reached. Upon calcination of the H-Zeolyst-*acid* sample a fast decrease for all peaks was observed above 573 K (Fig. 2B). If we define the crystallinity of H-Zeolyst-*parent* as 100 % a decrease to ~50 % was observed upon calcination of the H-Zeolyst-*acid* sample. The most likely explanation is that extra framework aluminum (efAl) species are formed during calcination [39-41], which remain close to the extraction site as the microporosity is not affected by calcination (Table 1). From an extensive study by Katada et al. [39, 40]

Table 1. Textural properties and crystallinities of mordenite samples (Zeolyst).

Sample	V_{micro} [a] ($cm^3 \times g^{-1}$)	A_{ext} [a] ($m^2 \times g^{-1}$)	V_{meso} [b] ($cm^3 \times g^{-1}$)	V_{total} [c] ($cm^3 \times g^{-1}$)	Si/Al [d] (at/at)	XRD (%)
NH_4-Zeolyst-parent	0.17	45	0.04	0.25	10	104
H-Zeolyst-parent	0.20	52	0.05	0.29	10	100
H-Zeolyst-acid	0.19	59	0.05	0.33	30	97
H-Zeolyst-acid-c	0.20	57	0.05	0.33	30	49
Na-Zeolyst-acid-at(M NaOH 60')	0.18	83	0.08	0.35	20	97
Na-Zeolyst-acid-at(0.1 M NaOH 30')	0.17	160	0.13	0.41	17	81
Na-Zeolyst-acid-at(0.2 M NaOH 5')	0.13	285	0.24	0.54	12	53
Na-Zeolyst-acid-c-at(0.1 M NaOH 30')	0.18	78	0.07	0.33	20	105
Na-Zeolyst-acid-c-at(0.2 M NaOH 5')	0.18	145	0.11	0.38	17	82

[a] t-plot method
[b] BJH-method (adsorption branch)
[c] @ $p/p_o = 0.995$
[d] ICP-AES

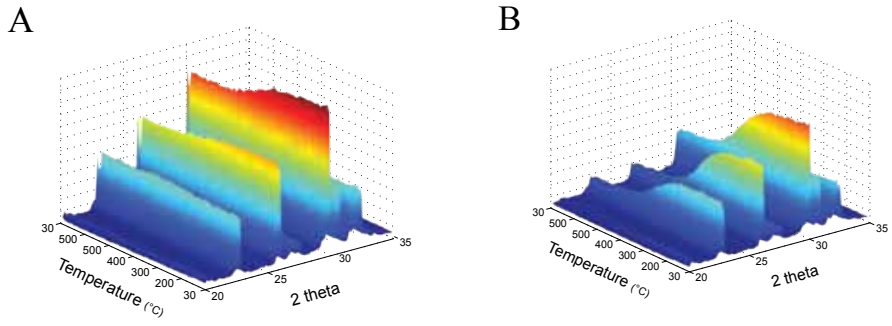

Fig. 2. In situ XRD: (A) NH4-Zeolyst-parent and (B): H-Zeolyst-acid.

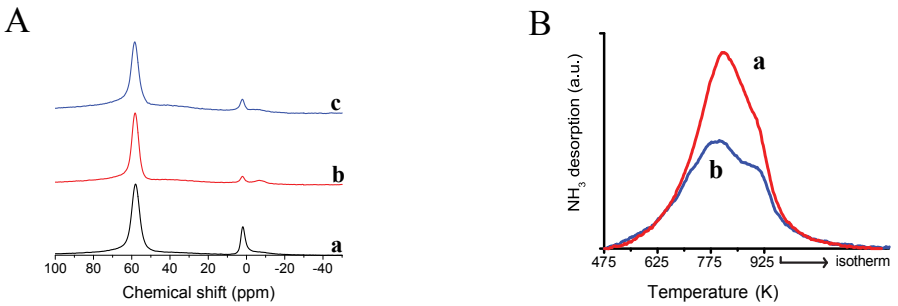

Fig. 3. (A) ^{27}Al MAS NMR: (a) H-Zeolyst-parent , (b) H-Zeolyst-acid and (c) H-Zeolyst-acid-c (B) NH_3-TPD desorption profiles: (a) H-Zeolyst-acid and (b) H-Zeolyst-acid-c .

it was concluded that extra framework aluminum in mordenite (Tosoh, Si/Al ratio 7.5) is formed at calcination temperatures above 673 by trace amounts of water. Muller et al. [41] however, observed large differences in efAl formation for different mordenite samples. ^{27}Al MAS NMR (Fig. 3A) confirmed that upon calcination of the acid treated mordenite additional efAl is created and NH_3 TPD measurements (Fig. 3B) show that the calcination resulted in a decrease of the Brønsted acid sites by ~50 %.

For the Zeolyst mordenite we can conclude that acid treatment is a powerful technique to increase the Si/Al ratio. Subsequent calcination at 773 K however, leads to the loss of crystallinity and Brønsted acid sites and to the formation of efAl. These changes most likely take place on a very local scale because the microporosity is unaffected.

3.1.2 Acid +alkaline treatment

Alkaline treatment was performed on the H-Zeolyst-*acid* sample in 0.05 M NaOH for 60 minutes, 0.1 M NaOH for 30 minutes and in 0.2 M NaOH for 5 minutes at 343 K. These conditions are slightly milder than those reported in the literature [32] because

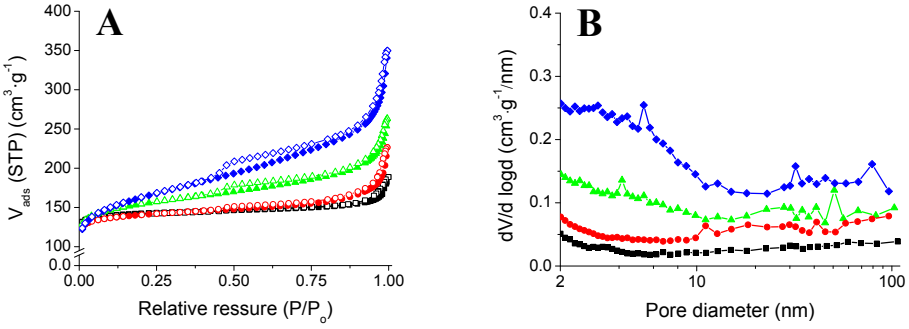

Fig. 4. (A) N_2 adsorption (solid symbols) and desorption (open symbols); and (B) BJH pore size distribution): ■ H-Zeolyst-parent, ● Na-Zeolyst-acid-at(0.05 M NaOH 60), ▲ Na-Zeolyst-acid-at(0.1 M NaOH 30) and ♦ Na-Zeolyst-acid-at(0.2 M NaOH 5).

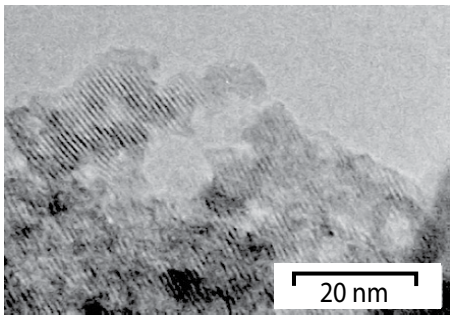

Fig. 5. TEM image Na-Zeolyst-acid-at(0.2 M NaOH 5').

of the smaller crystallite sizes (~150 nm vs. 10 μm). From nitrogen physisorption data (Table 1, Fig. 4) we can conclude that all three experiments led to increased porosity. The effect of the mild alkaline treatment in 0.05 M NaOH was limited, but treatment in 0.1 M for 30 minutes resulted in mordenite with an external surface area of 160 $m^2 \cdot g^{-1}$ and a slight decrease in crystallinity from 97 to 81 %. Treatment in 0.2 M NaOH resulted in an external surface area of 285 $m^2 \cdot g^{-1}$ and a mesopore volume of 0.26 $ml \cdot g^{-1}$. The BJH pore size distribution (Fig. S3-B) of the Na-Zeolyst-*acid-at(*0.2 M NaOH 5') sample shows a large volume of mesopores below 10 nm in size. A TEM image (Fig. 5) visualizes the mesopores as interruptions of the lattice planes, with dimensions between 4-8 nm. A decrease in micropore volume (0.20 to 0.13 $cm^3 \cdot g^{-1}$) was observed, which can possibly be attributed to the external surface area effect as described by Camblor et al. [6]. Besides the decrease in micropore volume there was also a significant decrease in crystallinity observed from 97 % for the H-Zeolyst-*acid* to 53% for Na-Zeolyst-*acid-at(0.2 M NaOH 5')*.

Similar experiments with 0.1 and 0.2 M NaOH were performed on the acid treated mordenite after calcination, H-Zeolyst-*acid-c*. Again for both samples an increase in porosity was observed although the volume of mesopores was considerably lower than for non-calcined sample (Table 1, Fig. 6). The 0.1 M NaOH and 0.2 M NaOH treatments resulted in external surface areas of 78 $m^2 \cdot g^{-1}$ and 145 $m^2 \cdot g^{-1}$, respectively, compared to 160 $m^2 \cdot g^{-1}$ and 285 $m^2 \cdot g^{-1}$ for the non-calcined samples. The crystallinity after treatment in 0.1 M NaOH was restored from 50 to 105% and to 82% after the 0.2 M NaOH treatment. The low mesoporosity that was obtained after 0.1 M NaOH treatment suggests that dissolution of amorphous material to increase the crystallinity is unlikely. More likely is that local defects close to the aluminum extraction site are the reason for the loss of crystallinity upon acid treatment and possibly that re-insertion of aluminum species into the zeolite framework occurs during alkaline treatment, thereby restoring

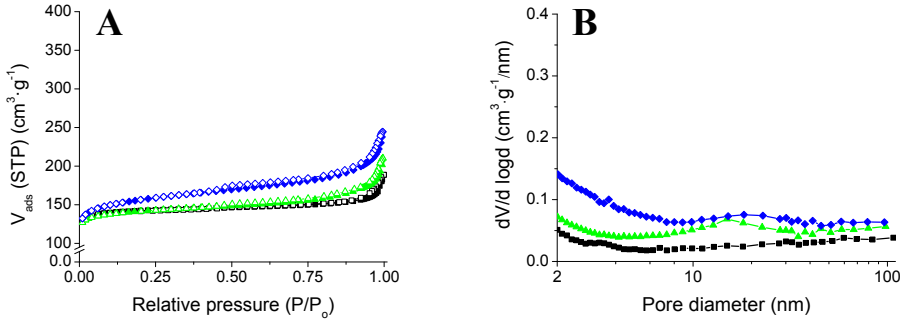

Fig. 6. (A) N_2 adsorption (solid symbols) and desorption (open symbols); and (B) BJH pore size distribution): ■ H-Zeolyst-parent, ● Na-Zeolyst-acid-c-at(0.05 M NaOH 60), ▲ Na-Zeolyst-acid-c-at(0.1 M NaOH 30) and ♦ Na-Zeolyst-acid-c-at(0.2 M NaOH 5),

crystallinity. Similar results were described by Groen et al. [31] for ZSM-5 in which a steam treatment at 873 K followed by alkaline treatment resulted in lower mesoporosity compared to a alkaline treatment only. The pore size distribution of the combined acid and alkaline treated samples (Fig. 4 and 6) show a comparable pattern for all samples, only the volume of mesopores varies.

A lower NaOH concentration leads to a lower degree of porosity, which could be related to a penetration gradient inside the particle or within the crystallite. The main difference between the non-calcined and the calcined samples is the nature of the aluminum species. The difference in porosity after identical alkaline treatment on non-calcined and calcined samples hence indicates that the nature of the aluminum species influence the alkaline treatment greatly. The different aluminum species before and after calcination are located within the micropores, and hence the differences in porosity are expected within the crystallites rather than within the particles. In summary we can conclude that highly porous mordenite can be obtained by sequential treatment acid and alkaline treatment on Zeolyst CBV 21A mordenite. The stability after post-synthesis treatments however, is considered poor and therefore a second mordenite supplied by BASF was studied.

3.2 Mordenite: BASF

3.2.1 BASF: acid treatment

Na-BASF-*parent* was ion exchanged with 1 M NH_4NO_3 followed by calcination to obtain H-BASF-*parent* that was subsequent stirred in 3 M HNO_3 at reflux conditions for 1 hour, resulting in a dealuminated mordenite with Si/Al ratio 22 (H-BASF-*acid(22)*). TEM/EDX measurements (Fig. 7) were performed on large and small crystallites that indicated the presence of local Si/Al ratio variations between 16 and 23 at/at. As

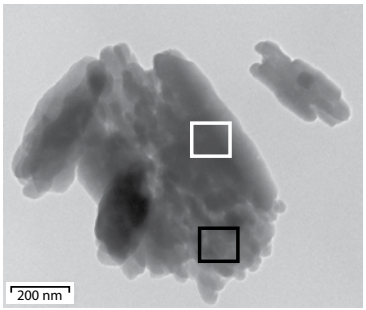

Fig. 7. TEM image with EDX Si/Al ratio area scans: Si/Al ratio 16 at/at (white square) and Si/Al ratio 23 at/at (black square).

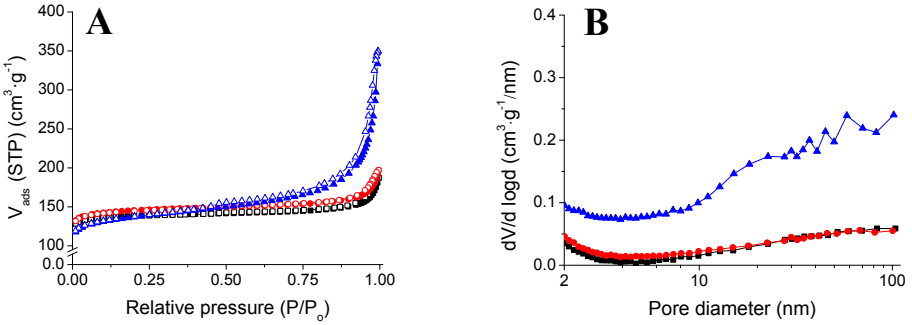

Fig. 8. (A) N_2 adsorption (solid symbols) and desorption (open symbols); and (B) BJH pore size distribution): ● H-BASF-parent, ■ H-BASF-acid(22)-c and ▲ H-BASF-at .

both these values are below the optimum Si/Al ratio for successful desilication [30], a second batch of acid treated mordenite was prepared. Acid treatment was similar as for the H-BASF-*acid(22)* sample with a longer reflux time of 1.5 hours, resulting in a Si/Al ratio of 30 (H-BASF-*acid(30)*). From nitrogen physisorption, listed in Table 2, it was determined that the porosity of the mordenite did not change significantly (Fig. 8), though a small increase in external surface area of ~20 m^2 was observed. After acid treatment only we observed that crystallinity was retained, which decreased upon calcination to 72 %. These results are in line with the results obtained for the Zeolyst mordenite, although the thermal stability of the acid treated BASF mordenite is superior to that of the acid treated Zeolyst mordenite.

3.2.2. BASF: alkaline treatment

In literature it is shown [34] that direct alkaline treatment on the Na-BASF-*parent* mordenite in 1 M NaOH solution at 343 K for 15 minutes resulted in the formation of mesopores. When these conditions were applied silicon, as well as aluminum were dissolved, though silicon was dissolved in slightly larger amounts thereby decreasing

Table 2 Textural properties and crystallinities of mordenite samples (BASF) and zeolite beta (Zeolyst).

Sample	V_{micro} [a] ($cm^3 \times g^{-1}$)	A_{ext} [a] ($m^2 \times g^{-1}$)	V_{meso} [b] ($cm^3 \times g^{-1}$)	V_{total} [c] ($cm^3 \times g^{-1}$)	Si/Al [d] (at/at)	XRD (%)
Na-BA*SF-Parent*	0.17	36	0.03	0.26	9	102
H-BASF-*Parent*	0.19	43	0.04	0.30	9	100
H-BASF-*at*	0.17	128	0.17	0.57	7	91
H-BASF-*acid(22)-c*	0.19	67	0.05	0.31	22	82
H-BASF-*acid(22)*-c-*at(NaOH)*	0.17	170	0.20	0.54	13	83
H-BASF-*acid(22)*-c-*at(NH_4OH)*	0.19	94	0.08	0.36	19	90
H-BASF-*acid(30)*	0.19	59	0.05	0.30	30	93
H-BASF-*acid(30)-c*	0.20	61	0.05	0.30	30	72
Na-BASF-*acid(30)-at(NaOH)*	0.15	289	0.30	0.71	-	89
NH_4-BASF-*acid(30)-at(NaOH)*	0.16	235	0.30	0.68	-	94
H-BASF-*acid(30)-at(NaOH)*	0.16	248	0.33	0.74	-	81
H-BASF-*acid(30)-at(NaOH)-acid*	0.16	250	0.33	0.78	22	89
H-Beta zeolyst CP814N CY [e, f]	0.17	225	0.38	0.81	9	-
NH_4-Beta CP 814E	0.18	230	0.36	0.83	12.5	-
H-Beta CP 814E	0.17	227	0.36	0.83	12.5	-

[a] t-plot method
[b] BJH-method (adsorption branch)
[c] @ p/p_o = 0.995
[d] ICP-AES

the bulk Si/Al ratio in the alkaline treated BASF mordenite. The alkaline treatment experiments were repeated with increased treatment time of 20 minutes resulting in an increase in the external surface area to 125 $m^2 \cdot g^{-1}$ compared to 45 $m^2 \cdot g^{-1}$ for the Na-BASF-Parent and a decrease in Si/Al ratio from 9 to 7 at/at (Table 2). From the BJH pore size distributions (Fig. 8B) we can conclude that after alkaline treatment and subsequent ion exchange and calcination (H-BASF-at) a wide range of meso- and macropores were obtained.

3.2.3 BASF: Acid + alkaline treatment

Alkaline treatment was performed on the H-BASF-*acid(22)-c* in a 0.2 M NaOH solution at 343 K for 8 minutes, followed by ion-exchange and calcination. This resulted in mesoporous mordenite with an external surface area of 170 $m^2 \cdot g^{-1}$ and micropore volume of 0.17 $cm^3 \cdot g^{-1}$ (Table 2). The pore size distribution in Figure 9-B indicates that small most likely intra-crystalline mesopores are formed with a predominant size of 8 nm. Besides

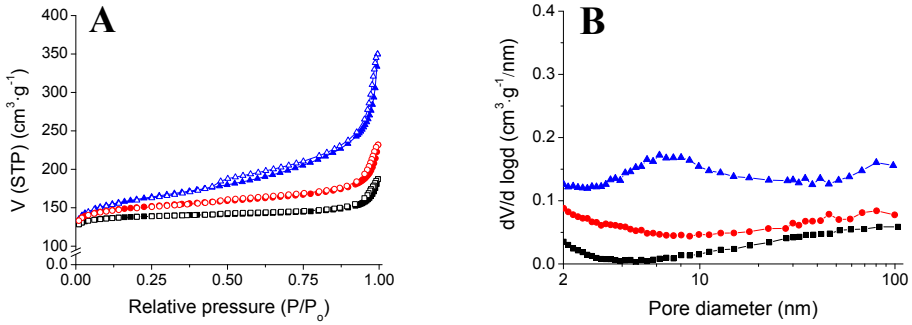

Fig. 9. (A) N_2 adsorption (solid symbols) and desorption (open symbols); and (B) BJH pore size distribution): ■ BASF H-parent, ● H-BASF-acid(22)-c-at(NH_4OH) and ▲ H-BASF-acid(22)-c-at(NaOH).

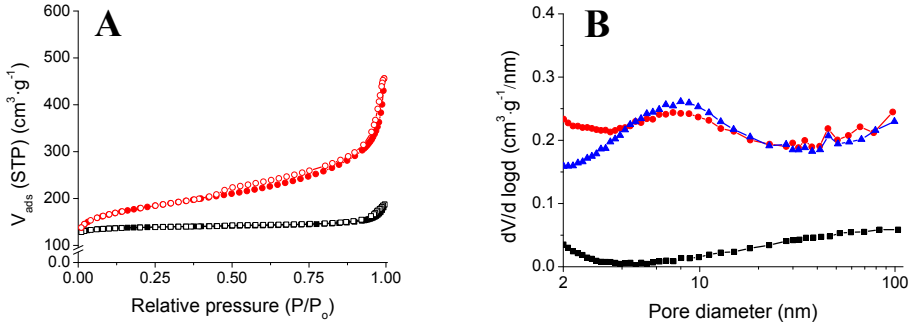

Fig. 10. Influence of ion exchange on porosity: (A) N_2 adsorption (solid symbols) and desorption (open symbols); and (B) BJH pore size distribution: ■ H-BASF-parent, ● Na-BASF-acid(30)-at(NaOH) and ▲ NH4-BASF-acid(30)-at(NaOH).

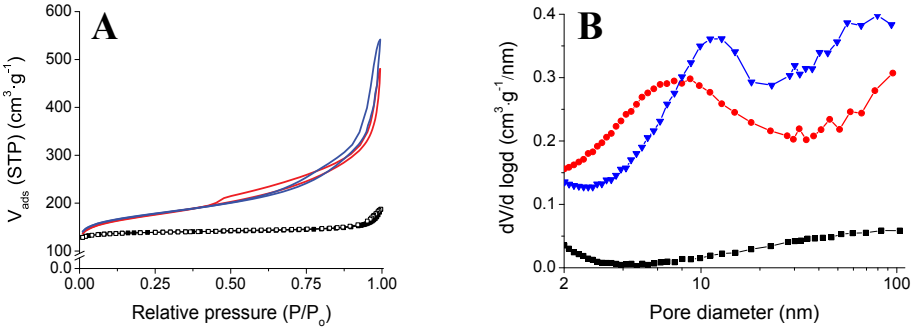

Fig. 11. (A) N_2 adsorption (solid symbols) and desorption (open symbols); and (B) BJH pore size distribution: ■ BASF H-parent (black), ● H-BASF-acid(30)-at(NaOH)-acid (red) and ▼ CP814E-cal (blue).

these small pores there is also a significant amount of large meso- and macro-pores that show similarities with the pores created with direct alkaline treatment on the Na-BASF-*parent*. Apparently treatment in 0.2 M NaOH at higher Si/Al ratios dissolves part of the outer layer of the crystallites, similar to the strong alkaline treatment in 1 M NaOH for lower Si/Al ratios. An alternative alkaline treatment on the H-BASF-*acid(22)-c* sample was performed with 1 M NH_4OH at 343 K. Treatment with NH_4OH has the advantage that a simple calcination would suffice to obtain the proton from, thereby avoiding additional ion exchange steps. Treatment with NH_4OH resulted in a limited increase in external surface area from 67 to 94 $m^2 \cdot g^{-1}$ after calcination. Important is that the micropore volume was preserved, and if we compare the pore size distribution of the 1 M NH_4OH treatment (Fig. 9-B) with the 0.2 M NaOH treatment we observe fewer and smaller (below 8 nm) mesopores and a significantly lower volume of large meso- and macropores. A third experiment was performed on the H-BASF-*acid(30)* sample that was not calcined after acid treatment. Alkaline treatment was performed with 0.2 M NaOH for 8 minutes at 343 K resulting in the formation of highly porous mordenite (Table 2) with an external surface area of 287 $m^2 \cdot g^{-1}$. The micropore volume decreased from 0.20 to 0.15 $cm^3 \cdot g^{-1}$, while the mesopore volume was increased from 0.04 to 0.30 $cm^3 \cdot g^{-1}$. The BJH pore size distribution (Fig. 10B) shows a similar pore size distribution as the identically treated H-BASF-*acid(22)*-c-*at(NaOH)* sample, although the mesopore volume is considerably higher. This indicates that the small difference in Si/Al ratio after acid treatment (30 vs. 22) and calcination after acid treatment have an influence on the mesopore volume but not on the size of pores, similar as what was observed for the Zeolyst mordenite. A difference is that the Zeolyst mordenite has smaller mesopores after acid and alkaline treatments, which could be related to the smaller crystallite size. To obtain the active catalyst Na-BASF-*acid(30)-at(NaOH)* was ion exchanged into NH_4-BASF-*acid(30)-at(NaOH),* which resulted in a decrease in external surface area (from 289 to 235 $m^2 \cdot g^{-1}$) and a slight increase in micropore volume (0.15 to 0.16 $cm^3 \cdot g^{-1}$). A third effect is visible in the mesopore size in which part of the 2-4 nm mesopores are converted into larger 4-10 nm mesopores (Fig. 10B). These changes are most likely because of removal of amorphous species. Calcination was performed at 723 K, which was reported to be the lowest calcination temperature to convert NH_4 sites into H-sites [39] thereby producing as few efAl species as possible. To remove possibly formed efAl species a mild acid treatment in 0.1 M HNO_3 at 323 K for 15 minutes was performed. The final product is a highly mesoporous H-mordenite with a Si/Al ratio of 22 at/at and a crystallinity of 89 %, which will be referred to as H-BASF-*acid(30)-at(NaOH)-acid* (Table 2, Fig. 11).

3.3 Zeolite Beta and mesoporous mordenite

Zeolite Beta (CP814E) has a large external surface area of 227 $m^2 \cdot g^{-1}$ combined with a micropore volume of 0.17 $cm^3 \cdot g^{-1}$ (Table 2). For the CP814N CY the textural properties are slightly different due to the added SiO_2, but the morphology of the two zeolite Beta samples is similar. If we compare zeolite Beta (CP814E) with the most porous mordenite sample (H-BASF-*acid(30)-at(NaOH)-acid*) we observe similar N_2-physissorption isotherms (Fig. 11A). The differences between these the two samples becomes visible when we compare the pore size distribution (Fig. 11B), which shows a predominant mesopore size of 12 nm for the CP814E sample against 8 nm for BASF mordenite. Although the porosities of these two zeolites are similar, their origin is very different with purely inter-crystalline mesopores for the CP814E sample while those of the mordenite are primarily intra-crystalline.

3.4 Electron tomography

The porosities of several BASF mordenite samples were further analyzed with electron tomography (ET) [42]. Low-dose TEM images were acquired to prevent degradation of the material during the tilt series. The ET results are described according to increasing porosity (Table 2): *H-BASF-acid(22)-c-at(NH_4OH), H-BASF-at, H-BASF-acid(22)-c-at(NaOH)* and *H-BASF-acid(30)-at(NaOH)-acid.*

In Figure 12 a TEM image, a numerical reconstructed cross-section and a segmented cross-section of *H-BASF-acid(22)-at(NH_4OH)* through the middle of the particle are shown. We observed that small intra-crystalline mesopores are located primarily in the small crystallites and at the edges of the large crystallites. Nonetheless, most of the crystallites have a dense interior and thus no mesoporosity. In Figure 13 similar data are shown for the *H-BASF-at* sample. The 1 M NaOH solution has dissolved part of the crystallites thereby creating large inter-crystalline mesopores. There are also small intra-crystalline mesopores present in the small and large crystallites. These intra-crystalline mesopores are present throughout the sample even at the center of the large crystallite at the left hand side (Fig. 13C). For the combined acid and alkaline treated sample with sodium hydroxide, H-BASF-*acid(22)-c-at(NaOH)*, a porous structure is observed (Fig. 14). The tomography and segmented data show the existence of a large number of pores (3-8 nm) inside the crystallites. The intra-crystalline mesopores however, are primarily located in the small crystallites and close to the outer surface of the larger crystallites. In Figure 15 the *H-BASF-acid(30)-at(NaOH)-acid* sample is depicted that indicates a highly porous material. In Figure 15C a manually segmented cross-section

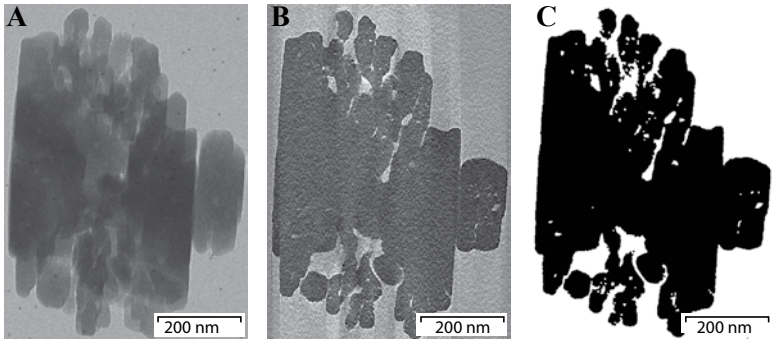

Fig. 12. H-BASF-acid(22)-c-at(NH_4OH) Aext = 94 $m^2 \cdot g^{-1}$: (A) TEM, (B) ET reconstruction cross-section (Thickness 1.1 nm) and (C) segmentation.

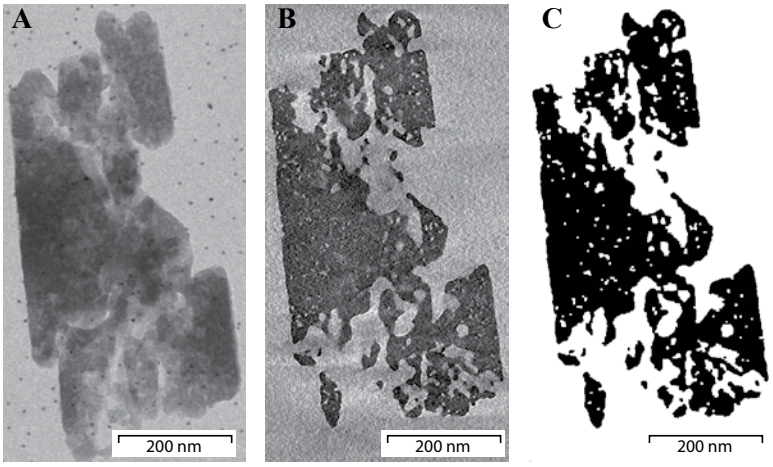

Fig. 13. H-BASF-at Aext = 128 $m^2 \cdot g^{-1}$: (A) TEM, (B) ET reconstruction cross-section (Thickness 1.1 nm) and (C) segmentation.

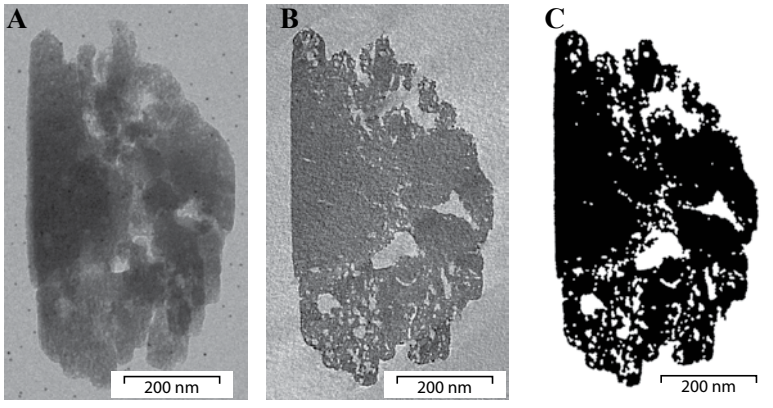

Fig. 14. H-BASF-acid(22)-c-at(NaOH) Aext = 170 $m^2 \cdot g^{-1}$: (A) TEM, (B) ET reconstruction cross-section (Thickness 1.1 nm) and (C) segmentation.

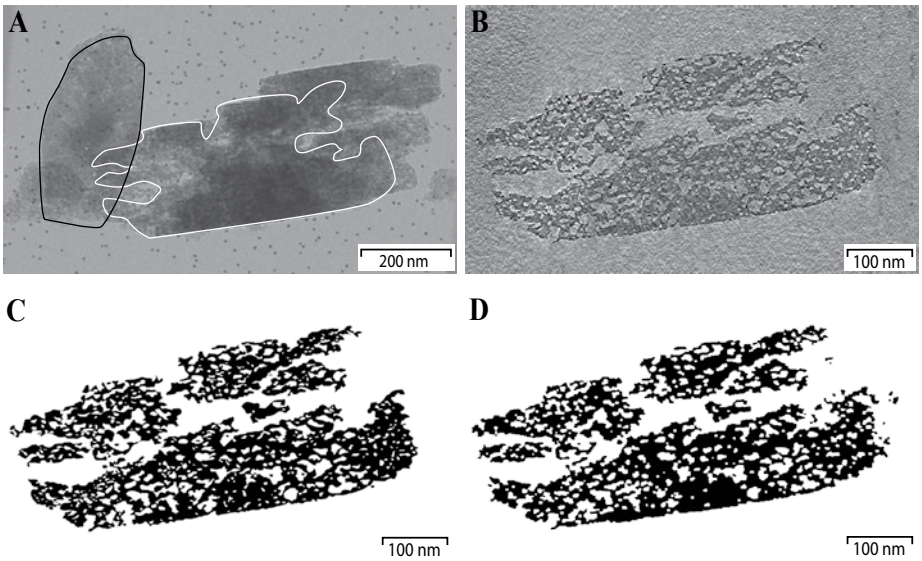

Fig. 15. H-BASF-acid(30)-at(NaOH)-acid Aext = 250 m2·g-1: (A) TEM, (B) ET reconstruction cross-section (Thickness 0.8 nm), (C) (manual) segmentation and (D) segmentation.

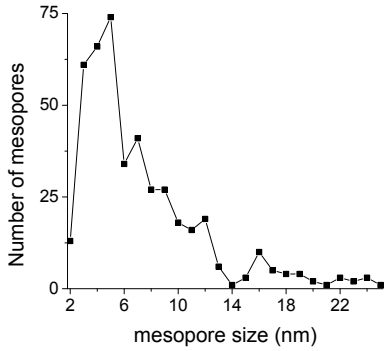

Fig. 16. Pore size distribution manual segmented cross-section (Fig. 15C).

(Fig. 15-A, white outline) through the agglomerate shows that a uniform distribution of the pores is present throughout the whole agglomerate. The added mesopores result in a shorter diffusion path length (half the length of the crystal) from ~70 nm for the parent to ~10 nm (Fig. 15C) for the mesoporous mordenite. Analysis of the pore sizes present in Figure 15C (Fig. 16) resembles the BJH pore size distribution (Fig. 11) for pores of 4 nm and larger. Below 4 nm less than expected pores are observed, which is most likely the result of the limited resolution due to the low dose TEM experiments. This suggests that the actual porosity is most likely higher than shown in Figure 15C. Automated segmented cross-sections visualize even less small mesopores (Fig. 15D).

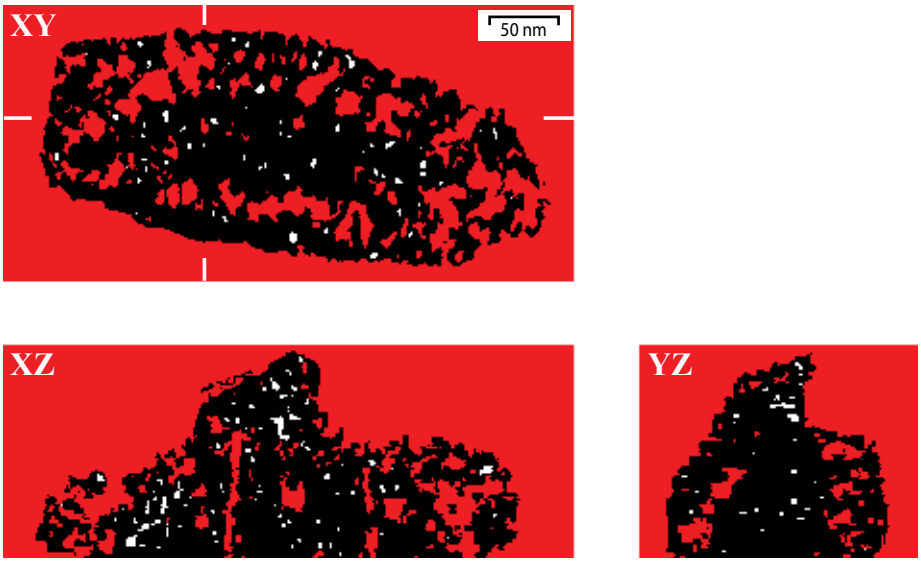

Fig. 17. Tomography cross-section XY, XZ and YZ planes: unconnected mesopores (white) and connected to the external surface (red).

A second isolated large particle ~300 nm (Fig. 15A, black outline) was manually segmented (Fig. 17). For this crystallite large differences in pore sizes are observed with large intra-crystalline mesopores (up to 40 nm) present close to the outer surface, while the pores in the center are few and small. A manually analyzed tomogram (Fig. 17) shows that the majority of the mesopores are in connection with the outer surface, thereby maximizing the mass-transport through the mordenite sample.

4 Catalysis

Alkylation of benzene with propylene to form cumene was chosen as a model reaction to evaluate the effect of the post synthesis treatments on the catalytic performance of BASF mordenite. As a reference material zeolite Beta (Zeolyst CP814N CY) was used that has catalytic properties close to the industrial catalyst.

The as-synthesized BASF mordenite (H-BASF-*parent*) has a low activity (Table 3) compared to zeolite Beta (CP814N CY), which is over 41 times as active. Besides a low activity H-BASF-*parent* produces a large amount of oligomers that leads to lower selectivity followed by deactivation. This is an uncharacteristic feature for mordenite in general as other mordenite samples in literature show at least 98 % selectivity [13, 34] towards the desired products: cumene + diisopropylbenzene (DIPB). The formation

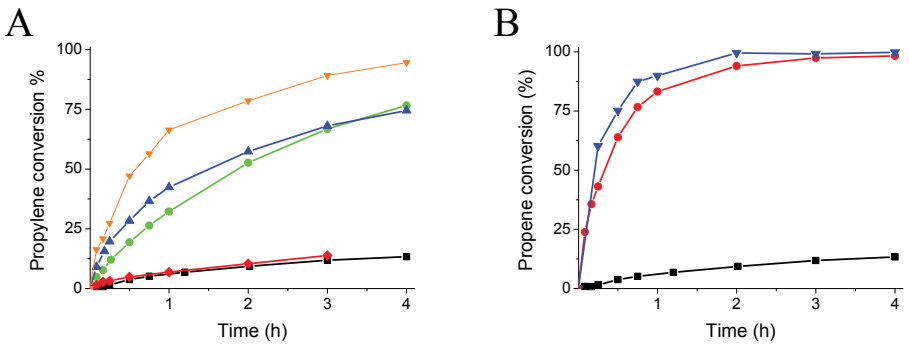

Fig. 18. Benzene alkylation with propylene:
(A) ■ H-BASF-parent, ♦ H-BASF-acid, ● H-BASF-at, ▲ H-BASF-acid(22)-c-at(NH_4OH) and ▼ H-BASF-acid(22)-c-at(NaOH).
(B) ■ BASF H-parent, ● H-BASF-acid(30)-at(NaOH)-acid, ▲ Zeolyst CP814E cal (zeolite Beta).

Table 3. Benzene alkylation with propylene; influence of post-synthesis treatments on BASF mordenite, with zeolite beta as a reference.

	H-BASF-Parent	H-BASF-acid(30)	H-BASF-at	H-BASF-acid(22)-c-at (NH_4OH)	H-BASF-acid(22)-c-at (NaOH)	H-BASF-acid(30)-at (NaOH)-acid	CP814N CY[a]
Activity							
Initial rate (mol×g^{-1}×s^{-1}) 10^{-3}	0.28	0.48	1.4	2.5	4.0	7.3	11
Initial rate (normalized)	1	1.6	5.4	9	15	27	41
Propene selectivity							
cumene (%)	75	73	79	69	72	68	84
di-isopropylbenzene (%)	15	17	20	25	23	25	15
oligomers (%)	10	10	1	6	5	7	1
dipb selectivity							
meta/para ratio	0.40	0.31	0.40	0.35	0.37	0.34	1
Side products							
Tri-isopropyl benzene (ppm)	87	--	640	370	808	700	1160
N-propyl cumene (ppm)	77	--	82	63	71	65	175

[a] 0.80 gram zeolite beta

of DIPB is comparable with zeolite Beta, with mordenite more selective towards the para-isomer (2.5:1 para/meta) while zeolite Beta produces similar amounts (1:1 para/meta). The formation of triisopropylbenzene (TIPB) and *n*-propylbenzene (NPB) is lower for mordenite [12, 13]. Upon acid treatment a negligible increase in porosity was observed and also the catalytic activity increases only marginal (Table 3) compared to the H-BASF-*parent*. The slight increase in activity could be the result of the increased Si/Al ratio from 8 to 30 at/at, that results in higher acid site strength [43]. The most significant change is a decrease in NPB that was below the detection limit of the GC.

The combined acid and mild alkaline treatment of H-BASF-*acid(22)-c-at(NH$_4$OH)* resulted in the formation of small mesopores close to the outer surface with an external surface area of 94 $m^2 \cdot g^{-1}$ (Table 2, Fig 12) .These intra-crystalline mesopores resulted in a 9 times higher activity compared to the parent. Besides the increased activity more DIPB and slightly less NPB was formed than for the parent. Direct alkaline treatment on the parent mordenite did result in inter- and intra-crystalline mesoporosity and a high external surface area of 128 $m^2 \cdot g^{-1}$, and also a 5 times increase in catalytic activity. Interesting is that upon alkaline treatment the production of oligomers is greatly suppressed and a 99 % selectivity is obtained. These propene oligomers are possibly formed at weak acid sites located on the external surface area, at these sites the benzene to propene ratio is similar as the feed ratio while the benzene to propene ratio on the inside of the micropore channels is, accordingly to simulations [44], expected to be significantly higher. Upon alkaline treatment in 1 M NaOH these species might be dissolved, leaving only the highly selective Brønsted acid sites in the micropores as catalytic sites. Unexpected is that the H-BASF-*at* sample is less active compared to the H-BASF-*acid(22)-c-at(NH$_4$OH)* sample, despite the higher degree of porosity. After 4 hours of reaction however, the higher selectivity of the H-BASF-*at* sample results in a higher conversion of propylene compared to H-BASF-*acid(22)- c-at(NH$_4$OH)* (Fig. 18A). The higher degree of porosity of the H-BASF-*acid(22)-c-at(NAOH)* (A_{ext} =170 $m^2 \cdot g^{-1}$) results in a 15 times enhanced catalytic activity compared to the parent, and has similar selectivities as the H-BASF-*acid(22)- c-at(NH$_4$OH)* sample. For the most porous H-BASF-*acid(30)-at(NaOH)-acid* sample we observed an enhanced catalytic activity of 27 times that of parent and an activity that is close to the activity of zeolite Beta (Fig. 18B). Selectivities for this sample are similar as for other combined acid and alkaline treatments, with a large DIPB production and oligomer formation and low NPB formation.

For all samples a significantly lower NPB concentration is measured than for zeolite Beta, this seems to be closely related to acid site strength. To verify this relation the acid

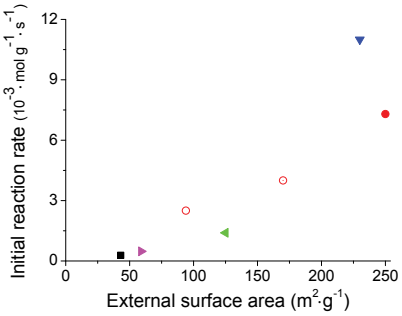

Fig. 19. Initial Reaction rate vs. Aext of ■ H-BASF-parent, ▶ H-BASF-acid, ◀ H-BASF-at, ○ H-BASF-acid(22)-c-at(NH_4OH), ⊙ H-BASF-acid(22)-c-at(NaOH), ● H-BASF-acid(30)-at(NaOH)-acid and ▼ zeolite Beta.

sites of the mordenite have to be studied in detail. This is possible by performing IR experiments with alkyl-pyridines as described by Thibault-Starzyk et al. [45]. In Figure 19 the catalytic activity is plotted against the external surface area. For the combined acid and alkaline treated samples (red circles) a positive relation between external surface area and catalytic activity is observed, which confirms strong mass transfer limitations. Strong mass transfer limitation implies a Thiele Modulus (φ) larger than 2 [46]. If φ>2 than the activity becomes proportional to the external surface area. The latter conclusion should not be confused with catalytic activity only occurring at the external surface. For φ>2 strong internal concentration gradients exists but still the catalysis predominantly takes place inside the micropores of the zeolite catalyst.

The activity of the direct alkaline treated mordenite is considerably lower despite the high porosity. The largest difference between the alkaline treated and the sequential acid and alkaline treated samples is the lower Si/Al ratio. This suggests that the best catalytic results with mordenite are obtained by raising both the porosity as well as the Si/Al ratio. Another effect of the added porosity might be that deactivation by pore blocking due to coke deposits [47] is expected to be lower. Despite the high porosities of the mesoporous mordenite zeolite Beta is still more active. The higher activity of zeolite Beta is most likely the result of the 3-dimensional micropore channel system.

5 Conclusion

The effect of acid and alkaline treatment and the combination of both treatments on the porosity of mordenite was investigated on commercial mordenite samples supplied

by Zeolyst and BASF. Both samples consist of small crystallites ~150 nm that have agglomerated into larger particles. It is shown that acid treatment does not lead to significant (meso) porosity, however, the Si/Al ratio can be increased significantly with preserved crystallinity and (micro) porosity. Calcination of the acid treated mordenite however, can lead to the formation of extra framework aluminum and loss of up to 50 % of the Brønsted acid sites and crystallinity. Direct alkaline treatment in 1 M NaOH on the parent mordenite leads to an increased porosity (A_{ext}: 128 $m^2 \cdot g^{-1}$), while at the same time the Si/Al ratio decreases from 9 to 7 at/at. Electron tomography studies indicate that large parts of the crystallites have been dissolved leading to large inter-crystalline meso- and macro-pores as well as small intra-crystalline mesopores that are present throughout the sample. If alkaline treatment is performed on an acid treated sample highly porous mordenite (A_{ext}: 250 to 300 $m^2 \cdot g^{-1}$) can be obtained. If a calcination is performed between acid and alkaline treatment significantly lower porosities (A_{ext} ~145 $m^2 \cdot g^{-1}$) are obtained, which is most likely the result of efAl formed during calcination that prohibits the formation of mesopores upon alkaline treatment. A series of subsequent acid and alkaline treated samples were prepared with increasing porosities (A_{ext}: 95, 170 and 250 $m^2 \cdot g^{-1}$, Si/Al ratios: 19, 13 and 22 at/at) and analyzed with electron tomography. It shows that mesopores start at the edges of the crystallites and progresses towards the centers at higher mesoporosities. For the most porous mordenite small mesopores (3-8 nm) throughout the sample were observed, although large (up to 40 nm) intra-crystalline mesopores were present as well.

Liquid phase alkylation of benzene with propylene to form cumene was performed to study the catalytic performance of the post synthesis treated mordenite samples. The parent mordenite displayed low activity as well as low selectivity towards cumene/DIPB (90 %) due to propene oligomerization, where > 98 % selectivity is expected based on literature values [13, 34]. The acid treatment did not result in a significant improvement of the catalytic performance, indicating that the Si/Al ratio is of limited influence. For the alkaline treated samples a 5 times higher catalytic activity was observed compared to the parent. Interesting is that after alkaline treatment a > 99 % selectivity towards cumene/DIPB was observed, which is likely the result of dissolution of weak Lewis acid sites on the external surface of the crystallites. The series of combined acid and alkaline treatment with increasing porosity resulted in increased catalytic activity by 9, 15 and 27 times, respectively, with a positive relation between external surface area and catalytic activity. The catalytic activity of the alkaline treated sample was significantly below the correlation obtained for the acid plus alkaline treated samples. This could indicate that the Si/Al

ratio can be an important parameter at higher porosities. Selectivity towards undesired *n*-propylbenzene was found to be decreasing with increasing Si/Al ratio, which could be the result of increased acid site strength. The activity of mesoporous mordenite (A_{ext}: 250 $m^2 \cdot g^{-1}$, Si/Al ratio: 22 at/at) was found to be close to the activity zeolite Beta (A_{ext}: 227 $m^2 \cdot g^{-1}$, Si/Al ratio: 9 at/at), which is 41 times as active as the parent mordenite and the commercial catalyst for cumene production [1]. The selectivity towards cumene/DIPB for the mesoporous mordenite (93 %) was lower compared to the zeolite Beta catalyst (99 %) due to the formation of propene oligomers. Formation of DIPB was also found to be higher than for zeolite Beta with primarily para DIPB formed, while selectivity towards NPB was found to be 3 times lower (~70 vs. 177 ppm). These results show that the acid-alkaline treatment route to obtain mesoporous mordenite can result in a viable catalyst in the cumene process as an alkylation or trans-alkylation catalyst. Finally, we point out that more detailed characterization, in particular of the acidic properties, is advocated for these mesoporous mordenites in order to arrive at a comprehensive understanding of their catalytic performance.

Acknowledgements

We would like to thank Dr. K.R. Bayense (BASF, Utrecht, The Netherlands) and Dr. F. Winter (Shell, Amsterdam, The Netherlands) for supplying mordenite samples, Prof. Dr. J.A. van Bokhoven and N. Danilina (ETH, Zurich) for ^{27}Al MAS NMR measurements and M.S.U. Samson, Dr. M.J. van der Aalst, and Dr. G. Meima (Dow Terneuzen, The Netherlands) for catalytic tests and ACTS-ASPECT for financial support.

Preferences

1. Perego, C.; Ingallina, P.; *Catal. Today*, **2002** (73) 3-22
2. Meima, G.R.; van der Aalst, M.J.M.; Samson, M.S.U.; Garces, J.M.; Lee, J.G.; *Erdoel, Erdgas, Kohle*, **1996** (112) 315-318
3. Kaeding, W.W.; Holland, R.E.; *J. Catal.*, **1988** (109) 212-216
4. Ruthven, D.M.; Post, M.F.M.; *Diffusion in zeolite molecular sieves*, in *Introduction to zeolite science and practice* (van Bekkum, H.; Flanigen, E.M.; Jacobs, P.A.; Jansen, J.C., Eds), Elsevier: Amsterdam. **2001** 525-577.
5. Corma, A.; Martínez-Soria, V.; Schnoeveld, E.; *J. Catal.*, **2000** (192) 163-173
6. Camblor, M.A.; Corma, A.; Valencia, S.; *Microporous Mesoporous Mat.*, **1998** (25) 59-74
7. Bearlocher, C.; McCusker, L.B.; Olsen, D.H.; *Atlas of zeolite framework types*. elsevier, 6th edition. **2007**
8. Cejka, J.; Wichterlova, B.; *Catal. Rev. - Sci. Eng.*, **2002** (44) 375 - 421
9. Wichterlová, B.; Cejka, J.; Zilková, N.; *Microporous Mat.*, **1996** (6) 405-414
10. Irina Ivanova, I.; Montouillout, V.; Fernandez, C.; Marie, O.; Gilson, J.-P.; *Microporous Mesoporous Mat.*, **2003** (57) 297-308

11. Peterson, G.A.; Schmidt, R.J.; *Handbook of Petroleum Refining Processes*, (Meyers, R.A., Editor. **2004**
12. Perego, C.; Millini, R.; Parker Jr, W.O.; Bellussi, G.; Romano, U.; E. van Steen, M.C.a.L.H.C.; *Stud. Surf. Sci. Catal*. **2004** (154) 2239-2246.
13. Perego, C.; Amarilli, S.; Millini, R.; Bellussi, G.; Girotti, G.; Terzoni, G.; *Microporous Mater*, **1996** (6) 395-404
14. Tromp, M.; van Bokhoven, J.A.; Garriga Oostenbrink, M.T.; Bitter, J.H.; de Jong, K.P.; Koningsberger, D.C.; *J. Catal.*, **2000** (190) 209-214
15. Hincapie, B.O.; Garces, L.J.; Zhang, Q.; Sacco, A.; Suib, S.L.; *Microporous Mesoporous Mat.*, **2004** (67) 19-26
16. van Donk, S.; Bitter, J.H.; Verberckmoes, A.; Versluijs-Helder, M.; Broersma, A.; de Jong, K.P.; *Angew. Chem. Int. Ed.*, **2005** (44) 1360-1363
17. Boveri, M.; Marquez-Alvarez, C.; Laborde, M.A.; Sastre, E.; *Catal. Today*, **2006** (114) 217-225
18. Chung, K.-H.; *Microporous Mesoporous Mater.*, **2008** (111) 544-550
19. Fernandes, L.D.; Bartl, P.E.; Monteiro, J.F.; da Silva, J.G.; de Menezes, S.C.; Cardoso, M.J.B.; *Zeolites*, **1994** (14) 533-540
20. O'Donovan, A.W.; O'Connor, C.T.; Koch, K.R.; *Microporous Mater.* , **1995** (5) 185-202
21. Giudici, R.; Kouwenhoven, H.W.; Prins, R.; *Appl. Catal., A*, **2000** (203) 101-110
22. Meyers, B.L.; Fleisch, T.H.; Ray, G.J.; Miller, J.T.; Hall, J.B.; *J. Catal.*, **1988** (110) 82-95
23. Olken, M.M.; Garces, J.M. *From the proceedings of the 9th International Zeolite Conference*. 1992. Montreal: Butterworth-Heinemann.559-566
24. Garcés, J.M.; Olken, M.M.; Lee, G.J.; Meima, G.R.; Jacobs, P.A.; Martens, J.A.; *Top. Catal.*, **2009** (52) 1175-1181
25. Lee, G.S.J.; Garces, J.M.; Meima, G.R.; Van Der Aalst, M.J.M., The Dow Chemical Company, US Patent 5 198 595, **1993**
26. van Donk, S.; Broersma, A.; Gijzeman, O.L.J.; Bitter, J.H.; de Jong, K.P.; *Stud. Surf. Sci. Catal.* **2001** (135) 269-269.
27. Koster, A.J.; Ziese, U.; Verkleij, A.J.; Janssen, A.H.; de Jong, K.P.; *J. Phys. Chem. B*, **2000** (104) 9368-9370
28. Ogura, M.; Shinomiya, S.; Tateno, J.; Nara, Y.; Kikuchi, E.; Matsukata, M.; *Chem. Lett.*, **2000** (29) 882
29. Ogura, M.; Shinomiya, S.; Tateno, J.; Nara, Y.; Nomura, M.; Kikuchi, E.; Matsukata, M.; *Appl. Catal., A*, **2001** (219) 33-43
30. Groen, J.C.; Jansen, J.C.; Moulijn, J.A.; Pérez-Ramirez, J.; *J. Phys. Chem. B*, **2004** (108) 13062-13065
31. Groen, J.C.; Moulijn, J.A.; Pérez-Ramírez, J.; *Microporous Mesoporous Mater.*, **2005** (87) 153-161
32. Groen, J.C.; Sano, T.; Moulijn, J.A.; Pérez-Ramírez, J.; *J. Catal.*, **2007** (251) 21-27
33. Li, X.; Prins, R.; van Bokhoven, J.A.; *J. Catal.*, **2009** (262) 257-265
34. van Laak, A.N.C.; Gosselink, R.W.; Sagala, S.L.; Meeldijk, J.D.; de Jongh, P.E.; de Jong, K.P.; *Appl. Catal., A: Gen*, **2010** (382) 65-72
35. Kremer, J.R.; Mastronarde, D.N.; McIntosh, J.R.; *J. Struct. Biol.*, **1996** (116) 71-76
36. Nickell, S.; Förster, F.; Linaroudis, A.; Net, W.D.; Beck, F.; Hegerl, R.; Baumeister, W.; Plitzko, J.M.; *J. Struct. Biol.*, **2005** (149) 227-234
37. Ridler, T.W.; Calvard, S.; *IEEE T Syst Man Cyb.*, **1978** (8) 630-632
38. Bellussi, G.; Pazzuconi, G.; Perego, C.; Girotti, G.; Terzoni, G.; *J. Catal.*, **1995** (157) 227-234
39. Katada, N.; Takeguchi, T.; Suzuki, T.; Fukushima, T.; Inagaki, K.; Tokunaga, S.; Shimada,

H.; Sato, K.; Oumi, Y.; Sano, T.; *Appl. Catal., A*, **2005** (283) 63-74
40. Katada, N.; Takeguchi, T.; Suzuki, T.; Fukushima, T.; Inagaki, K.; Tokunaga, S.; Shimada, H.; Sato, K.; Oumi, Y.; Sano, T.; *Appl. Catal., A*, **2005** (283) 75-84
41. Müller, M.; Harvey, G.; Prins, R.; *Microporous Mesoporous Mater.*, **2000** (34) 281-290
42. Friedrich, H.; de Jongh, P.E.; Verkleij, A.J.; de Jong, K.P.; *Chem. Rev.*, **2009** (109) 1613-1629
43. Corma, A.; *Chem. Rev.* , **1997** (97) 2373-2420
44. Ban, S.; van laak, A.N.C.; de Jongh, P.E.; van der Eerden, J.P.J.M.; Vlugt, T.J.H.; *J. phys. Chem. C*, **2007** (111) 17241-17248
45. Thibault-Starzyk, F.; Stan, I.; Abelló, S.; Bonilla, A.; Thomas, K.; Fernandez, C.; Gilson, J.P.; Pérez-Ramírez, J.; *J. Catal.*, **2009** (264) 11-14
46. Kapteijn, F.; Marin, G.B.; Moulijn, J.A.; *Catalytic Reaction Engineering*, in *Catalysis: An Integrated Approach.*,(van Santen, R.A.; van Leeuwen, P.W.N.M.; Moulijn, J.A.; Averill, B.A., Eds), Elsevier: Amsterdam. **1999** 405-406
47. Guisnet, M.; Costa, L.; Ribeiro, F.R.; *J. Mol. Catal. A: Chem.*, **2009** (305) 69-83

.

4

Alkaline Treatment of Template containing Zeolites: Introducing Mesoporosity while preserving Acidity

Abstract

Alkaline treatment (desilication) is an effective treatment to increase mesoporosity. However, the concomitant decrease in Si/Al ratio affects the strengths of the acidic sites and hence catalytic activity and selectivity. Therefore instead we subjected *template containing* zeolites to 1 M NaOH to induce additional porosity. All zeolites tested (ZSM-5, ZSM-12 and Beta) consisted of small crystallites (30 to 200 nm) that were agglomerated into larger particles between 1 and 5 μm. Inter-crystalline mesopore formation occurred by slowly removing outer layers of individual crystallites, thereby preserving the Si/Al ratio as well as the crystallinity. The external surface area of ZSM-5 was increased from 90 to 149 $m^2 \cdot g^{-1}$ and for zeolite Beta from 70 to 158 $m^2 \cdot g^{-1}$. The catalytic performance was tested for etherification of 1,2-propylene glycol with 1-octene to form octyl-ether. For ZSM-5, conversion increased from 1.2 to 5.6 % upon alkaline treatment in the presence of a template, while only to 5 % for the template-free treated sample with a significantly higher external surface area (205 $m^2 \cdot g^{-1}$). The parent zeolite Beta was significantly more active (30 % conv., 88 % sel.) compared to ZSM-5. Nevertheless upon alkaline treatment in the presence of the template a significant increase in activity (40 % conv., 88 % sel.) was observed. As only the mesoporosity was changed upon alkaline treatment it suggests that the etherification of 1,2-propylene glycol with 1-octene is affected by intra-crystalline diffusion. Our work illustrates the possibilities to use alkaline treatment of templated zeolites to decouple accessibility changes from acidity, and to gain further insight in zeolite catalysis.

1 Introduction

Zeolites are microporous crystalline aluminosilicates that represent an important class of catalysts in the petrochemical industry. Finding new and improved synthesis routes has been essential to the success of zeolites. An important development in zeolite synthesis was the use of organic molecules ,such as the tetramethylammonium (TMA) halide or hydroxide, that can facilitate the synthesis of known and new zeolites [1-4]. Nowadays these structure directing agents, such as alkyl-ammonium hydroxides and amines, have greatly contributed to the content of the Atlas of Zeolites [5] that contains over 190 structures.

Post-synthesis treatments, such as steaming and acid-leaching, are important to induce mesoporosity and further enhance the catalytic performance of zeolites, especially in diffusion limited reactions [6]. Recently also alkaline treatment (desilication) was explored as a post-synthesis tool to increase the porosity, and thereby the activity, of zeolites [7, 8]. The desilication process was further improved by Groen et al. [9, 10] who determined that the best results for ZSM-5 are obtained with 0.2 M NaOH for 30 min at 328 K with a Si/Al ratio between 25 and 50 at/at. At lower values the aluminum prevents desilication, thereby limiting mesopore formation, while at higher values complete dissolution occurs. It was also observed that alkaline treatment can affect tetrahedrally coordinated aluminum, resulting in loss of acidic properties of zeolite Beta [11] thereby decreasing the catalytic activity. Recently Holm et al. [12] showed that desilication of ZSM-5 zeolite results in the formation of strong Lewis sites most likely as a result from extra framework aluminum. Groen et al. [13] and Fernandez et al. [14] showed that desilication leads to redistribution of aluminum and enrichment of aluminum at the external surface and near the pore mouths.

Several studies show that templates can be helpful for successful alkaline treatment. Perez-Ramirez et al. reported that partial de-templation followed by alkaline treatment [15] can be used to tune the desilication process and that the addition of template molecules (TPA^+ or TBA^+) during desilication can be used as pore growth moderators [16]. Holm et al. showed that a TMA-hydroxide solution can be used a to obtain mesoporous zeolite Beta [17]. A study by Wei et al. [18] showed that templated ZSM-12 samples with Si/Al ratio up to 500 (at/at) were protected from silicon extraction during alkaline treatment.

In this study alkaline treatment on template containing zeolites with industrial importance, such as ZSM-5, ZSM-12 and zeolite Beta, is discussed. It is shown that alkaline treatment on templated zeolites can be used to increase the porosity without

changing the crystallinity or acidity of the zeolites regardless of the framework type and Si/Al ratio. This enables the decoupling of accessibility and acidity, and can be used to improve the scope as well as the understanding of zeolite catalyzed reactions.

2 Experimental

2.1 Zeolite synthesis

ZSM-5 was synthesized at the laboratories of ExxonMobil European Technology (Machelen, Belgium) according to US Patent 5 672 331 [19] starting from a mixture with molar composition: $0.065Na_2O$: $0.025Al_2O_3$: SiO_2: 0.1TPABr: $15H_2O$. Based on the total weight of the synthesis mixture 40 ppm of colloidal silicalite seeds were added as a slurry. The mixture was heated in a stainless steel autoclave at 423 K for 72 h under static conditions.

ZSM-12 was synthesized according to ref [20] with some modifications. In a typical synthesis, 0.041 g of $NaAlO_2$ (technical grade, Riedel de Häen) was dissolved into 1.35 g of H_2O (Millipore water, resistivity > 18 MΩ•cm at 25 ˚C) and 5.15 g of tetraethylammonium hydroxide solution (TEAOH, 35 wt%, Sigma-Aldrich). To this solution, 10 g of colloidal silica was added (Ludox HS30, 30 wt. % suspension in H_2O, Sigma-Aldrich), which resulted in a clear gel with a molar composition of 1.0 SiO_2: 0.005 Al_2O_3: 0.1225 TEA_2O: 13.0 H_2O. The mixture was stirred at room temperature for 1 h, and then transferred into a teflon-lined steel autoclave with a full capacity volume of 50 ml (inner diameter of the teflon bottle of 34 mm and height of 55 mm). The autoclave was placed in an oven at 433 K for 5.5 days, and afterwards quenched with tap water. The precipitated product was washed with three batches of hot water (343-353 K). The powder product was obtained by filtration, and dried at 333 K overnight. The ZSM-12 sample has a Si/Al ratio of 105 and is referred to as ZSM-12-(105). A second ZSM-12 was prepared analogous to MTW-1, except that 0.071 g of $NaAlO_2$ was used resulting in a gel with molar composition of 1.0 SiO_2: 0.0086 Al_2O_3: 0.1225 TEA_2O: 13.0 H_2O. This sample has a Si/Al ratio of 63 and is referred to as ZSM-12-(63Zeolite Beta was synthesized according to ref [21] with some modifications. In a typical synthesis, 2.40 g of silica (Sipernat 50, Evonik Degussa), 0.156 g of $Al(OH)_3$ (> 63.5 % Al_2O_3, Acros), and 0.592 g of NH_4F (> 98%, Sigma-Aldrich) were added to 7.57 g of a tetraethylammonium hydroxide solution (TEAOH, 35 wt%, Sigma-Aldrich), which resulted in a gel with a molar composition of 1.0 SiO_2: 0.025 Al_2O_3: 0.225 TEA_2O: 0.4 NH_4F: 7.14 H_2O. The

mixture was stirred at room temperature for 1 hour, and then transferred into a teflon-lined steel autoclave with a full capacity volume of 50 ml (inner diameter of the teflon bottle of 34 mm and height of 55 mm). The autoclave was treated in a preheated oven at 443 K for 3 days, and afterwards quenched with tap water. The precipitated product was washed with three batches of hot water (343-353 K). The powder product was obtained by filtration, dried at 333 K overnight.

2.2 Alkaline treatment

Alkaline treatment was performed by adding 0.7 g of zeolite to 40 ml pre-heated alkaline solution (0.2, 0.5 or 1.0 M NaOH) (p.a., Merck) at 343 K, while stirring. This was followed by centrifugation (Eppendorf centrifuge 5804, 5000 rpm, 5 min.), for zeolite Beta by ultra-centrifugation (Sorvall *RC5*$^{+}$ SS34 rotor, 18000 rpm, 1 min.) and decantation of the liquid followed by re-suspension with hot demineralized water. This procedure was repeated until the pH was 7 or less. The obtained sample will be referred to as zeolite-*at[treatment time]*, after calcination (823 K, 3h, 1K·min^{-1}) zeolite- *at[treatment time]-cal* is obtained.

To obtain the proton form of the zeolites, ion-exchange was performed in an aqueous 1 M NH_4NO_3 (p.a., Acros) solution at 353 K for 24 h, followed by filtering and washing. Per gram of zeolite 12 ml of ammonium nitrate solution was used. This procedure was repeated three times followed by calcination in air at 773 K for 3h using a heating rate of 1 K·min^{-1}. After the additional ion-exchange followed by calcination the obtained zeolite is referred to as *H-zeolite-at[treatment time]-cal.*

2.3 Structural characterization

Powder X-ray diffraction (XRD) patterns were obtained using a Bruker-Axs D8 series 2 with a $Co_{\alpha 1,2}$ source (λ = 0.179 nm). The porosity of the samples was studied using N_2 physisorption isotherms, which were recorded with a Micromeritics Tristar 3000 at 77 K. Prior to the physisorption measurements, the samples were dried overnight at 573 K in flowing nitrogen. The t-plot method [22] was applied to obtain the micro pore volume and the external surface area. Pore size distributions were obtained from the adsorption branch using the BJH-method [23]. The mesopore volume was calculated by integrating these plots from 2 to 50 nm. Ammonia temperature programmed desorption (TPD) was performed with a Micromeritics Autochem II. About ~150 mg of sample was dried at 573 K with a heating ramp of 5 K·s^{-1} and kept there for 30 min after which the sample was cooled down to 473 K. After saturating the sample with ammonia, a 30

min dwell time was applied to obtain a stable baseline. Subsequently the temperature was increased to 923K with a heating rate of 10 $K \cdot s^{-1}$ and was kept there for 30 min. *n*-Hexane adsorption measurements were performed with a tapered element oscillating microbalance (TEOM) as described by Bitter et al. [24]. Morphology and crystal sizes were determined with a Tecnai FEI XL 30SFEG Scanning Electron Microscope (SEM) at 15 kV and with a Tecnai 20 Transmission Electron Microscope operated at 200 kV.

2.4 Catalysis

In a typical etherification reaction 0.05 mol of glycerol, 0.15 mol of 1-octene and 0.3 g of catalyst were loaded in a 100 ml stainless steel Parr autoclave. The autoclave was flushed with argon three times and then pressurized with argon to 10 bar. The autoclave was heated to 413 K and the solution was continuously mechanically stirred (750 rpm). The starting point of the reaction was taken when the autoclave reached the reaction temperature. After 3 h the reaction was stopped, the autoclave was cooled to 313 K and the reaction mixture was dissolved in a known amount of ethanol. The catalyst was separated by filtration, and a sample of the solution was taken for further analysis. More information about the procedure and analytical methods is described elsewhere [25]. Four ZSM-5 samples as well as four zeolite Beta samples were tested: H-ZSM-5-*cal,* H-ZSM-5-*cal-at(0.2, 20),* H-ZSM-5-*cal-at(0.5, 20),* H-ZSM-5-*at(60)-cal,* Beta-cal, Beta-at(*15)-cal*, Beta-at(*120)-cal* and H-Beta-at(*120)-cal*.

3 Results and discussion

Figure 1 shows SEM images of three template containing zeolites: ZSM-5 (MFI), ZSM-12 (MTW) and zeolite Beta (BEA). All zeolites samples consist of small crystallites that have agglomerated into larger particles.

3.1 ZSM-5 (MFI)

The ZSM-5-parent had uniform particles with dimensions between 1 and 1.5 μm (Fig. 1A), that consisted of agglomerated nano-crystallites ranging from approximately 20 to

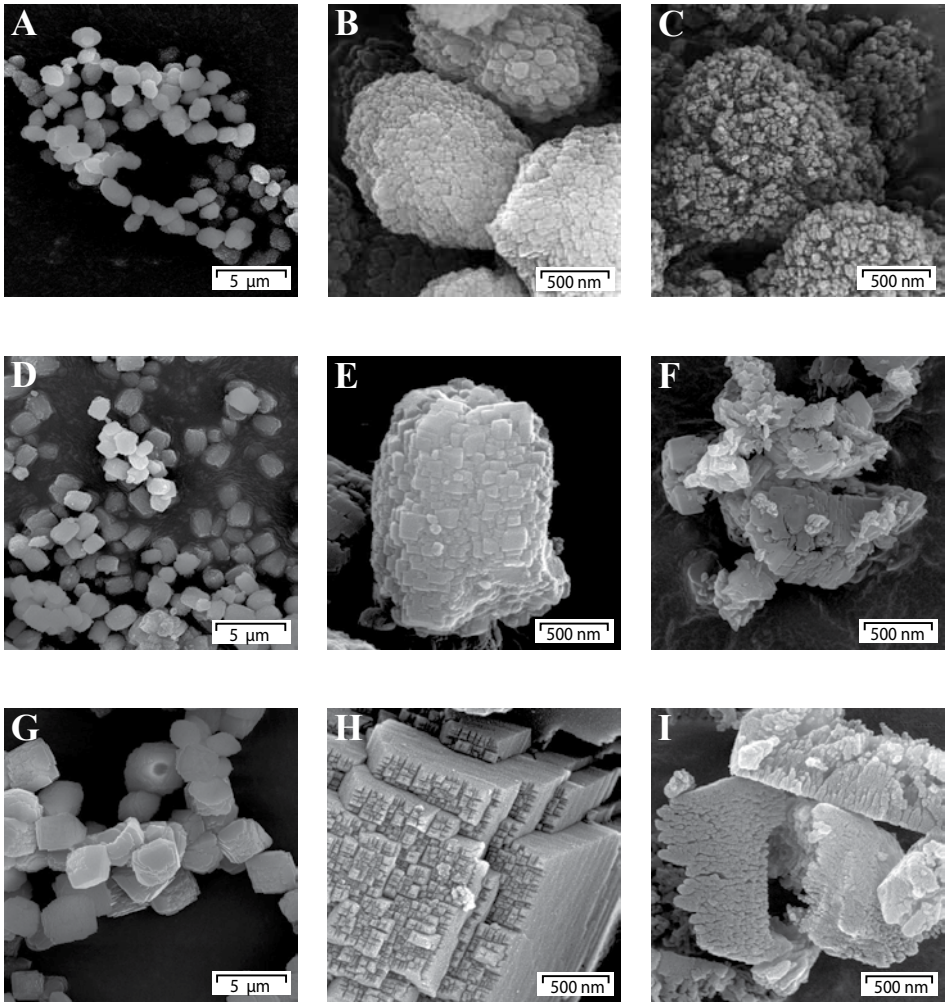

Fig. 1. SEM images of (A) ZSM-5-parent, (B) ZSM-5-parent, (C) ZSM-5-at(60), (D) ZSM-12-(105)-parent, (E) ZSM-12-(105)-parent, (F) ZSM-12-(105)-at(60), (G) Beta-parent, (H) Beta-parent, (I) Beta-at(120).

100 nm in size (Fig 1B). The ZSM-5-parent displayed no micropore volume due to the presence of the TPA template and a low external surface area of 21 $m^2 \cdot g^{-1}$ (Table 1). The mesopore volume is almost nil as a result of the dense packing of the crystallites. Upon calcination a micropore volume of 0.13 $cm^3 \cdot g^{-1}$ was obtained while the external surface area (A_{ext}) had increased to 94 $m^2 \cdot g^{-1}$. For direct comparison we will now first discuss the impact of alkaline treatment on template-free ZSM-5, and then the results for alkaline treatment on template-containing ZSM-5.

Alkaline treatment on template free ZSM-5 (after calcination) is described to be most effective for Si/Al ratios between 25 and 50 at/at with 0.2 M NaOH for 30 min [9, 10]. Because of the small crystallites of the present ZSM-5 samples, a shorter treatment of 20 min in 0.2 M NaOH was performed. This resulted in the formation of a highly porous H-ZSM-5 sample with an external surface area of 205 $m^2 \cdot g^{-1}$ (Table 1, Fig. 2). Alkaline treatment in 0.5 M NaOH solution for 20 min resulted in an even higher external surface area of 233 $m^2 \cdot g^{-1}$ (Table 1, Fig. 2). For both treatments the micropore volume was preserved. BJH analysis shows a predominant pore size of ~10 nm for the 0.2 M and ~20 nm for the 0.5 M NaOH treated samples. These results are close to the literature values described by Groen et. al. [10] for which an external surface area of 235 $m^2 \cdot g^{-1}$ and a predominant pore size of 10 nm is observed upon desilication of ZSM-5 zeolites. The initial Si/Al ratios (37-42 at/at) in Groen's study of desilicated ZSM-5 zeolites are significantly higher compared to the Si/Al ratio (18 at/at) of the ZSM-5 zeolite used in this study. Although desilication is a powerful tool to enhance accessibility it is accompanied by a decrease in Si/Al ratio [8]. For our samples a decrease in Si/Al ratio from 18 to 13 and 9 at/at was observed (Table 1). This implies that the acidity is changed, which can negatively affect catalysis [11-14].

A different approach to increase the accessibility of the ZSM-5 zeolite was performed

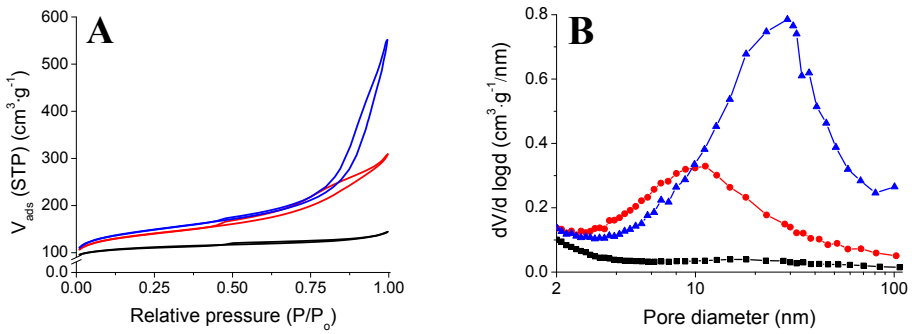

Fig. 2. Nitrogen physisorption isotherms (A) and BJH desorption curves (B) of ■ ZSM-5-cal, ● H-ZSM-5-cal-at(0.2, 20) and ▲ H-ZSM-5-cal-at(0.5, 20).

by treating the parent ZSM-5 with the template still present, in alkaline solution of 1 M NaOH at 343 K for 20 to 60 min. Nitrogen physisorption (Fig. 3A) showed that alkaline treatment for 20 min resulted in an increased nitrogen uptake due to the formation of mesopores. A longer treatment time of 30 and 60 min. shows an increased uptake of nitrogen that occurs at higher relative pressures indicating the formation of larger mesopores. From the BJH pore size distribution (Fig. 3B) we observe that mesopores of ~20 nm are present after 20 min of alkaline treatment that slowly grow with increased treatment time into large meso- and macro-pores with an predominant size of 30 and 60 nm. In Table 1 the textural properties of the samples are listed. A continual increase in the external surface area is observed from the 21 $m^2 \cdot g^{-1}$ for the parent to 77 $m^2 \cdot g^{-1}$ for ZSM-5-*at(60)*. A likely explanation for these observations is that upon alkaline treatment small layers of the external surface area of the crystallites are dissolved, thereby increasing the mesoporosity of the agglomerates [26]. This hypothesis is further strengthened by the fact that neither the bulk Si/Al ratio (Si/Al=18 at/at both before and after alkaline treatment) nor the crystallinity (Fig. 5A) changed upon treatment. SEM (Fig. 1C) confirms that after alkaline treatment added mesoporosity is apparent

Table 1. Textural properties of ZSM-5 samples.

Sample	V_{micro} [a] ($cm^3 \times g^{-1}$)	A_{ext} [a] ($m^2 \times g^{-1}$)	V_{meso} [b] ($cm^3 \times g^{-1}$)	V_{total} [c] ($cm^3 \times g^{-1}$)	Si/Al [d] (at/at)	*n*-hexane uptake (wt.%)
ZSM-5-*parent*	-	21	0.04	0.05		
ZSM-5-*cal*	0.13	94	0.06	0.22		2.9
H-ZSM-5-*cal*	0.13	92	0.06	0.23	18	
Treated without template						
H-ZSM-5-*cal-at(0.2, 20)*	0.12	205	0.26	0.48	13	
H-ZSM-5-*cal-at(0.5, 20)*	0.12	233	0.49	0.80	9	
Treated with template						
ZSM-5-*at(20)-cal*	0.13	121	0.15	0.33	18	3.0
ZSM-5-*at(30)*	-	61	0.22	0.28		
ZSM-5-*at(30)-cal*	0.13	129	0.26	0.47		
ZSM-*5-at(20)*	-	52	0.12	0.15		
ZSM-5-*at(60)*	-	77	0.20	0.58		
ZSM-5-*at(60)-cal*	0.13	144	0.23	0.73	18	
H-ZSM-5-*at(60)-cal*	0.13	149	0.21	0.69	18	

[a] t-plot method
[b] BJH-method (adsorption branch)
[c] @ $p/p_o = 0.995$
[d] ICP-AES

between the crystallites within particles. If the ZSM-5 is calcined prior to the alkaline treatment in 1 M NaOH complete dissolution occurred within minutes. After calcination all ZSM-5 samples show, whether alkaline treated or not, a similar micropore volume (Table 1). The mesoporosity is unaffected by the calcination step (Fig. 4). *n*-Hexane uptake measurements indicated that the micropores are fully accessible also for large molecules with similar values as those described in literature (Table 1, Fig. 6) [24]. NH_3 TPD measurements were performed on the proton form of the ZSM-5 to probe the acid sites. Similar curves for parent and alkaline treated ZSM-5 indicate that the acid sites are completely preserved (Fig. 5B). A slight shift is observed towards lower temperatures, which could be the result of faster transport of NH_3 [27] because of the added mesoporosity.

Comparing the alkaline treatment with and without template, we can conclude that without a template a significantly larger increase in external surface area is obtained. A second advantage is that the combination of intra- and inter-crystalline mesopores provides an effective reduction of the path length towards the active sites [13]. However,

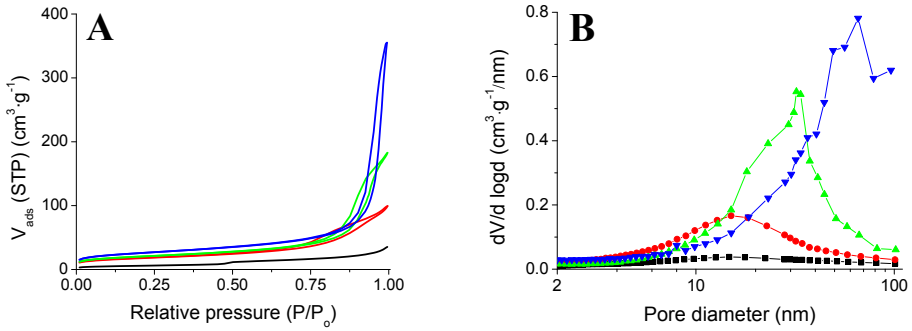

Fig. 3. Nitrogen physisorption isotherms (A) and BJH desorption curves (B) of ■ ZSM-5-parent, ● ZSM-5-at(20), ▲ ZSM-5-at(30) and ▼ ZSM-5-at(60).

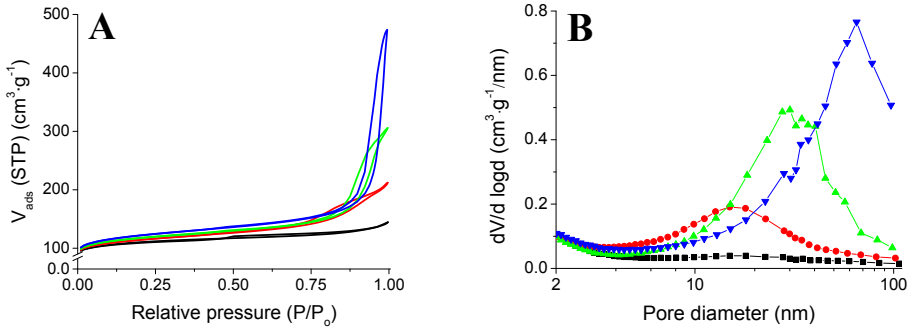

Fig. 4. Nitrogen physisorption isotherms (A) and BJH desorption curves (B) of ■ ZSM-5-cal, ● ZSM-5-at(20)-cal, ▲ ZSM-5-at(30)-cal and ▼ ZSM-5-at(60)-cal.

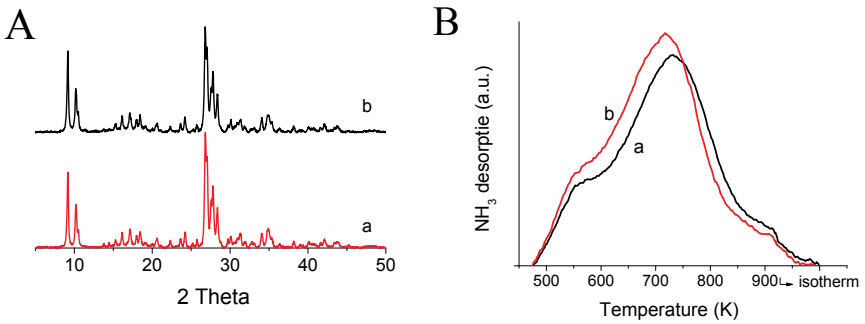

Fig. 5. (A) XRD pattern and (B) Ammonia TPD curves of H-ZSM-5-cal (a) and H-ZSM-5-at(60)-cal (b).

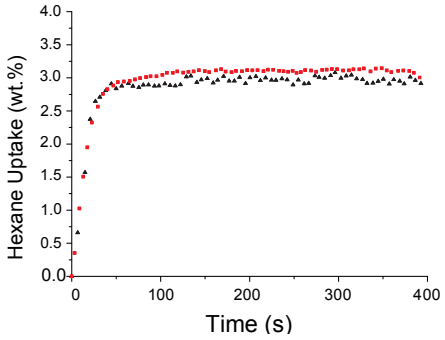

Fig. 6. *n*-Hexane uptake curve of parent ZSM-5-parent and ZSM-5-at(20).

the Si/Al ratio decreases, and hence the strength of the acid sites. Although alkaline treatment on template-containing samples gives a more modest increase in surface area, this is obtained without altering the acid site strength. Hence alkaline treatment in the presence of a template might provide a very useful strategy if extra mesoporosity is desirable, but the properties of the acid sites, such as for instance reflected in the selectivity when used as a catalyst, should not be affected.

3.2 ZSM-12 (MTW)

ZSM-12 samples were synthesized in two different gel compositions resulting in two samples ZSM-12-(105) and ZSM-12-(63) with Si/Al ratios of 105 and 63, respectively. The morphology of the two samples was very similar, consisting of agglomerates (1 μm × 2 μm, Fig. 1D) that contained small crystallites ranging in size from approximately 50 to 200 nm (Fig. 1E).

Alkaline treatment was performed in 1 M NaOH at 343 K on the non-calcined ZSM-12 samples (Table 2). Only minor differences between the two samples are observed.

Table 2. Textural properties of ZSM-12 samples.

Sample	V_{micro} [a] ($cm^3 \times g^{-1}$)	A_{ext} [a] ($m^2 \times g^{-1}$)	V_{meso} [b] ($cm^3 \times g^{-1}$)	V_{total} [c] ($cm^3 \times g^{-1}$)	Si/Al [d] (at/at)
ZSM-12-(105)	-	1	-	0.01	105
ZSM-12-(105)-*at(15)*	-	36	0.05	0.06	-
ZSM-12-(105)-*at(30)*	-	47	0.15	0.24	-
ZSM-12-(105)-*at(60)*	-	39	0.07	0.26	99
ZSM-12-(63)	-	2	-	0.01	63
ZSM-12-(63)-*at(15)*	-	42	0.05	0.06	-
ZSM-12-(63)-*at(30)*	-	46	0.11	0.13	-
ZSM-12-(63)-*at(60)*	-	44	0.07	0.27	60

[a] t-plot method
[b] BJH-method (adsorption branch)
[c] @ $p/p_o = 0.995$
[d] ICP-AES

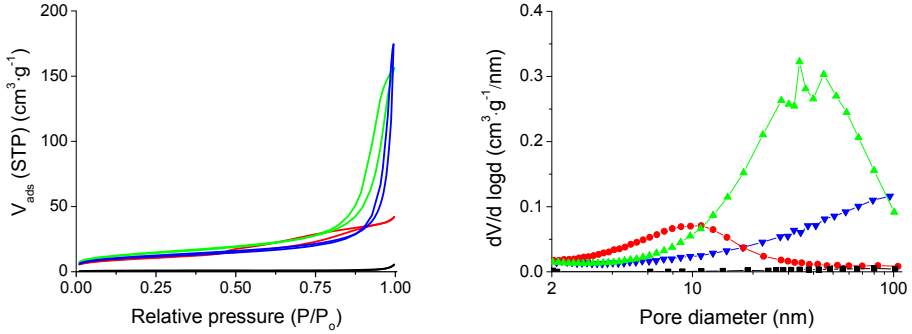

Fig. 7. Nitrogen physisorption isotherms (A) and BJH desorption curves (B) of ■ ZSM-12-(105), ● ZSM-12-(105)-at(15), ▲ ZSM-12-(105)-at(30) and ▼ ZSM-12-(105)-at(60).

The mesopore formation after 30 min is slightly higher for the aluminum poor ZSM-12-(105) (0.15 $cm^3 \cdot g^{-1}$) compared to the more aluminum rich ZSM-12-(63) (0.10 $cm^3 \cdot g^{-1}$). This is in agreement with Wei et al. [18] who observed a slightly faster rate of desilication for higher Si/Al ratio, although this could not be proven due to the presence of different amounts of template. After treatment for 60 min we observed a decrease in both mesopore volume and external surface area, and the formation of large meso- and macropores (Fig. 7). SEM images (Fig. 1F) show that the agglomerates have fallen apart into various sized smaller agglomerates. The small differences between the two samples suggest that there is a minor influence of the aluminum content on alkaline treatment, and that the alkaline treatment is primarily controlled by the presence of the template.

Our results show that alkaline treatment in 1 M NaOH at 343 K enhances the

mesoporosity when applied to different commercially available zeolites. The results on the low aluminum content ZSM-12 demonstrate that mesoporosity can be introduced by alkaline treatment in the presence of a template , regardless of the Si/Al ratio, whereas without a template present this is limited to a upper Si/Al ratio of ~50 (at/at) [9]. The differences that exist between the tested samples seem to be the result of the particle/crystallite size of the parent material.

3.3 Beta (BEA)

The morphology of the synthesized zeolite Beta (Fig. 1G) was slightly different from the other two zeolites. No individual crystallites were observed, but instead large truncated bipyramidal crystals with smooth surfaces and a width of 5 μm. Higher magnification reveals that the top of the crystallites is covered with small extrusions between 20 and 30 nm in size (Fig. 1H).

Alkaline treatment in 1 M NaOH for 15 min on the template containing zeolite Beta followed by calcination resulted in an increase in external surface from 70 to 181 $m^2 \cdot g^{-1}$

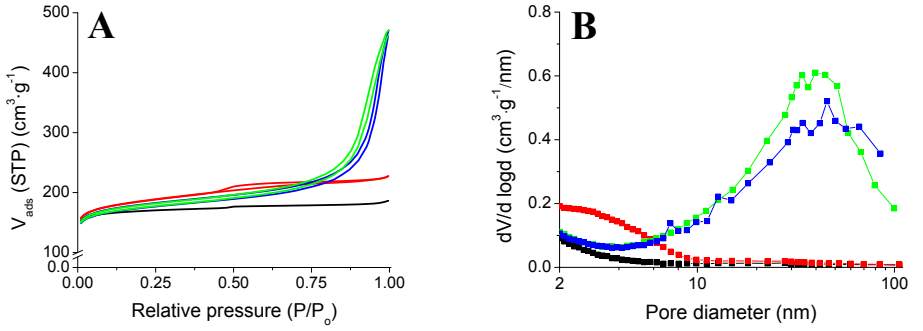

Fig. 8. Nitrogen physisorption isotherms (A) and BJH desorption curves (B) of ■ Beta-cal, ● Beta-at(15)-cal, ▲ Beta-at(120)-cal and ▼H-Beta-at(120)-cal.

Table 3. Textural properties of zeolite Beta samples.

Sample	V_{micro} [a] ($cm^3 \times g^{-1}$)	A_{ext} [a] ($m^2 \times g^{-1}$)	V_{meso} [b] ($cm^3 \times g^{-1}$)	V_{total} [c] ($cm^3 \times g^{-1}$)	Si/Al [d] (at/at)
Beta-cal	0.23	77	0.03	0.29	17
Beta-at(*15*)-*cal*	0.21	181	0.09	0.35	-
Beta-at(*120*)-*cal*	0.21	164	0.34	0.73	16
H-Beta-at(*120*)-*cal*	0.20	158	0.29	0.54	-
Zeolyst-*CP 814E-cal*	0.17	227	0.36	0.83	12.5

[a] t-plot method
[b] BJH-method (adsorption branch)
[c] @ p/p_o = 0.995
[d] ICP-AES

and similar micropore volume (Table 3, Fig. 8A). The BJH pore size distribution (Fig. 8B) shows that upon alkaline treatment for 15 min small mesopores between 2 and 10 nm have formed. Another alkaline treatment was performed for 120 min, which resulted in a slightly lower external surface area of 164 $m^2 \cdot g^{-1}$ compared to the 15 min treatment. This sample has large mesopores of ~ 40 nm (Fig. 8B) and SEM images (Fig. 1I) show that some of the particles have fallen apart into smaller fragments, similar to what is observed for the ZSM-12 sample after 60 min of treatment. To prevent the loss of small clusters of zeolite Beta all washing steps were followed by ultra-centrifugation, from which clear fluids were decanted. The smaller agglomerate fractions allowed the use of TEM to look at the crystallites (Fig. 9). The interior of zeolite Beta consisted of smaller crystallites that are aligned parallel with inter-crystalline porosity.

No sodium was present during synthesis, hence calcination resulted in the proton form of zeolite Beta. NH_3 TPD measurements were performed to measure if the alkaline treatment affects the acidity. For the Beta-parent two peaks (Fig. 10a) were observed, the first peak at ~ 475 K is ascribed to weak Lewis acid sites, and the second peak at ~670 K [28] to Brønsted acid sites [29]. For comparison a commercially available zeolite

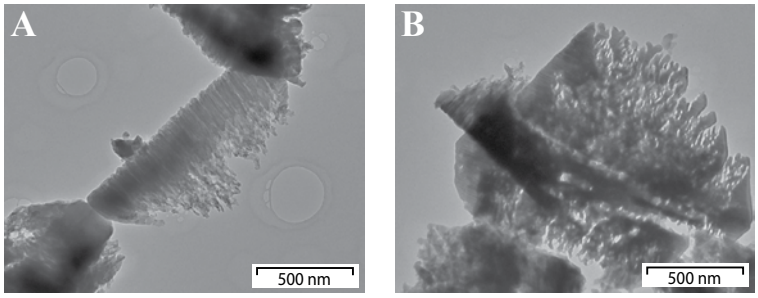

Fig. 9. TEM images of Beta-at(120).

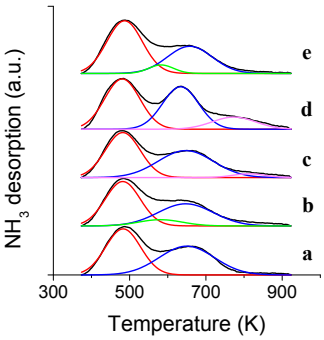

Fig. 10. Ammonia TPD curves of Beta-parent (a), Beta-at(120)-cal (b), H-Beta-at(120)-cal (c), Zeolyst Cp814N (d) and Beta-at(15)-cal (e).

Beta from Zeolyst was analyzed (Fig. 10d). A similar pattern was observed with slightly more Brønsted acid sites. This is a direct result of the lower Si/Al ratio (12.5 at/at) and confirmed the assignment of the peak. For the Zeolyst material a third peak or shoulder is observed at ~ 780 K, which could be the result of strong Lewis acid sites. Compared to the parent no change for the weak Lewis acidity (~475) was observed after 15 min of alkaline treatment (Fig. 10e). The Brønsted acidity (~670 K) is slightly lower compared to the parent and deconvolution revealed a fourth peak at 570 K. This peaks might be the result of NH_3 adsorption on Na^+ sites, which is a weaker than NH_3 adsorption on H^+ sites and desorption therefore occurs at lower temperatures [30]. After 120 min of alkaline treatment a similar pattern as for 15 min was observed although the peak at ~780 K is slightly increased (Fig. 10b). The percentage NH_3 adsorbed onto Na^+ ions is approximately between 15 and 20 % of the total cationic sites of the zeolite. Upon ion exchange and calcination of the Beta-at(120)-cal sample the Na^+ peak at 570 K disappears (Fig. 10c), thereby restoring Brønsted acidity. Clearly during alkaline treatment some cationic sites are ion-exchanged with sodium. Presumably this ion-exchange occurs close to the external surface area as the template is still present inside the micropores after ion exchange. This implicates that an additional ion exchange/calcination step is necessary to obtain a fully active catalyst.

3.4 Catalysis

We have sofar seen that the porosity can be increased with alkaline treatment without changing the acidity (or bulk Si/Al ratio). It is hence interesting to test if the catalytic performance is enhanced. The influence of the alkaline treatment on the catalytic properties of Beta and ZSM-5 zeolites was investigated in the etherification of 1,2-propylene glycol with 1-octene (Scheme 1). The direct etherification of biomass-based glycols was recently reported to take place with high activity and selectivity over the H-Beta zeolites [25, 31,

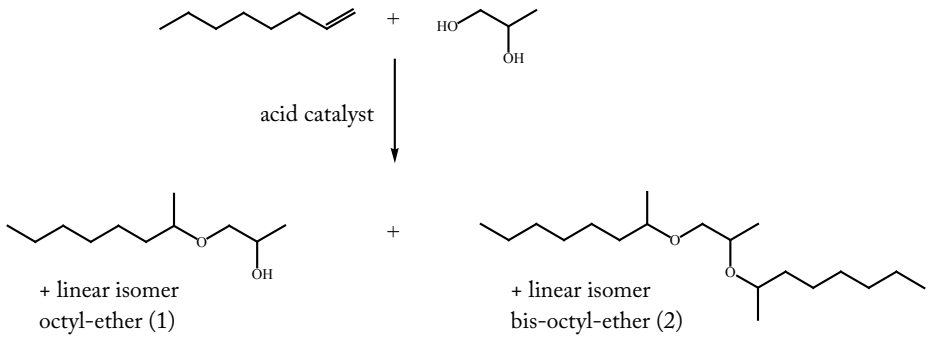

Scheme 1. Etherification of 1,2-propylene glycol with 1-octene.

32]. Furthermore, the etherification activity of the H-Beta zeolites was correlated to both the crystal size and the external surface area of the zeolite, [25, 31, 32], where most probably the reaction takes place as observed by confocal fluorescence microscopy [32]. ZSM-5 was found to be less active and selective than zeolite Beta [25]. The etherification of 1,2-propylene glycol with 1-octene was therfore chosen as a test reaction for the effect of the alkaline treatment on the catalytic activity of the zeolites. The tests were performed at low conversions of the alcohol substrate in order to be able to relate catalytic activity of the zeolite with the pretreatment process. The results of the etherification of 1,2-propylene glycol with 1-octene are presented in Table 4 and are compared to a commercial Beta and ZSM-5 zeolites (Zeolyst-*CP 814E)*, with smaller particle size which previously showed a very high activity for this reaction [25, 31]. The etherification of 1,2-propylene glycol with 1-octene over all H-ZSM-5 and H-Beta zeolites were produced with high selectivity towards octyl-ether (Table 4). Side products were small amounts of di-ether (C16), and dehydrated and cyclic derivatives of 1,2-propylene glycol, consistent with previously reported results [25, 31]. The untreated H-ZSM-5-cal has a low conversion (1.2 %) similar to values obtained in literature [25]. The selectivity is with 95 % towards the mono-isomer (Table 4) significantly better than the values described in literature (<82 % after 5 hours of reaction) [25]. The alkaline treated H-ZSM-5-cal-at(0.2, 20) showed a fourfold increase in conversion (5.0 %) as well as a slightly better selectivity. The alkaline treatment on the template containing ZSM-5 (H-ZSM-5-at(60)-cal) resulted in the best catalytic performance with a conversion of 5.6 % and a selectivity of 98%. This is at first sight unexpected, as the porosity of the H-ZSM-5-at(60)-cal is considerably

Table 4. Etherification of 1,2-propylene glycol with 1-octene over ZSM-5 and Beta zeolites

Sample	Conv. (%)	$Sel._{C8\text{-}ether}$ (%)	$Sel._{C16\text{-}ether}$ (%)	$Sel._{other}$ (%)
H-ZSM-5-*cal*	1.2	95	0	5
H-ZSM-5-*cal-at(0.2, 20)*	5.0	97	1	2
H-ZSM-5-*cal-at(0.5, 20)*	3.8	96	2	2
H-ZSM-5-*at(60)-cal*	5.6	98	1	1
Beta-cal	33	88	3	9
Beta-at(*15)-cal*	26	91	4	5
Beta-at(*120)-cal*	23	91	4	5
H-Beta-at(*120)-cal*	40	88	5	7
Zeolyst-*CP814N*	45	90	4	6

Reaction conditions: 0.3 g catalyst, 0.05 mol 1,2-propylene, 0.15 mol 1-octene, 413 K, 3 h, 10 bar Ar.

lower than that of H-ZSM-5-cal-at(0.2/0.5, 20) (149 vs. 205 and 233 $m^2 \cdot g^{-1}$). A plausible explanation is that the pore entrances of the H-ZSM-5-cal-at(0.2/0.5, 20) samples are partly obstructed by extra framework aluminum [14].

Prior to testing, the parent and alkaline treated zeolite Beta samples (Table 3) were calcined to obtain the proton form. One sample, H-Beta-at(*120)-cal*, received an NH_4-ion exchange in 1 M NH_4NO_3 followed by calcination in air. The etherification of 1,2-propylene glycol with 1-octene over all H-Beta zeolites produced mainly the octyl-ethers with selectivities over 88 % (Table 4). The mono-ether (C_8-ether) was obtained for all the catalysts as the main reaction product and the side products mostly consists of small amounts of dehydrated and cyclic derivatives of 1,2-propylene glycol, consistent with other results [25, 31]. The most active catalyst was the commercial zeolite, with a ratio of Si/Al of 12.5 and with the highest external surface (Table 3). With this catalyst a conversion of 1,2-propylene glycol of 45 % was observed after 3 h of reaction. The in-house synthesized Beta-cal (initial particle size of about ~2 μm) presented lower conversions, but a similar product distribution and selectivity was found as for the commercial zeolite. The higher external surface area of the alkaline treated zeolite Beta samples was expected to result in an increased conversion for this reaction. However, a short alkaline treatment of just 15 min was found to result in a decrease of the 1,2-propylene glycol conversion from 33 to 26 % (Table 4). This is despite the increase in external surface of 72 to 185 $m^2 \cdot g^{-1}$ upon alkaline treatment. A longer alkaline treatment of 120 min (Beta-at(120)-cal) resulted in an even lower conversion of 23 %. The selectivity towards the C_8-ether increased slightly from 88 % to 91 %, while the selectivity of the by-products decreased from 9 to 5 %. The decreased conversion can be attributed to the presence of Na^+ ions that remained after alkaline treatment (Fig.8b). As discussed in section 3.4 the Na^+ ions are expected to be located near the external surface area as the interior of the zeolite and thus the acid sites were protected from alkaline treatment by the template. After removal of the Na^+-ions upon ion exchange with NH_4NO_3 followed by calcination (H-Beta-at(120)-cal) the conversion almost doubled from 23 to 40 %. This conversion is also significantly higher than the parent Beta (33% conversion), which is expected given the higher external surface area 77 vs. 158 $m^2 \cdot g^{-1}$.

The strong increase in conversion for higher external surface areas suggests that the etherification of 1,2-propylene glycol with 1-octene is affected by intra-crystalline diffusion, as suggested earlier [25, 31]. An important factor are the pore systems of the zeolites. Comparing samples with similar Si/Al atomic ratio (~ 17 at/at) and surface area (~155 m^2 g^{-1}), zeolite Beta is much more active and not as prone to pore blocking as

ZSM-5. This is explained by their different pore geometries, with a 10-ring (5.1 × 5.5 Å) for ZSM-5 and a 12-ring channel (7.1 × 7.3 Å) for zeolite Beta. Most importantly, we can conclude that in both cases alkaline treatment of template containing zeolites results in added porosity and enhanced catalytic activity, while selectivity is unaffected or even improved.

4 Conclusions

Template containing ZSM-5 (Si/Al ratio 18 at/at) was subjected to alkaline treatment in 1 M NaOH at 343 K to induce additional mesoporosity. The ZSM-5 samples consisted of small crystallites between 20 and 100 nm in size that were agglomerated into larger particles of ~1 μm. After alkaline treatment for 60 min the external surface area was increased from 21 to 77 $m^2 \cdot g^{-1}$. Because of the presence of the template the micropores were unaffected by the alkaline treatment and after calcination the full micropore volume was obtained, while the added mesoporosity was preserved. Alkaline treatment without the template present resulted in higher external surface areas, but also in a decrease in Si/Al ratio to 13 (0.2 M NaOH) and 8 (0.5 M NaOH). SEM showed that the nature of the mesoporosity upon alkaline treatment on template containing zeolites was inter-crystalline and intra-particle. Additional experiments on ZSM-12 gave similar results and showed that the treatment can be applied to a range of zeolites regardless of the Si/Al ratio. It was also determined that the morphology of the parent zeolite, i.e. crystallite/particle size, determines the amount of added mesoporosity in which smaller crystallites give rise to higher porosities. Alkaline treatment on sodium-free zeolite Beta for 120 min led to an increase in the external surface from 77 to 164 $m^2 \cdot g^{-1}$. As a result the large Beta particles (5 μm) showed de-agglomeration, which made it possible to study the individual crystallites by TEM. NH_3-TPD measurements showed that after alkaline treatment 15 to 20 % of the total protonic sites were ion exchanged with sodium cations. The sodium cations were probably located near the external surface area, as the interior of the crystallites is protected by the templates molecules. Subsequent ion exchange/calcination was performed to convert the zeolite fully into the proton form. As a showcase reaction the catalytic performance of alkaline treated ZSM-5 and zeolite Beta were tested for the etherification of 1,2-propylene glycol with 1-octene. This reaction was previously [25, 31, 32] expected to be a surface catalyzed reaction. A 1 % conversion of 1,2-propylene glycol for the ZSM-5-parent was measured. Upon alkaline treatment

on template containing ZSM-5 the conversion increased to 5.6 % and selectivity increased from 95 % to 98 %. Conversion of 1,2-propylene glycol for the alkaline treated ZSM-5 zeolite was with 5.0 and 3.8 % lower than with a template despite a higher external surface area. For zeolite Beta significantly higher conversions were measured although upon alkaline treatment initially a decrease in conversion (33 to 23 %) was observed despite the higher porosity. However, after the NH_4-ion exchange/calcination the conversion increased to 40 %, in line with the previous studies. The presence of the sodium cations near the external surface apparently inhibited the reaction, which makes it likely that the etherification of 1,2-propylene glycol with 1-octene over zeolite Beta is affected by intra-crystalline diffusion.

During alkaline treatment of templated zeolites silicon as well as aluminum species are slowly dissolved. This process created smaller crystallites and inter-crystalline mesoporosity. The presence of the template inside the micropores assures that the acid sites are not affected by the treatment. The increase in porosity leads to enhanced catalytic performance, and provides an opportunity to decouple the acidity from accessibility of zeolites, and can be used to optimize and gain insight in zeolite catalysis.

Acknowledgements

We would like to thank Dr. M. Mertens and Dr. M.J. Janssen (ExxonMobil, Belgium) for supplying the ZSM-5 sample. S.L. Sagala for experimental work, J. Zečević for TEM, M. Versluijs-Helder for SEM, V. Koot for NH_3-TPD and ACTS-ASPECT for financial support.

References

1. Barrer, R.M.; Denny, P.J.; *J. Chem. Soc.*, **1961** 971-982
2. Barrer, R.M.; Dicks, L.W.R.; *J. Chem. Soc. A*, **1967** 1523-1529
3. Kerr, G.T., US Patent 4 703 025, **1966**
4. Barrer, R.M.; Denny, P.J.; Flanigane, E.M., US Patent 3 306 922, **1967**
5. Bearlocher, C.; McCusker, L.B.; Olsen, D.H.; *Atlas of zeolite framework types*. elsevier, 6th edition. **2007**
6. van Donk, S.; Janssen, A.H.; Bitter, J.H.; de Jong, K.P.; *Catal. Rev. Sci. Eng.*, **2003** (45) 297 - 319
7. Ogura, M.; Shinomiya, S.; Tateno, J.; Nara, Y.; Kikuchi, E.; Matsukata, M.; *Chem. Lett.*,

2000 (29) 882
8. Ogura, M.; Shinomiya, S.; Tateno, J.; Nara, Y.; Nomura, M.; Kikuchi, E.; Matsukata, M.; *Appl. Catal., A*, **2001** (219) 33-43
9. Groen, J.C.; Jansen, J.C.; Moulijn, J.A.; Pérez-Ramirez, J.; *J. Phys. Chem. B*, **2004** (108) 13062-13065
10. Groen, J.C.; Peffer, L.A.A.; Moulijn, J.A.; Pérez-Ramírez, J.; *Chem. Eur. J.*, **2005** (11) 4983-4994
11. Groen, J.C.; Abelló, S.; Villaescusa, L.A.; Pérez-Ramírez, J.; *Microporous Mesoporous Mater.*, **2008** (114) 93-102
12. Holm, M.S.; Svelle, S.; Joensen, F.; Beato, P.; Christensen, C.H.; Bordiga, S.; Bjørgen, M.; *Appl. Catal., A*, **2009** (356) 23-30
13. Groen, J.C.; Bach, T.; Ziese, U.; Paulaime-van Donk, A.M.; de Jong, K.P.; Moulijn, J.A.; Pérez-Ramírez, J.; *J. Am. Chem. Soc.*, **2005** (127) 10792-10793
14. Fernandez, C.; Stan, I.; Gilson, J.P.; Thomas, K.; Vicente, A.; Bonilla, A.; Pérez-Ramírez, J.; *Chem. Eur. J.*, **2010** (16) 6224-6233
15. Pérez-Ramírez, J.; Abelló, S.; Bonilla, A.; Groen, J.C.; *Adv. Funct. Mater.*, **2009** (19) 164-172
16. Pérez-Ramírez, J.; Verboekend, D.; Bonilla, A.; Abelló, S.; *Adv. Funct. Mater.*, **2009** (19) 3972-3979
17. Holm, M.S.; Hansen, M.K.; Christensen, C.H.; *Eur. J. Inorg. Chem.* , **2009** 1194-1198
18. Wei, X.; Smirniotis, P.G.; *Microporous Mesoporous Mater.*, **2006** (97) 97-106
19. Verduijn, J.P., Exxon Chemical Patents Inc.,**1997**
20. Gopal, S.; Yoo, K.; Smirniotis, P.G.; *Microporous Mesoporous Mat.*, **2001** (49) 149-156
21. Lu, B.W.; Jon, H.; Kanai, T.; Oumi, Y.; Itabashi, K.; Sano, T.; *J. Mater. Sci*, **2006** (41) 1861-1864
22. Lippens, B.C.; de Boer, J.H.; *J. Catal.*, **1965** (4) 319-323
23. Barrett, E.P.; Joyner, L.G.; Halenda, P.P.; *J. Am. Chem. Soc.* , **1951** (73) 373-380
24. Bitter, J.H.; Battiston, A.A.; van Donk, S.; de Jong, K.P.; Koningsberger, D.C.; *Microporous Mesoporous Mater.*, **2003** (64) 175-184
25. Ruppert, A.M.; Parvulescu, A.N.; Arias, M.; Hausoul, P.J.C.; Bruijnincx, P.C.A.; Klein Gebbink, R.J.M.; Weckhuysen, B.M.; *J. Catal.*, **2009** (268) 251-259
26. van Laak, A.N.C.; Gosselink, R.W.; Sagala, S.L.; Meeldijk, J.D.; de Jongh, P.E.; de Jong, K.P.; *Appl. Catal., A: Gen*, **2010** (382) 65-72
27. Lónyi, F.; Valyon, J.; *Microporous Mesoporous Mater.*, **2001** (47) 293-301
28. Miyamoto, Y.; Katada, N.; Niwa, M.; *Microporous Mesoporous Mater.*, **2000** (40) 271-281
29. Camiloti, A.M.; Jahn, S.L.; Velasco, N.D.; Moura, L.F.; Cardoso, D.; *Appl. Catal., A: Gen*, **1999** (182) 107-113
30. Costa, C.; Lopes, J.M.; Lemos, F.; Ribeiro, F.R.; *J. Mol. Catal. A: Chem.*, **1999** (144) 221-231
31. Parvulescu, A.N.; Hausoul, P.J.C.; Bruijnincx, P.C.A.; Klein Gebbink, R.J.M.; Weckhuysen, B.M.; *Catal. Today*, **2010** (158) 130-138
32. Parvulescu, A.N.; Mores, D.; Stavitski, E.; Teodorescu, C.M.; Bruijnincx, P.C.A.; Gebbink, R.J.M.K.; Weckhuysen, B.M.; *J. Am. Chem. Soc.*, **2010** (132) 10429-10439

5a

Summary and Concluding Remarks

The aim of the research described in this thesis was to introduce mesoporosity in zeolites to enhance the catalytic performance with the emphasis on mordenite for the production of cumene. The activity of zeolites is closely related to the accessibility of reactants to the active sites inside the micropore channels. Improved synthesis recipes have led to smaller zeolite crystals and post-synthesis treatments using steam and acid (dealumination) have introduced mesopores to improve mass transport. These developments have made zeolites one of the most important class of heterogeneous catalysts today. Alkaline treatment (or desilication) was recently studied in detail as a post synthesis treatment that makes high levels of mesoporosity possible, thus enhancing catalytic performance even further. An alkaline treatment of ZSM-5 is typically performed in 0.2 M NaOH at 333 K for 30 minutes. Important is that the Si/Al ratio of the zeolite should be between 25 and 50 at/at. At lower Si/Al ratios the alkaline treatment is ineffective while at higher ratios the zeolite will be dissolved. In this thesis we describe that alkaline treatment to obtain mesoporosity can be applied to a broader range of Si/Al ratios.

In chapter 2 we apply alkaline treatment to generate mesopores in mordenite with a high aluminum content (Si/Al ratios 6-10 at/at). Three mordenite samples LZM-5, BASF and Zeolyst 21A were studied and the key approach was to apply more severe conditions (1 M NaOH 343 K) than those described in literature. The stronger alkaline medium made it possibly to not only dissolve silicon species but aluminum species as well. As a result of the alkaline treatment the external surface area increased from ~30 to over 100 $m^2 \cdot g^{-1}$. The type of mesopores for the mordenite with Si/Al ratio 6 at/at (LZM-5) was found to be mainly inter-crystalline, while for the slightly higher Si/Al ratios (8-10 at/at) of BASF and Zeolyst mordenites intra-crystalline mesopores were formed as well. Alkylation experiments were performed on LZM-5 and BASF (chapter 3) mordenite. Interestingly about the parent mordenites is that the BASF sample is 10 times more active than LZM-5, while the selectivity is significantly lower (90 vs. 99 %). This illustrates the importance of studying multiple samples when catalytic performances of zeolites are studied. The added porosity after alkaline treatment resulted in ~20 times higher catalytic activity for the LZM-5 mordenite, while selectivity was similar. Alkaline treatment on the BASF mordenite resulted in a 5 times more active catalyst and more importantly the poor selectivity of the parent BASF (90 %) was improved to 99 %. This is most likely a result of dissolved species with low acidity removed from the external surface area during the alkaline treatment.

In chapter 3 the effects of acid, alkaline and sequential acid and alkaline treatments on mesopore formation were studied with mordenites Zeolyst 21A and BASF.

Dealumination with 3 M nitric acid increased the Si/Al ratio to 22 and 30 at/at, but mesopore formation was negligible for both mordenite samples. Sequential alkaline treatments in 1 M NH_4OH and 0.2 M NaOH at 343 K resulted in a series of highly mesoporous mordenite with surface areas increasing from 94 $m^2 \cdot g^{-1}$ up to 250 $m^2 \cdot g^{-1}$. This series of increasingly porous mordenite was analyzed with electron tomography and showed that mesopore formation started at the edges of the crystallites and progressed to the centers at higher mesoporosities. For the most porous mordenite small mesopores (3-8 nm) were observed throughout the sample. This highly porous BASF mordenite was ~27 times more active than the parent and close in activity to zeolite Beta, which is the industrially used catalyst. The selectivity of the mesoporous mordenite of 93 % was less than that of zeolite Beta (99 %). The selectivity can most likely be improved by careful acid washing to remove redistributed aluminum from the surface. More importantly is that mordenite has three times lower n-propylbenzene formation (a contaminant for downstream processes) compared to zeolite Beta. This indicates that mesoporous mordenite can be a viable catalyst in the cumene process as an alkylation or trans-alkylation catalyst.

Chapter 4 provides an approach to generate mesoporosity of template containing zeolites. The treatment is similar as to what is described in chapter 2, with the difference that a template is present. Because of the presence of the template the acid sites in the interior of the micropores are not affected by the alkaline solution. As a result outer layers of the individual crystallites were removed, thereby adding inter-crystalline mesoporosity. This treatment was successfully applied on three different zeolites ZSM-5, ZSM-12 and zeolite Beta with Si/Al ratios ranging from 17 to 105 at/at. The external surface area for ZSM-5 was increased from 92 to 149 $m^2 \cdot g^{-1}$ and from 77 to 158 $m^2 \cdot g^{-1}$ for zeolite Beta. The added mesoporosity resulted in an enhanced catalytic activity for the etherification of 1,2-propylene glycol with 1-octene to form octyl-ether for ZSM-5 and zeolite beta. For ZSM-5 conversion of 1,2-propylene glycol increased from 1.2 to 5.6 % and selectivity increased from 95 % to 98 %. Additional alkaline treatment experiments were performed without the template present. Despite the larger mesoporosity lower catalytic performance was measured (5.0 % conv., 97 % sel.), possibly the result of aluminum deposits near the micropore mouth. Zeolite Beta was considerably more active with a 30 % conversion and 88 % selectivity. Upon alkaline treatment of zeolite Beta the conversion increased to 40 % with equal selectivity. These results show that alkaline treatment on templated zeolites provides a new route to enhance the accessibility without changing the acidity, and provides an opportunity to expand our understanding of zeolite catalysis.

The results described in this thesis show that zeolites, after decades of research, can still be improved upon. The question that remains is if these post-synthesis routes will be implemented in actual industrial processes. For the most exciting result of this PhD research, the sequential acid and alkaline treatment I would say that there are possibilities, especially as a trans-alkylation catalyst of diisopropylbenzene where mordenite showed its potency before, when it was industrially applied at Dow Terneuzen. However, before any such implementation is possible, further refinement of the sequential acid and alkaline treatment is necessary. For that a high-throughput experiment would be ideal, for which the results described in this thesis provide excellent boundary conditions. After that scaling up of the whole process will be another hurdle to take. Thus there are possibilities for commercial application for sequential acid and alkaline treatment, but it will need some additional work to get there.

5b

Nederlandse Samenvatting

Het doel van het onderzoek dat beschreven staat in dit proefschrift was het genereren van mesoporiën in zeolieten met de nadruk op mordeniet ten einde de katalytische activiteit en selectiviteit voor de productie van cumeen te verbeteren. Zeolieten zijn kristallijne en microporeuze materialen die opgebouwd zijn uit zuurstof-, aluminium- en silicium-atomen. Daarnaast zijn er in de microporiën (~1 nm) vaak lading compenserende kationen aanwezig zoals natrium (Na^+) of een proton (H^+). Het proton werkt als een Brønsted zuur waarmee zuur gekatalyseerde reacties kunnen worden uitgevoerd. Een voorbeeld daarvan is de alkylering van benzeen met propene tot cumeen (iso-propylbenzeen). Het grote voordeel van zeolieten is dat deze reactie voornamelijk plaats vindt in microporoririën waardoor de productie van ongewenste bijproducten verkleind wordt. De activiteit van zeolieten is nauw verwant aan de toegankelijkheid van de actieve plekken in de microporiën voor reactanten. In de afgelopen decennia hebben aangepaste syntheses geleid tot kleinere zeolietkristallen en kunnen door nabehandelingen met stoom en zuur (dealuminatie) mesoporiën (2 tot 50 nm) worden geïntroduceerd, zodat het massa transport aanzienlijk versneld wordt. Recent zijn behandelingen met alkalische oplossingen (loog) uitgevoerd op zeolieten waarbij veel werk is gedaan met ZSM-5. Een alkalibehandeling op ZSM-5 wordt typisch uitgevoerd in 0.2 M NaOH bij 333 K voor 30 minuten. Belangrijk is dat de Si/Al ratio van de zeoliet tussen de 25 en 50 at/at is. Bij lagere Si/Al verhouding zal de alkalibehandeling niet effectief zijn doordat de hoge hoeveelheid aluminium een bescherming vormt terwijl bij hogere Si/Al verhouding de zeoliet zal oplossen. In dit proefschrift beschrijven we hoe mesoporiën kunnen worden verkregen met behulp van een alkali behandeling in een breder gebied van Si/Al verhoudingen.

In hoofdstuk 2 passen we een alkalibehandeling toe om mesoporiën te verkrijgen in mordeniet waarin veel aluminium aanwezig is (lage Si/Al verhouding). Drie mordeniet monsters, LZM-5, BASF en Zeolyst 21A werden bestudeerd waarbij het verhogen van de NaOH concentratie tot 1 M belangrijk bleek. Deze alkalibehandeling maakte het mogelijk om zowel silicium als aluminium gecontroleerd op te lossen, met als resultaat dat het externe oppervlakte van het mordeniet monster steeg van ~30 $m^2 \cdot g^{-1}$ tot boven de 100 $m^2 \cdot g^{-1}$. Het type mesoporiën voor LZM-5 mordeniet met een Si/Al-ratio van 6 at/at was voornamelijk tussen de kristallen ofwel inter-kristallijn. Voor de mordenietkristallen van BASF en Zeolyst die een iets hogere Si/Al-ratio hebben (8-10 at/at), werden daarnaast ook mesoporiën in de kristallen gevonden (intra-kristallijn). Alkylatie-experimenten werden uitgevoerd met zowel de LZM-5 mordeniet (hoofdstuk 2) als met de BASF mordeniet (hoofdstuk 3). Wanneer we de katalytische activiteit van de mordenieten vergelijken zonder behandelingen te hebben gedaan blijken er grote verschillen te zijn.

De BASF mordeniet is 5 keer actiever maar is daarnaast ook veel minder selectief (90 %) naar bruikbare producten (cumeen + diisopropylbenzeen) ten opzichte van LZM-5 (99 %). Dit geeft aan dat er grote verschillen zijn tussen verschillende mordeniet monsters en dat voor het screenen van zeolieten meerdere monsters moeten worden geanalyseerd om een juist inzicht te krijgen. De toegevoegde porositeit na de alkalibehandeling resulteerde in een ~20 keer hogere activiteit voor de LZM-5 mordeniet bij gelijkblijvende selectiviteit. Voor de BASF-mordeniet werd een 5 keer hogere activiteit gemeten en nog belangrijker de selectiviteit nam toe van 90 naar 99 %. Hoogstwaarschijnlijk is de lage selectiviteit van het oorspronkelijke BASF mordeniet het gevolg van oppervlakte actieve plaatsen die tijdens de alkali behandeling worden verwijderd waardoor de selectiviteit toeneemt. Met de methode beschreven in hoofdstuk 2 kan de activiteit van mordeniet met lage Si/Al-ratio voor de productie van cumeen worden verbeterd terwijl de selectiviteit gelijkblijft of zelfs hoger is.
In hoofdstuk 3 worden de effecten van zuur-, alkali- of opeenvolgende zuur- en alkalibehandeling voor het verkrijgen van mesoporiën bestudeerd voor de mordenieten Zeolyst 21A en BASF. Zuur behandeling met 3 M salpeterzuur resulteerde in een verhoging van de Si/Al ratio van 8 naar 30 (at/at), waarbij mesoporie formatie vrijwel nihil was. Een opeenvolgende alkalische behandeling in 1 M NH_4OH of 0.2 M NaOH op 343 K resulteerde in een serie mesoporeuze mordenieten met externe oppervlaktes tussen 94 en 250 $m^2 \cdot g^{-1}$. Deze serie met oplopende porositeit werd geanalyseerd met elektronentomografie. Na reconstructie van de mordeniet kristallen in 3D werd duidelijk dat mesoporie formatie begon aan de randen van de kristallen en steeds verder voortging naar het hart van de kristallen. Voor de meest poreuze mordeniet werden kleine mesoporiën (3-8 nm) door het gehele kristal aangetroffen. Deze zeer poreuze mordeniet bleek ~27 keer meer actief te zijn dan de oorspronkelijke mordeniet. Deze activiteit is dicht bij die van zeoliet Beta, welke de katalysator voor het commerciële proces is. De selectiviteit (cumeen + diisopropylbenzeen) van de poreuze mordeniet was met 93% wel lager dan dat van zeolite Beta (99 %). Deze selectiviteit kan waarschijnlijk door optimalisaties van de zuur- en alkalibehandeling nog wel worden verbeterd. Belangrijk is dat de mesoporeuze mordeniet een drie keer lagere hoeveelheid n-propylbenzeen maakt dan zeoliet Beta. Dit n-propylbenzeen is schadelijk in latere processen en een zo laag mogelijk concentratie is gewenst. Deze resultaten geven aan dat mesoporeuze mordeniet door opeenvolgende zuur- en alkalibehandelingen een levensvatbare katalysator kan geven in het cumeen-proces als een alkylatie- of trans-alkylatiekatalysator.
Hoofdstuk 4 beschrijft een methode om mesoporiën te verkrijgen in templaat bevattende zeolieten. De alkalibehandeling is vergelijkbaar met die beschreven in hoofdstuk 2, met

als verschil dat de microporiën van de zeoliet gevuld zijn met templaatmoleculen (bv. tetra-ethyl ammonium). Door de aanwezigheid van de templaatmoleculen worden de katalytisch actieve plekken in de microporiën niet beïnvloed door de alkali behandeling. Het resultaat is dat de buitenste lagen van de kristallen werden verwijderd waarbij inter-kristallijne mesoporiën worden gevormd. Deze behandeling werd succesvol toegepast op drie verschillende zeolieten: ZSM-5, ZSM-12 en zeoliet Beta met Si/Al verhoudingen variërend van 17 tot 105 at/at. Het externe oppervlak van ZSM-5 werd door de alkalibehandeling verhoogd van 92 naar 149 $m^2 \cdot g^{-1}$ en dat van zeoliet Beta van 77 naar 158 $m^2 \cdot g^{-1}$. De toegevoegde mesoporositeit resulteerde in verbeterde katalytische werking voor de etherificatie van 1,2-propyleen glycol met 1-octene ter vorming van octyl-ether door ZSM-5 en zeoliet Beta. De conversie van 1,2-propyleen glycol door ZSM-5 nam toe van 1.2 % naar 5.6 % en de selectiviteit steeg van 95 % naar 98 %. Ook werd alkali behandelde ZSM-5 gemeten zonder het templaat aanwezig. Deze monsters hadden ondanks significant hogere externe oppervlaktes (233 $m^2 \cdot g^{-1}$) minder goede katalytische eigenschappen (5.0 % conv., 97 % sel.). Mogelijk is dit het gevolg van ophoping van aluminium aan het oppervlak. Zeoliet Beta was actiever dan ZSM-5 met een conversie van 30 %, selectiviteit daarentegen was met 88 % lager. Na alkalibehandeling was de conversie 40 % met gelijkblijvende selectiviteit. Deze resultaten laten zien dat alkalibehandeling op templaat bevattende zeolieten een nieuwe route biedt om de toegankelijkheid van zeolieten te verbeteren zonder daarbij de actieve sites te veranderen. Deze ontkoppeling van de aard van de actieve plekken en de toegankelijkheid ervan geeft de mogelijkheid om ons begrip van zeolietkatalyse verder te vergroten.

De resultaten zoals die beschreven staan in dit proefschrift laten zien dat zeoliten na decennia van onderzoek nog steeds verbeterd kunnen worden. De vraag die overblijft is of deze post synthese routes kunnen worden geïmplementeerd in bestaande industriële processen. Voor het meest in oog springende resultaat van dit proefschrift, de opeenvolgende zuur en alkali behandeling, zou ik zeggen dat er mogelijkheden zijn, in het bijzonder als een trans-alkylerings katalysator van diisopropylbenzeen, welke al eerder in de industrie gebruikt werd door Dow Terneuzen. Echter voordat dit geïmplementeerd kan worden moet de opeenvolgende zuur en alkaline op mordenite behandeling verder worden verfijnd. Hiervoor zou een high-throughput experiment uikomst bieden, waarvoor de randvoorwaarden in dit proefschrift worden gegeven. Hierna zal de laatste horde het opschalen van het proces zijn. Er zijn dus mogelijkheden voor een commerciële toepassing voor de opeenvolgende zuur en alkali behandeling op mordeniet maar daarvoor zal er eerst nog wat aanvullend werk uitgevoerd moeten worden.

List of Publications and Presentations

Patent application

- Van Donk, S., Lacroix, M., Kenmogne-Catchuisse, R., Fajula, F., Bulut, M., Dath, J., De Jong, K.P., De Jongh P.E. Zecevic, J., Van Laak A.N.C. "Modified Y-type zeolite having a trimodal intracrystalline structure, method for making same, and use thereof", WO 2010/072976 A1

Publications

- van Laak, A.N.C.; de Jong, K.P.; de Jongh, P.E., *Benzene adsorption and desorption in mordenite*, in *Stud. Surf. Sci. Catal.* 2007 (170) 934-941.

- Ban, S.; van laak, A.N.C.; de Jongh, P.E.; van der Eerden, J.P.J.M.; Vlugt, T.J.H., *Adsorption Selectivity of Benzene/Propene Mixtures for Various Zeolites*, in *J. Phys. Chem. C*. 2007 (111) 17241-17248.

- Zhang, L.; Zmelik, C.; van Laak, A.N.C.; Karger, J.; de Jongh, P.E.; de Jong, K.P., *Direct assessment of molecular transport in mordenite: Dominance of surface resistances*, in *Chem. Commun.* 2009 6424-6426

- Ban, S.; Van Laak, A.N.C.; Landers, J.; Neimark, A.V.; De Jongh, P.E.; De Jong, K.P.; Vlugt, T.J.H., *Insight into the effect of dealumination on mordenite using experimentally validated simulations*, in *J. Phys. Chem. C*. 2010. (114) 2056-2065.

- van Laak, A.N.C.; Gosselink, R.W.; Sagala, S.L.; Meeldijk, J.D.; de Jongh, P.E.; de Jong, K.P., *Alkaline treatment on commercially available aluminum rich mordenite*, in *Appl. Catal., A: Gen*. 2010 (382) 65-72.

- van Laak, A.N.C.; Sagala, S.L.; Zecevic, J.; Friedrich, H.; de Jongh, P.E.; de Jong, K.P., *Mesoporous mordenites obtained by sequential acid and alkaline treatments - Catalysts for cumene production with enhanced accessibility*, in *J. Catal.* 2010 (276) 170-180.

- van laak, A.N.C.; Zhang, L.; Parvulescu, A.N.; Bruijnincx, P.C.A.; Weckhuysen, B.M.; de Jong, K.P.; de Jongh, P.E., *Alkaline Treatment of Template Containing Zeolites: Introducing Mesoporosity while Preserving Acidity*, in *Catal. Today*. 2010. doi:10.1016/j.cattod.2010.10.101

- Zhang, L.; van Laak, A.N.C.; de Jongh, P.E.; de Jong, K.P.; Zeolites and Catalysis: Synthesis, Reactions and Applications: Chapter 8, (Cejka, J.; Corma, A.; Zones, S., Eds). Weinheim. Wiley-VCH., 2010 237-282

Oral presentation:

- van Laak, A.N.C.; de Jong, K.P.; de Jongh, P.E., *Benzene adsorption and desorption in mordenite*, 15th International Zeolite Conference, August 12-17, 2007, Beijing, China

Acknowledgements - Dankwoord

For a PhD to succeed there are numerous things that have to be taken care of, one of which is the writing of this book, for which I'm very happy that it is finished now. At the core of this book, however, there is the necessary raw scientific data, which is often acquired through hard work, persistence and the occasional (educated?) luck. But most important of all is the knowledge that a PhD research isn't done alone. There is help on a lot of different levels; colleagues, friends, family and last but not least students.

In our group I would say master students are by far the most hardworking people, not only do they have to perform scientific related stuff like experiments and reporting, they also have to earn some money for the occasional beer or road trip, hone their gaming skills, keeping in touch with their social contacts, play sports or breaking a leg, bring back exotic parasites (or think they do) and they have to do all that within a given timeframe. I had the luxury that two talented master students were interested in my PhD work and I was lucky that, in contrast to the general aspects described above ,these students were absolutely 100 % dedicated to their (my) scientific work. And I can say for certain that without their work my PhD would have been fundamentally different. Therefore I would like to thank Rob and Sophia for all their efforts and I wish you all the help from dedicated master students in your own PhD research (break a leg). Also the help of bachelors students Stefan, Maarten and Philip is greatly appreciated.

I would also like to thank my colleagues Nadia, André, Shuai, Thijs, Heiner and Jovanna (thanks for the amazing cover tomo cross-section on the cover) for the cooperation that has led to several publications. Lei, special thanks to you for the beautiful mordenite crystals and joint work with the TEOM. Ard en Rien heel veel succes gewenst met de TEOM en dat ie na de verhuizing nog een lang leven mag hebben.

Vanuit de samenwerking binnen NWO/ASPECT wil ik Marcel Janssen en Machteld Mertens van Exxonmobil bedanken voor de Al-NMR analyses en de prachtige MFI kristallieten. Ferry en Jelle (Shell) bedankt voor de mordeniet monsters en de katalytische experimenten. Daarnaast zijn door DOW katalytische alkylerings testen uitgevoerd die essentieel waren voor hoofdstuk 2 en 3. Garry Meima, Mathieu van der Aalst en Jeff Samson bedankt voor al jullie medewerking en expertise.

Daarnaast wil ik ook graag de technische staf van Anorganische Chemie bedanken. Fred, bedankt voor al het werk met de TEOM. Ad^{m}, bedankt voor de antwoorden op al die talloze kleine/korte vraagjes. Marjan en Hans bedankt voor al die mooie SEM/TEM/

TOMO plaatjes die toch een aanzienlijk deel van dit proefschrift in gebruik nemen. Ad[e], Fouad, Vincent en natuurlijk Dymph en Monique bedankt voor al die andere dingen die jullie in de afgelopen jaren hebben geregeld.
Ingmar, Alwies, Johan, Tamara, Mariska, Bart, Arjan, Annelie, Eli, Lukasz en alle anderen bedankt voor al het vertier tijdens de koffiepauzes, op de fiets, in de gang, tijdens uitjes en op NCCC's. Harry bedankt voor al die mooie anekdoten, hou die van die Espace er in elk geval in ☺, en niet alleen van de vorige eigenaar maar ook dat andere. Niels bedankt voor het delen van je glutenkennis, zonder die kennis had dit boekje waarschijnlijk wat langer op zich laten wachten. Daarnaast wil ik Rudy, Simona, Hirsa, Inge, Upakul en Rene bedanken de gezelligheid in N205.
Krijn ik wil je bedanken voor de mogelijkheid die je mij hebt gegeven en al het advies en tips die ik in de afgelopen jaren ontvangen heb zeker gaan toepassen in de rest van mijn carrière. Ook Petra bedankt voor de ideeën, manuscript correcties en natuurlijk de reis naar China.
Pap en mam mijn dank voor alles wat jullie in die afgelopen eenendertig jaar gedaan hebben. Jullie hebben mij het belang van een goede opleiding meegeven en daar is dit boekje het resultaat van. Ook ben ik dankbaar voor al die keren dat jullie in de afgelopen jaren klaarstonden voor mij, Marleen en de kinderen en elke dinsdagochtend de A2 spits trotseerden om op de kinderen te passen.
Als laatste wil ik mijn gezin bedanken. Veere, super dat je mij de maximale hoeveelheid uren in een etmaal liet meemaken door gemiddeld om 6.00 's ochtends klaarwakker te zijn. Thomas, bedankt voor het toevoegen van de nachtelijke uren en het laten zien dat de aanhouder wint. Jesse, dank voor je inzicht dat er ook een tijd van slapen moet zijn. Maar vooral bedankt voor al die lachjes en knuffels die ik kreeg van jullie drie als ik terug kwam van de uni, dat maakte de promotie en het schrijven van dit boekje een stuk makkelijker. Mijn allerlaatste woorden zijn voor jou Marleen, want zonder jou was dit boekje er niet geweest. Bedankt voor alles wat je in de afgelopen jaren hebt gedaan voor mij en voor onze kinderen, mijn dank en mijn liefde voor jou.

Adri

Curriculum Vitae

Adri van Laak werd op 15 januari 1980 geboren te Vught. Na het behalen van zijn VWO diploma aan het Maurick College te Vught startte hij in 1998 aan de studie Scheikunde aan de universiteit Utrecht. In november 2004 studeerde hij af na universitaire stages bij de secties Biochemie van Membranen (dr. M.A. Kol, prof. dr. B. de Kruijff) en Anorganische Chemie en Katalyse (dr. L. Bezemer, prof. dr. K.P. de Jong).
Vanaf februari 2005 was hij werkzaam als Assistent in Opleiding bij prof. dr. K.P. de Jong en dr. P.E. de Jongh in de sectie Anorganische Chemie en Katalyse van de Universiteit Utrecht. Het onderzoek werd gefinancierd door ACTS-ASPECT en een deel van de verkregen resultaten is gebundeld in dit boekje.

Adri van Laak was born on the 15th of January 1980 in Vught. After graduating from secondary school, Maurick College in Vught, he started in 1998 with a Chemistry study at Utrecht University. In November 2004 he obtained his master's degree after university traineeships at the groups of Biochemistry of Membranes (dr. M.A. Kol, prof. dr. B. de Kruijff) and Inorganic Chemistry and Catalysis (dr. L. Bezemer, prof. dr. K.P. de Jong).
From February 2005 he worked as a PhD-student under the supervision of prof. dr. K.P. de Jong en dr. P.E. de Jongh in the group of Inorganic Chemistry and Catalysis at Utrecht University. The Research was funded by ACTS-ASPECT and part of the obtained results is described in this thesis.